CORA Cork Open Research Archive
Cartlann Taighde Oscailte Chorcaí

| | |
|---|---|
| Title | Quantum behavior in mesoscopic systems |
| Authors | Lo Gullo, Nicolino |
| Publication date | 2013-01 |
| Original Citation | Lo Gullo, Nicolino. 2013. Quantum behavior in mesoscopic systems. PhD Thesis, University College Cork. |
| Type of publication | Doctoral thesis |
| Link to publisher's version | http://arxiv.org/pdf/1107.0750v2.pdf, http://arxiv.org/pdf/1011.2125v3.pdf, http://arxiv.org/pdf/0912.1305v2.pdf |
| Rights | © 2013, Nicolino Lo Gullo - http://creativecommons.org/licenses/by-nc-nd/3.0/ |
| Download date | 2026-11-06 17:49:56 |
| Item downloaded from | https://hdl.handle.net/10468/964 |



UCC
University College Cork, Ireland
Coláiste na hOllscoile Corcaigh

**UNIVERSITY COLLEGE CORK**

# Quantum behavior in mesoscopic systems

by

Nicolino Lo Gullo

A thesis submitted in partial fulfillment for the degree of Doctor of Philosophy

in the
Faculty of Science
Department of Physics

January 2013

# Declaration of Authorship

I, Nicolino Lo Gullo, declare that this thesis titled, 'Coherences in mesoscopic systems', and the work presented in it are my own. I confirm that:

- This work was done wholly or mainly while in candidature for a research degree at this University.
- Where any part of this thesis has previously been submitted for a degree or any other qualification at this University or any other institution, this has been clearly stated.
- Where I have consulted the published work of others, this is always clearly attributed.
- Where I have quoted from the work of others, the source is always given. With the exception of such quotations, this thesis is entirely my own work.
- I have acknowledged all main sources of help.
- Where the thesis is based on work done by myself jointly with others, I have made clear exactly what was done by others and what I have contributed myself.

Signed: _____

Date: _____

UNIVERSITY COLLEGE CORK

# *Abstract*

Faculty of Science
Department of Physics

Doctor of Philosophy

by Nicolino Lo Gullo

In this thesis I present the work done during my PhD. The Thesis is divided into two parts; in the first one I present the study of mesoscopic quantum systems whereas in the second one I address the problem of the definition of Markov regime for quantum system dynamics. The first work presented is the study of vortex patterns in (quasi) two dimensional rotating Bose Einstein condensates (BECs). I consider the case of an anisotropy trapping potential and I shall show that the ground state of the system hosts vortex patterns that are unstable. In a second work I designed an experimental scheme to transfer entanglement from two entangled photons to two BECs. This work is meant to propose a feasible experimental set up to bring entanglement from microscopic to macroscopic systems for both the study of fundamental questions (quantum to classical transition) and technological applications. In the last work of the first part another experimental scheme is presented in order to detect coherences of a mechanical oscillator which is assumed to have been previously cooled down to the quantum regime. In this regime in fact the system can rapidly undergo decoherence so that new techniques have to be employed in order to detect and manipulate their states. In the scheme I propose a micro-mechanical oscillator is coupled to a BEC and the detection is performed by monitoring the BEC with a negligible back-action on the cantilever. In the second part of the thesis I give a definition of Markov regime for open quantum dynamics. The importance of such definition comes from both the mathematical description of the system dynamics and from the understanding of the role played by the environment in the evolution of an open system. In the Markov regime the mathematical description can be simplified and the role of the environment is a passive one.

# *Acknowledgements*

The first person I want to thank is my supervisor *Thomas Busch*. I am really grateful to him for all the time he spent preparing me for research. Only now can I see what he did to the student I was in order to make him into a scientist. Each of his suggestions were aimed at tailoring, day by day, a good physicist. He has been a strong guide without supressing my enthusiasm and creativity. In fact he shaped them and made me use them in a profitable way. I hope I gave him something back.

I also want to thank *Mauro Paternostro*, who looked after me in the last three years. I am grateful to him for guiding me and for the great patience he had in listening to my concerns. I owe him most of the physicist I am now.

Another person I want to thank is *Francesco Plastina*, my mentor at the Universitá della Calabria. I thank him for the continuous suggestions and tips and I am greatful for all he keeps teaching me about physics. I still enjoy talking with him about physics and I admire for his no nonsense straightforward approach.

There is a long list of people I want to thank I will try to order them by "age". First the last ones as somebody would like to say.

I thank this country and its people that have welcomed me and made me feel at home in this cold weather. In particular, I thank them for introducing to Beamish and Irish music. I thank *Mossy Fogárty*, *Tadhg Morgan* and *Tara Hennessy* for all the scones we had, the search the best scone ever is still on, but we definitely gave it our best try. I thank Dave Rea for all his stories and continuous support, it is refreshing to experience his passion for physics. I thank the rest of the group of Ultracold Gases in UCC for many enjoyable moments and drinks.

I can not forget the two cornerstones of the group: *John Goold* and *Brian O'Sullivan*. Before being my great friends, they were my English teachers, so blame them for any mistakes you will find in this thesis.

I thank *John* for all the discussions we had and for his enthusiasm, which was really helpful in many moments during the past three years. I thank him for sharing with me his ideas, his new discoveries and his doubts. This kept me going in difficult moments.

About *Brian*, what can I say, we spent the last three years supporting each other and having fun, making the PhD an almost painless experience. He kept alive the childhood side of the physicist I am. He taught me that it is never stupid to ask questions you already answered and made me understand that most of the time the answer was wrong or unclear.

I want to thank *Shane Cameron*, a very good friend and my Bodhràn teacher. He helped me more than what he can imagine in improving my communication skills. It was really tough to answer all of his questions about science, he probably thought I was a kind of encyclopedia. He made me understand the importance of having concepts clear in your mind before you try to tell people.

I want to thank all my friends I studied with in college for many helpful discussions. I find it wonderful that, separated by distance, we keep supporting each other on this journey without end that is the research. I thank *Michele Pisarra* and *Michele Lucente*, *Daniel Francesco Filice*, *Giuseppe Pucci*, *Aldo Brunetti* , *Francesco Carbone*, *Giuseppe Nisticò*, *Denise Perrone*, *Beatrice Murdaca*, *Sandro Donato Serena Dalena*, *Melissa Infusino*.

A particular thanks goes to *Antonello Palermo*, a brother more than a friend for the way he believes in me.

I also want to thank *Tony Apollaro*, for beautiful discussions. I really enjoy listening to him and for me he is the example of physicist I would like to be. I have always been amazed by his passion for physics and knowledge in general.

I want to thank the *A.G.E.S.C.I.* group *Sartano 1* and their components for keeping alive a very important reality in our small village.

Another thank goes to the *Associazione Ginmarco de Maria* and particularly to the Clown group *Cucusettete*. The memories of the moments spent together have been a light ray in dark days, thanks to *Raffaele Salerno*, *Stelio Marano*, *Claudia Giordano*, *Sara Oliviero*, *Giada Andretti*, *Violetta Soave*, *Aldo Barca*, *Fran Bescia*, *Annalisa Orlando* and *Franco de Maria*.

I want to thank the *Nanpu Dojo* in Cosenza and particularly *Sensei Marco Massarotto* for the time he spent teaching me Traditional Japanese Martial Arts and for the passion he shows no matter what. He really embodies the Issho Kenmei motto. Thanks a lot.

A thank goes to *Fabio Pucci*, for hilarious moments during intensive trainings. I would have gone mad if he has not been there with me.

A massive thank goes to *Giuseppe Argento*, *Antonio Mura*, *Sonia De Rose*, *Domingo De Seta*, *Silvia Cicirelli*, *Lucia Micieli* , *Francesco De Rose*, *Francesco Balzamino* very good friends with who I enjoyed many moments of my life. They are my reference when I get lost, the idea of having such good friends makes me feel stupid when I think of giving up something. I feel like I am betraying them.

Thanks even to *my brother*, *Francesco*, who again managed to be there every time I needed him. That is why he is a great brother.

I suppose there is no thank big enough for *my mother* and *my father*, They have been my strength when I was weak and I am grateful for every single word they had for me.

Oh, I was nearly forgetting her, *Rossana, the Princess.* It is amazing that after all these years she is still here, fixing my mistakes and walking with me. She is the only person that really knows who I am and what I want even when I do not know it myself. I learned how to solve equations and how to link causes and effects, but I still can not figure out how this strange thing works. With her life is never boring or sad, and from her I get inspiration for my thoughts and motivations to do instead of thinking. I love the way she put all her efforts in doing one thing, I love her tenacity when she wants to achieve something. I could not really wish for anything more. I am grateful for every day we spend together.

I want to thank the Irish Council for Science Engineering ad Technology, the Science Foundation Ireland and the Okinawa Institute for Science and Technology for financial support.

# Contents

**Declaration of Authorship** i

**Abstract** ii

**Acknowledgements** iii

**List of Figures** viii

**List of Tables** xi

**1 Bose Einstein condensates** 5
- 1.1 Introduction . . . 5
- 1.2 Theoretical background . . . 6
  - 1.2.1 Gross-Pitaevskii equation . . . 6
  - 1.2.2 Quantum vortices . . . 11
- 1.3 Atom Cooling and Trapping . . . 14
  - 1.3.1 Cooling techniques . . . 14
  - 1.3.2 Zeeman slowing and chirping . . . 15
  - 1.3.3 Optical trapping . . . 16
  - 1.3.4 Magnetic trapping . . . 18

**2 Structural change of vortex patterns in 2D BEC** 21
- 2.1 Introduction . . . 21
- 2.2 Vortex gas . . . 23
- 2.3 Hydrodynamic description . . . 26
- 2.4 Patterns modes . . . 29
- 2.5 Conclusions and Outlooks . . . 30

**3 Mesoscopic entanglement in BEC** 32
- 3.1 Introduction . . . 32
- 3.2 Phase space representation . . . 33
- 3.3 Wigner function and non-classicality . . . 36
- 3.4 Angle and angular momentum variables . . . 37
- 3.5 The model . . . 39
- 3.6 Three-mode expansion and light-induced transfer of OAM entanglement . 45

3.6.1 Bosonic-mode expansion . . . 45
3.6.2 Entanglement transfer process . . . 47
3.6.3 Assessment of entanglement . . . 50
3.7 Detection of vortex entanglement . . . 53
3.8 Conclusions and outlook . . . 55

**4 Detection of quantum coherence by means of a BEC 56**
4.1 Introduction . . . 56
4.2 "Cooling" of a mechanical oscillator . . . 59
4.2.1 Resolved sideband cooling . . . 59
4.3 The set up and the Hamiltonian . . . 60
4.3.1 Hamiltonian of the system . . . 61
4.3.2 Mapping into a rotor . . . 64
4.4 Probing quantum coherences . . . 65
4.4.1 Dynamics . . . 65
4.4.2 Detection scheme . . . 68
4.5 Conclusions . . . 71

**5 Markov regime for open quantum dynamics 72**
5.1 Introduction . . . 72
5.2 Classical stochastic systems . . . 73
5.3 Open quantum systems' dynamics . . . 76
5.4 The dynamical map . . . 78
5.5 Multivariate time correlation functions . . . 79
5.6 Decay of a two-level atom . . . 82
5.6.1 Exact solution . . . 82
5.6.2 Density matrix propagator . . . 84
5.7 Decoherence of a two-level atom . . . 86
5.7.1 Exact solution . . . 86
5.7.2 Density matrix propagator . . . 87
5.7.3 Trace over the environment . . . 88
5.8 Conclusions . . . 89

**Bibliography 94**

# List of Figures


2.1 Distance $\Delta x$ of the vortices from the soft trapping axis (units of $\sqrt{2Ng_{2D}\Omega/\hbar\omega_x}$) against the eccentricity $\lambda$. We show the cases of $N_v = 7$ and 8 (panel **(a)** and **(b)** respectively) and plot only the changes in positions of four vortices in the lattice (the association with the curves is irrelevant). At $\lambda = \lambda_L$ the vortices suddenly align along the y-axis ($\Delta x = 0$). We have used a BEC of $10^6$ $^{87}$Rb atoms with $a = 5.23 \times 10^{-9}$m in a trap with $\omega_z/2\pi = 100$Hz and $\sqrt{\omega_x\omega_y}/2\pi = 50$Hz (regardless of $\lambda$). . . . . 23

2.2 Phase distribution ($\arg(\psi(\mathbf{x}))$) of a vortex-lattice in the $x-y$ plane with $N_v$=7, 8 (upper and lower row respectively)for different values of $\lambda$. Black dots mark the positions of the vortices (in units of $\sqrt{2Ng_{2D}\Omega/\hbar\omega_x}$). . . . 24

2.3 Phase distribution ($\arg(\psi(\mathbf{x}))$) of a vortex-lattice in the $x-y$ plane with $N_v$=18 for different values of $\lambda$. Black dots mark the positions of the vortices (in units of $\sqrt{2Ng_{2D}\Omega/\hbar\omega_x}$). . . . . 25

2.4 Superfluid velocity field in the rotating frame for $N_v$=8 (other parameters as in Fig. 2.1). From **(a)** to **(d)** we have $\lambda$=1, 0.76, 0.56, 0.36. Dark purple regions correspond to zero velocity. The velocities close to the cores are not shown on the chosen colourmap. . . . . 28

2.5 Spectrum of a BEC with $N_v = 7$ vortices against the eccentricity $\lambda$. The points $\lambda_{C,L}$ where the vortex pattern undergoes a structural change are visible. . . . . 29

3.1 Sketch of the proposed setup. An OAM-entangled two-photon state is produced by spontaneus parametric down conversion (SPDC) of a Gaussian pump. Each output mode interacts with a respective trapped Bose-Einstein condensate (BEC), which is also pumped by an intense field with no OAM. The local matter-light interaction transfers the OAM entanglement from the field modes to the condensates rotational degree of freedom. 40

3.2 Six-level configuration for OAM transfer. We show a schematic representation of the relevant energy levels of a single $^{87}$Rb atom interacting with Laguerre-Gauss (LG) driving fields and classical Gaussian pumps with frequency $\omega_p$. The ground-state triplet comprises states having angular momentum 0 and $\pm\hbar l$. The excited-state triplet is adiabatically eliminated from the dynamics by a double off-resonant Raman transition with the one-photon detunings $\Delta$ and $\Delta_0$. Two-photon detunings $\delta_{\pm l}$ are also introduced for the stabilization of the entanglement-transfer process. The component in Eq. 3.12 carrying zero OAM [being in a Hermite-Gauss (HG) spatial mode] drives off-resonantly the $|0\rangle \leftrightarrow |E\rangle$ transition. . . . . 41

3.3 Evolution of the state probabilities $|f_i(t)|^2$ against the interaction time $t$ (in $\mu$s) for $N_0^I = 10^5$ atoms per condensate. Here $f^I_{j,j'} = 5nm$, $\Omega_I = 27.5$kHz, $\chi_{I,\pm l} = 1.18$kHz, $\Delta = 90$kHz and the two-photon detunings having the functional form $\delta_{\pm l}(t) = 2\Omega_I(1-\Omega_I t/2)-\omega_t$. The trap frequencies are $\omega_t = 70$Hz and $\omega_z = 500$Hz. The photonic resource is tailored at a wavelength of 702nm at an angle of $4^o$ off the initial pumping gaussian beam's axis . . . . . 49

3.4 Time behavior of the populations of the atomic states in $\rho_{AB}(t) = \mathrm{Tr}_{\alpha\beta}(|\Psi(t)\rangle_{AB\alpha\beta}\langle\Psi(t)|)$. The same parameters as in Fig. 3.3 have been used here. The (dashed) green curve is for $|N_0^A, N_0^B\rangle_{AB}$, the (solid) yellow one is for state $|B\rangle$. The low-lying (dotted) red curves represent the probability that the remaining two-BEC basis states are excited. The incomplete population transfer from $|0\rangle_I$ to $|\pm l\rangle_I$ $(I = A, B)$ is due to the zero-OAM terms in $|\Phi_Z\rangle_{\alpha\beta}$. . . . . 50

3.5 Linear entropy $S_L(\rho_{AB})$ against time $t$ (units of $\mu$s). The same parameters as in Fig. 3.3 have been used here. . . . . 51

3.6 Negativity $N(\rho_{AB})$ against the interaction time $t$ (units of $\mu$s). The same parameters as in Fig. 3.3 have been used here. We obtain a maximum of entanglement in correspondence of the range of decreasing trend of $S_L(\rho_{AB}(t))$, which witnesses a larger purity of the two-vortex state and smaller quantum correlations between light and matter. Inset: Negativity against $t$ for $N_0^A = 10N_0^B = 10^4$ and $\Omega_B = 10\ \Omega_A = 27.5$ kHz. Other parameters as in Fig. 3.3. . . . . 52

3.7 Analysis of the Wigner function for $\rho_{AB}(t)$. **(a)**: The blue circle shows a projection the Wigner function on the unit circle for $t = 0$, while the red butterfly structure is associated with $t \simeq 800\mu$s, where OAM entanglement has been transferred. **(b)** and **(c)**: We plot $W_{0,0}(\theta_A, \theta_B)$ at the two instants of time considered for panel **(a)**. Notice the different vertical-axis scales in the two plots. The visibility of the fringes of interference in the Wigner function is an indication of quantum correlations. . . . . 54

4.1 Sketch of the set-up for BEC-based probing of mechanical coherences. A BEC is placed in close proximity to a nano-mechanical cantilever endowed with a magnetic tip. The coupling between the magnetic field generated by the mechanical *quantum antenna* and the ultra-cold atoms embodies a mechanism for the effective probing of coherences in the state of the mechanical system. . . . . 61

4.2 Mean value of $\hat{\mathcal{L}}_x(t)$ for a cantilever in the initial state as given by Eq. (4.10) with $C_0$=$C_1/\alpha$=$1/\sqrt{1+\alpha^2}$and $C_n = 0$ otherwise. The BEC consists of $N$=$10^3$ $^{87}$Rb atoms and $\langle\hat{\mathcal{L}}_{x,y}(0)\rangle = 0$, $\langle\hat{\mathcal{L}}_z(0)\rangle = 100$. We have used $B_z^0$=$3\times10^{-6}\mu T$ and $G_c \approx 1.8\times10^3\mu T/\mu$m. . . . . 67

4.3 Mean value of $\hat{\mathcal{L}}_x(t)$ for a cantilever in the initial state as given by Eq. (4.10) with $C_0 = C_1 = C_2/\alpha = 1/\sqrt{2+\alpha^2}$ and $C_n = 0$ otherwise. The BEC parameters are the same as in Fig. 4.2. The inset shows that the change in $|\alpha|$ amounts to a shift of the oscillations [we have taken $= e^{i\pi/6}(0.5, 1, 2)$]. . . . . 69

4.4 Time evolution of $\hat{\mathcal{L}}_x$ for a coherent initial state of the cantilever with $|\alpha|^2 = 1$ **(a)**, 5 **(b)**, 15 **(c)**, 20 **(d)**. For the same parameter as in **(d)**, the plot **(e)** shows that the carrier frequency $\omega_L$ is not significantly affected. . 70

5.1 Plots of the relative errors for the correlation function $\langle\hat{\sigma}_+(0.1+\tau)\hat{\sigma}_-(0.1)\rangle$ for the case of the decay of a two level atom initially in its excited state interacting with a bosonic bath with spectral density in Eq. (5.35) initially in the vacuum state. The parameter used are $\omega_0 = 10,\ \lambda = 2.1,\ \Delta = 0.2$ . 85

# List of Tables

3.1 Coupling rates in the effective Hamiltonian after the introduction of the effective matter-like bosonic operators [see Eqs. (3.28)] and their expressions in terms of the non-interacting atomic wave-function for a pancake-like potential. . . . . 46

*A Pino*

# Introduction

Since its first formulation quantum mechanics has received great attention both from the scientific community and lay people. With no doubt the reason has to be sought in its predictions, which are often in contrast with our everyday experiences. The idea that an object can be in an undefined state until a measurement is performed is something that even the founders of quantum mechanics themselves were not comfortable with. The power of quantum mechanics and its predictions were, however, immediately recognized due to the excellent agreement between theory and experiments. The quantum formalism was able to explain phenomena that would otherwise be inexplicable such as the wave-like behavior of electron and atoms [1], the magnetic properties of certain materials [2], the structure of proteins [3]. Nevertheless the more we used (and abused) quantum mechanics the more uncomfortable we were: the quantum world is something far away from our classical existence. Then fundamental questions arise. Is there a border between the classical and the quantum realm? We do not know what would happen when we cross this border or in which way this border can be crossed. The first attempts to shed light on this problem were done by trying to explain measurement in the quantum framework. The main problem was to explain the reading out process. Since the quantum world is not equipped with a reader it has to be provided by the classical world. Here, again, the same question arises: how does this reading process, which involves the interfacing between classical and quantum realms, occur? What allows us to perform such a reading out process has been readily identified (or introduced ad hoc) to be "decoherence". We are not really used to such effects in our classical world; nevertheless in the quantum realm coherences are exactly what makes a system "quantum". "The system is affected by decoherence" means that it is losing its quantum properties. Decoherence is the carrier which drives a system across this quantum to classical border in an irreversible way: a one way journey. In the explanation of the (real) measurement process the picture is more or less like this: the (quantum) system to be measured and the (quantum) apparatus first interact and then decoherence drives both across the border. We needed this process because the very last measurement (reading process) has to be classical: we, the ultimate apparatus, are classical objects. On the

other hand this very useful "tool" turns out to be the greatest enemy for any quantum device. If we want to develop quantum technologies we have to learn more about the process of decoherence to counteract it. We then are asked for a better understanding of the mechanism responsible for this "crossover" from quantum to classical. To further complicate the problem there is the old misconception that quantum is synonymous with small whereas a classical object is large. Now we know that this is not the case; a superfluid is a macroscopic object made up of millions of particles, very well organized though, and which shows "quantum behavior". A gravity-wave detector whose mass might be a ton can behave as a quantum oscillator. But we already knew that there are no classical or quantum systems *per se*. Roughly speaking a system involved in a particular process follows classical or quantum laws depending on the ratio of its de Broglie wavelength to the characteristic length scale for that process. It is the essence of the particle-wave duality, there are no particles or waves, it depends upon the physical process. The border between quantum and classical world is then not as easy as the division between "small" and "large". How can we investigate such a crossover? Nature offers plenty of systems that change their behavior from classical to quantum, sometimes showing even both features at the same time. Natural systems are often to complex to be controlled and for this reason in the last decade we have been trying to simulate or emulate them with *ad hoc* designed experiments. In particular we need to have systems that by construction are really close to the border and we require an unprecedent degree of control over them.

The end of the XX century has been the era of technology based on the application of the scientific discoveries made during the end of the XIX / beginning of the XX century itself. The current century holds the potential to be that of quantum based technology. On one hand we dream of this technology because of its intrinsic potential predicted by the quantum mechanical laws. On the other hand we are pushing our current technology to very small scales and to regimes where quantum effects play an important role. That is why in the last couple of decades the so-called hybrid systems received much interest. They are the first attempt to join up different, and well developed, techniques coming from different fields in order to build quantum devices. These techniques come from quantum optics, (ultra) cold gases, condensed matter, soft-matter, biological physics, thermodynamics, etc. [4] These hybrid systems are a very nice playground even for the study of the transition from quantum to classical case.

In this thesis I give my contribution to the study of mesoscopic quantum systems. We borrow the term "mesoscopic" from studies on charge transport in solid state devices [5] where the hallmark of mesoscopic systems is the presence of coherent motion of the charges over the transport process. Mesoscopic systems can have sizes ranging from few elementary components, such as atoms or molecules, up several millions of them. A

mesoscopic system is usually a macroscopic systems whose dynamics occur in presence of a certain degree of quantum coherences. It can be divided into two parts.

We start with a study of vortex patterns in two dimensional Bose-Einstein condensates (BECs) held in anisotropic rotating traps. BECs are ultra-cold gases showing quantum properties; even though they are made up of about thousands to millions of atoms they show interference patterns if two of them collide. It is similar to what happens when two waves on the surface interfere, hence the name matter wave interference for this phenomenon. Nevertheless in this case the phenomenon is even richer because of non linearities in the interaction between atoms. Another remarkable property is super-fluidity whose signature are vortices with quantized circulation. This phenomenon is similar to the occurrence of magnetic vortices in type-II superconductors of the [18]; the microscopic mechanism behind this type of super-fluidity is not clear yet. This makes the study of vortex system particularly interesting and BECs offer a very clean and fully tunable system giving us access to a broad set of configurations. In our work we study the geometry of vortex patterns as a function of the anisotropy of the trapping potential. In particular we address the case of few vortices in the trap finding that, as the anisotropy changes, the ground state of the BEC accommodates vortices in different geometries going from the hexagonal one, reminiscent of the Abrikosov lattice in the case of a large number of vortices, to the linear one in which vortices align. Nevertheless a study of the stability of these patterns shows that they are all unstable. This can be explained by the fact that the anisotropic trap acts as a forcing potential that excite quadrupole modes. Since the number of vortices allowed in the system is fixed by the value of the angular velocity of the trapping potential itself, the system reacts to the external perturbation by setting the vortices in rotation. This allows to store an extra amount of orbital angular momentum without introducing new vortices into the system.

We resort again to the superfluid properties of a BEC to design an experimental scheme aiming at transferring entanglement from micro to the macro world. The transfer can be achieved by means of two photons, initially entangled in orbital angular momentum degree of freedom, that interact with two spatially separated BECs, transferring their angular momentum to them through a Raman-like scattering scheme. The pair of entangled photons are produced via spontaneous parametric down conversion, which has been shown to conserve the total angular momentum. The atoms that acquired the angular momentum are thus set in a frictionless motion through the BEC. This allows for a long-lived entangled mesoscopic system, which can be exploited for quantum repeaters or for more fundamental studies on the quantum behavior of large systems.

We then propose a second scheme in order to investigate quantum properties of micro/-nano objects. Mechanical oscillators are currently used for different purposes such as

monitoring of chemical reactions or biological processes, as thermostats or else to measure small displacements as in the atomic force microscope. These objects turned out to be very good candidates for the study of quantum to classical transition, or as a building block for future quantum technologies. Many efforts are focused on cooling these objects to very low temperatures in order for them to end up in the quantum regime. Nevertheless particular schemes are required to extract information about their state in order not to induce decoherence and thus lose their quantum properties. We assume that a cantilever supplied with a magnetic tip has been cooled down to the quantum regime. Because of the magnetic tip it can interact with a BEC of atoms in a hyperfine level with spin $s = 1$. Because of the mutual interaction the total spin of the BEC undergoes a precession motion and it will carry information about the cantilever state. This precession motion can be continuously monitored with a negligible back-action by means of the Faraday rotation effect, *i.e.* the polarization of light traveling through an active medium rotates by an amount that is proportional to the average magnetic field in the medium. We then have way for monitoring the state of a micro mechanical oscillator in its quantum regime with a negligible perturbation.

In the second part of this thesis a definition for the Markov regime for quantum systems is presented in analogy with the Markov assumption for classical stochastic processes. Every time we neglect part of our system, as it happens when we have no experimental control on it or we are simply not interested in its dynamics, we unavoidably add extra uncertainty to its description. In complex systems this is often the case since one part of the total system, called environment, makes our system open. In the past decade an extensive amount of work has been dedicated to the study of both new mathematical tools to describe such situation and different and diverse experiments have been proposed and realized to better understand these systems. The Markov assumption allows for a really simple mathematical description of these systems. Nevertheless there has been no clear definition of the Markov regime in the quantum case and we detail our attempts to rectify this here.

# Chapter 1

# Bose Einstein condensates

In this chapter we will give a brief theoretical overview of the Bose Einstein condensation phenomenon and the related cooling and trapping techniques exploited to create and manipulate these systems. Bose Einstein condensates are a perfect example of mesoscopic quantum systems for instance they are are used to produce atomic beams [8] or for matter waves interference. They are controlled by mean of optical lasers and/or magnetic fields and due to the high levels of precision reached with these techniques BECs offer a very clean and fully tunable setup to study many-body problems [6] and quantum simulations [7].

## 1.1 Introduction

It is commonly taught in school that the matter surrounding us can appear in three different phases: solid, liquid and gaseous. The simplest example is given by water. It appears in our everyday life in all these phases and we can "switch" from one to another by changing its temperature. From a microscopic point of view the temperature is associated to the mean kinetic energy of the molecules so we can imagine that the higher their temperature the less confined they are; this is why we can drive phase transitions by varying the temperature. Of course things are not as easy as this but this kind of picture matches pretty well our experience. On the other hand during the last two centuries we have developed a better and more sophisticated view of the world around us and in particular of what matter is made of and how its components interact. We have two new phases of matter to the above list, namely the Bose-Einstein condensate (BEC) and the plasma. Roughly speaking we can say that the BEC corresponds to really low temperature whereas the plasma to really high ones, so high that electrons are no longer bounded to their nuclei due to scattering energy. That is why we do not

see plasmas in our daily life (except when looking at the Sun or lighting a match). The BEC phase was first predicted by A. Einstein [9] (1924) who used a previous work by S. N. Bose [10] (1924) on the statistical description of photons. A. Einstein predicted a phase transition for a gas of non-interacting bosons whose effect is "condensation" of particles in the lowest energy state of the system. These particles, named after Bose, are characterized by the fact that their spin is an integer in contrast to fermions, named after E. Fermi, which have half integer spin.

The following decades gave an abundant production of works on this subject. First there was the mathematical formulation of super-fluids by L.D. Landau [11] with the definition of an order parameter; from there Bogoliubov [12] developed a mathematical framework to describe excitation in an interacting Bose-Einstein gas. Historically the first super-fluid has been the achieved with $^4$He, but it does not show the BEC transition due to strong interaction between atom. First attempts to reach the BEC phase were made using dilute atomic clouds, but cooling techniques did not allow reaching low enough temperatures. Nevertheless in 1995 [13] by employing new laser cooling and trapping techniques (Magneto-Optical Trap (MOT)), 70 years after its prediction and in a different physical system, Bose-Einstein condensation of a gas of Rubidium atoms was achieved. More recently the condensation of photons, exactly as predicted in the original works, has been achieved as well [14] by means of a dye which is able to create an effective chemical potential and thus allowing for the conservation of the mean number of photons. In the reminder of the chapter we shall first give a brief theoretical description of Bose Einstein condensation and focus on the equations for a multimode BEC that will be useful throughout the thesis. We will briefly talk about the experimental techniques that allow the achievement of alkali BECs.

## 1.2 Theoretical background

### 1.2.1 Gross-Pitaevskii equation

We start from a microscopic description of Bose Einstein condensation and show how the BEC "emerges" from a theoretical point of view. Let us consider a gas of $N$ atoms of mass $m$ trapped in a potential $V_\lambda(\mathbf{x}, \mathbf{t})$ where $\mathbf{x}$ is the position of the atom and $\lambda$ is a multi-index that labels the internal degrees of freedom. It is in fact possible to "tailor" potential for atoms depending on their hyperfine state as shown in Sec. 1.3. This technique is used for instance in the so-called optical super-lattices where atoms can be displaced according to their internal states. We assume atoms have integer spin so that, by the spin-statistic theorem, they are bosons.

Let us introduce an important quantity: the two point spatial correlation function, also called the single particle density matrix,

$$n_\lambda(\mathbf{x},\mathbf{y}) = \langle \hat{\Psi}^\dagger_\lambda(\mathbf{x})\hat{\Psi}_\lambda(\mathbf{y})\rangle, \tag{1.1}$$

and where the average is meant to be taken with the help of the many-body density operator. The single particle operator $\hat{\Psi}_\lambda(\mathbf{x})$ is such that $\hat{\Psi}_\lambda(\mathbf{x})|0\rangle = 0$ where $|0\rangle$ is the vacuum state, *i.e.* no atoms. We can diagonalize the correlation function such that

$$n_\lambda(\mathbf{x},\mathbf{y}) = \sum_i n_i^\lambda (\phi_i^\lambda(\mathbf{x}))^* \phi_i^\lambda(\mathbf{y}), \tag{1.2}$$

where the $\{\phi_{i(\lambda)}(\mathbf{x})\}$ are given such that

$$\int_{\mathcal{V}} d\mathbf{y}\; n_\lambda(\mathbf{x},\mathbf{y})\phi_i^\lambda(\mathbf{y}) = n_i^\lambda\; \phi_i^\lambda(\mathbf{x}), \tag{1.3}$$

where the integral is over the volume $\mathcal{V}$ occupied by the gas of bosons. Since the relation $n_\lambda(\mathbf{x},\mathbf{y}) = (n_\lambda(\mathbf{y},\mathbf{x}))^*$ holds the eigenvalues $n_i$ are real. Moreover, as we will see below, they are the eigenvalues of the number operator in second quantization and their value is thus bounded from below by zero. We then interpret these eigenvalues as the population of the corresponding modes. The correlation function plays an important role from a theoretical point of view since through it we can properly define the BEC phase as we shall see. The transition to the Bose Einstein condensate phase occurs when a macroscopic number of particles (bosons) are in the same quantum state. Assuming the bosons are at equilibrium, they follow the Bose-Einstein distribution

$$f(\epsilon) = \frac{1}{e^{\beta(\epsilon-\mu)} - 1}, \tag{1.4}$$

where $\beta^{-1} = k_B T$, $k_B$ is the Boltzman constant and $\mu$ is the chemical potential that fixes the average number of particles at equilibrium. The function $f(\epsilon)$ gives the number of particles having energy $\epsilon$ at equilibrium at temperature $T$. The total number of particles can then be written as

$$N = N_0 + \Delta N = f(\epsilon_0) + \sum_{\epsilon > \epsilon_0} f(\epsilon), \tag{1.5}$$

where $\epsilon_0$ is the lowest energy of the system. At low temperature there is a non vanishing probability of finding particles only at energies such that $\beta(\epsilon - \mu) \ll 1$, in the limit

$T \to 0$ all the particles end up in the ground state at energy $\epsilon_0$. In order to give a precise mathematical definition we would need deeper thermodynamical arguments that we shall skip here but a complete discussion can be found in ref. [17]. Here we are interested in the fact that there exist a critical temperature ($T_c$) such that (for $T < T_c$)

$$\frac{N_0}{N} = 1 - \left(\frac{T}{T_c}\right)^{\frac{3}{2}}. \tag{1.6}$$

Whenever a macroscopic number of particles $N_0^\lambda$ occupy the same single particle state $\phi_0^\lambda(\mathbf{x})$ then we speak about Bose Einstein condensation in the 0-th "mode". The function $\phi_0^\lambda(\mathbf{x})$ is often called an "order parameter" having in mind that the appearance of BEC is a phase transition in the sense of Landau's theory. It is worth noticing that with the above definition we allow for the so called multimode BECs. A multimode BEC is a system of different, and possibly mutually interacting, BECs which will be labeled with different multi-indices $\lambda$. Since the index $\lambda$ often runs over the spin degrees of freedom of particles the collection of field operators $\hat{\mathbf{\Psi}}(\mathbf{x}) = \{\hat{\Psi}_\lambda(\mathbf{x})\}$ is often referred to as "spinor". We shall use such a system in Chapter 3 and Chapter 4.

The basis of the mathematical description of BEC phenomenon is the following. Let us assume that there exist a set of multi-indices $\{\lambda_i\}$ for which we have condensation of particles in those modes as the temperature of the systems drops below a certain critical temperature $T_c$. We expand the field operator with multi-index $\lambda \in \{\lambda_i\}$ as

$$\hat{\Psi}_\lambda(\mathbf{x}) = \phi_{0,\lambda}(\mathbf{x})\hat{a}_{0,\lambda} + \sum_{i\neq 0} \phi_{i,\lambda}(\mathbf{x})\hat{a}_{i,\lambda}. \tag{1.7}$$

The operators $\{\hat{a}_{i,\lambda}\}$ are bosonic operators obeying the commutation relations $[\hat{a}_{i,\mu}, \hat{a}^\dagger_{j,\nu}] = \delta_{i,j}\delta_{\nu,\mu}$. As the phase transition to BEC phase occurs ($T = T_c$) a macroscopic number of atoms ends up in mode $\phi_{0,\lambda}(\mathbf{x})$ *i.e.* $O(N_{0,\lambda}/N) \approx 1$, as it can be seen from equation 1.6. We have

$$[\hat{a}_{0,\lambda}, \hat{a}^\dagger_{0,\lambda}]|GS\rangle = (\sqrt{N_{0,\lambda}}\sqrt{(N_{0,\lambda}+1)} - N_{0,\lambda})|GS\rangle, \tag{1.8}$$

where $|GS\rangle$ is the ground state of the system. Since $N_{0,\lambda} \gg 1$ we have $N_{0,\lambda} + 1 \approx N_{0,\lambda}$. Physically this approximation means that it makes no difference if one boson is removed from the condensed part because there is a macroscopic number of them in mode $\phi_0^\lambda(\mathbf{x})$. Most importantly it implies that the operators for the condensate modes can be treated as c-numbers and since $\hat{a}^\dagger_{0,\lambda}\hat{a}_{0,\lambda} = N_{0,\lambda}$ we set $\hat{a}^\dagger_{0,\lambda} \approx \hat{a}_{0,\lambda} = \sqrt{N_{0,\lambda}}$. This is known as Bogoliubov approximation.

Let us now assume that particles mutually interact and that this interaction can be expressed through the potential $U_{\lambda,\lambda'}(|\mathbf{x}-\mathbf{y}|)$. The fact that the potential does depend

on the relative position of the two particles matches the requirement that their center of mass motion is constant if no external forces are applied. It is worth noticing that the potential has been labeled by the internal degrees of freedom of the two atoms. This is not at all surprising; for instance the interaction between two atoms does depend on their spin and/or on their electron configuration.

The total Hamiltonian of the system can then be written as:

$$\begin{aligned}\hat{H} =& \sum_{i,\lambda} \int_{\mathcal{V}_\lambda} d\mathbf{x}\ \hat{\Psi}^\dagger_{i,\lambda}(\mathbf{x}) \frac{\hat{\mathbf{p}}2}{2m} \hat{\Psi}_{i,\lambda}(\mathbf{x}) + \sum_{i,\lambda} \int_{\mathcal{V}_\lambda} d\mathbf{x}\ V_\lambda(\mathbf{x},t) \hat{\Psi}^\dagger_{i,\lambda}(\mathbf{x}) \hat{\Psi}_{i,\lambda}(\mathbf{x}) \\ &+ \sum_{i,j>i} \sum_{\lambda,\lambda'} \int_{\mathcal{V}_\lambda} \int_{\mathcal{V}_{\lambda'}} d\mathbf{x} d\mathbf{y}\ \hat{\Psi}^\dagger_{i,\lambda}(\mathbf{x}) \hat{\Psi}^\dagger_{j,\lambda'}(\mathbf{y}) U_{\lambda,\lambda'}(|\mathbf{x}-\mathbf{y}|) \hat{\Psi}_{i,\lambda}(\mathbf{x}) \hat{\Psi}_{j,\lambda'}(\mathbf{y}).\end{aligned} \tag{1.9}$$

The first term is the kinetic energy operator, the second the potential one and the third is the atom-atom interaction energy operator. Let us now focus on the inter-atomic scattering potential $U_{\lambda,\lambda'}(|\mathbf{x}-\mathbf{y}|)$. Regardless of its details it can be thought of as to be made up of two contributions: a short range and a long range one. The first one is usually a strong repulsive potential whereas the second one is a smooth attractive potential that vanishes at infinity. The prototype for such potentials is the Lennard-Jones potential which describes the interaction between neutral atoms or molecules well.

This term in the Hamiltonian can be very difficult to deal with and a partial waves expansion is commonly used to simplify it. First the center of mass motion is separated from the relative motion of the two atoms since the potential only depends upon the relative distance. We are thus left facing the problem of one body moving in a potential $U(r)$, where $r = |\mathbf{x}-\mathbf{y}|$ is the modulus of the relative distance. Since the potential is a central one the total angular momentum is conserved and thus it is convenient to write wave function for the relative motion near the contact point ($r \to 0$) as:

$$\psi(z,r,\theta) = e^{\imath kz} + f(\theta)\frac{e^{\imath kr}}{r}. \tag{1.10}$$

The function $f(\theta) = \sum_l f_l P_l(\cos(\theta))$ can be written in terms of Legendre polynomials. It is further assumed that scattering off this potential has no effect at large distances apart from a phase shift. The two solutions then have to match. By assuming that the de Broglie-wavelength of the incoming particle is small compared to the typical length scale over which the trapping varies it is possible to retain only terms with $l = 0$ and this approximation is then called s-wave approximation because of the spherical symmetry of the l=0 terms.

In this approximation the interaction energy can be written as $U_{\lambda,\lambda'}(|\mathbf{x}-\mathbf{y}|) = g_{\lambda,\lambda'}\delta(|\mathbf{x}-\mathbf{y}|)$ where $g_{\lambda,\lambda'} = 4\pi\hbar^2 a_{\lambda,\lambda'}/m$. The coefficient $a_{\lambda,\lambda'}$ is the so-called scattering length and contains all the information about the (short range) scattering process between two particles in the state $\lambda$ and $\lambda'$ respectively.

In what follows we assume that even in the presence of multiple components the BEC phase exist [15]. Moreover we restrict our discussions to the case of complete Bose Einstein condensation, which means that no particles are found in any of the modes $\phi_i^\lambda(\mathbf{x})$ with $i \neq 0$ and which corresponds to $T \ll T_c$. In this case the treatment is simplified since everything is reduced to the dynamics of classical fields. With the above assumptions and by means of the Bogoliubov approximation the Hamiltonian becomes:

$$\begin{aligned}\hat{H} = \mathcal{H}[\phi,\phi^*] =& \sum_\lambda N_{0,\lambda} \int_{\mathcal{V}} d\mathbf{x}\ (\phi_{0,\lambda}(\mathbf{x}))^* \frac{\hat{\mathbf{p}}2}{2m}\phi_{0,\lambda}(\mathbf{x}) \\ &+ \sum_\lambda N_{0,\lambda} \int_{\mathcal{V}} d\mathbf{x}\ |\phi_{0,\lambda}(\mathbf{x})|^2 V_\alpha(\mathbf{x},t) \\ &+ \sum_{\lambda,\lambda'} N_\lambda N_{\lambda'} g_{\lambda,\lambda'} \int_{\mathcal{V}} d\mathbf{x}\ |\phi_{0,\lambda}(\mathbf{x})|^2 |\phi_{0,\lambda'}(\mathbf{x})|^2.\end{aligned} \tag{1.11}$$

The fields $\phi_{0,\lambda}(\mathbf{x})$ and their complex conjugates can be regarded as pairs of canonically conjugate variables. In this spirit one can define the action

$$S[\Phi,\Phi^*] = \int dt \int \Pi_\lambda D[\Phi_\lambda] D[\Phi_\lambda^*] \sum_\lambda (\Phi_{0,\lambda}(\mathbf{x}))^* \imath \frac{\partial}{\partial t}\Phi_{0,\lambda}(\mathbf{x}) - \mathcal{H}[\Phi,\Phi^*], \tag{1.12}$$

where $\Phi_{0,\lambda}(\mathbf{x}) = \sqrt{N_{0,\lambda}}\phi_{0,\lambda}(\mathbf{x})$. In this way it is possible to derive the equation of motion for the fields by means of the least action principle $\delta S = 0$:

$$\frac{\partial S[\Phi,\Phi^*]}{\partial \Phi_{0,\lambda}(\mathbf{x})} = 0, \qquad \frac{\partial S[\Phi,\Phi^*]}{\partial (\Phi_{0,\lambda}(\mathbf{x}))^*} = 0. \tag{1.13}$$

We thus obtain a set of the so-called Gross-Pitaevskii equations:

$$\begin{aligned}\frac{\partial}{\partial t}\Phi_{0,\lambda}(\mathbf{x}) =& \frac{\hat{\mathbf{p}}2}{2m}\Phi_{0,\lambda}(\mathbf{x}) + V_\lambda(\mathbf{x},t)\ \Phi_{0,\lambda}(\mathbf{x}) \\ &+ 2g_{\lambda,\lambda}\ |\Phi_{0,\lambda}(\mathbf{x})|^2 \Phi_{0,\lambda}(\mathbf{x}) + \sum_{\lambda\neq\lambda'} g_{\lambda,\lambda'}\ |\Phi_{0,\lambda'}(\mathbf{x})|^2 \Phi_{0,\lambda}(\mathbf{x}).\end{aligned} \tag{1.14}$$

These are also often called non-linear Schhödinger equations because of the presence of an atom-atom interaction term that is cubic in the field variables. The solution of this equation is a quite difficult task and numerical simulations are the most common

tools used to tackle this problem in both the static (ground state) and the dynamical case [16]. Nevertheless a very useful approximation is the Thomas-Fermi one, which allows for an analytical treatment of strongly interacting BEC. This approximation amounts to neglect the kinetic term in the GP equation in favor of the trapping and the atom-atom interaction energies [17].

### 1.2.2 Quantum vortices

An interesting feature of BEC is super-fluidity: frictionless motion of an impurity (*i.e.* any particle that does not belong to the BEC) through the fluid as long as its velocity is smaller than a threshold value. It was first discovered and studied in $^4$He. Although the description of the super-fluid part of liquid $^4$He was satisfactorily achieved by means of the GP equation, the latter was not enough to give a good description of the full system. The description of super-fluid Helium required special attention because together with super-fluid part there always is a normal component (*i.e.* non super-fluid) and thus so called two-fluids model was recognized to be more appropriate. On the other hand BEC of ultra-cold alkali gas is a purer system: the non-condensate fraction can be kept small for the whole duration of the experiment. In this sense the GP equation describes BEC of alkali gas better than super-fluid $^4$He.

A clear signature of super-fluidity in liquids BECs is the occurrence of vortex-like excitations. A vortex is a collective motion of particles of a liquid that undergo a rotation around a common center.

It is advantageous talking about vortices to make use of the Madelung representation [17] for the order parameter (in what follows we consider a one component BEC so we drop the label $\lambda$): $\phi_0(\mathbf{x}) = \sqrt{n(\mathbf{x},\mathbf{t})}e^{\imath S(\mathbf{x},\mathbf{t})}$ where $n(\mathbf{x})$ is the density of the gas and $S(\mathbf{x},\mathbf{t})$ its phase.

By inserting this expression into the GP equation it is possible to obtain the so-called hydrodynamic equations for the BEC:

$$\begin{aligned}
&\frac{\partial}{\partial t}n(\mathbf{x},\mathbf{t}) + \nabla\left(n(\mathbf{x},\mathbf{t})\ \mathbf{v}(\mathbf{x},\mathbf{t})\right) = 0 \\
&m\frac{\partial}{\partial t}n(\mathbf{x},\mathbf{t}) + \nabla\left(-\frac{\hbar^2}{2m\sqrt{n(\mathbf{x},\mathbf{t})}}\nabla^2\sqrt{n(\mathbf{x},\mathbf{t})} + m\frac{|\mathbf{v}(\mathbf{x},\mathbf{t})|^2}{2} + V(\mathbf{x},\mathbf{t}) + g\ n(\mathbf{x},\mathbf{t})\right) = 0,
\end{aligned} \tag{1.15}$$

where we have defined the velocity of the fluid as

$$\mathbf{v}(\mathbf{x},\mathbf{t}) = \frac{\hbar}{m}\nabla S(\mathbf{x},\mathbf{t}). \tag{1.16}$$

The first of the above equations is simply the continuity equation and it is equivalent to the conservation of probability density of the single particle wave-function $\phi_0(\mathbf{x})$. The second is similar to the Navier-Stokes (NS) equation with the exception of the term containing $\hbar$. This term is called "quantum pressure" since it vanishes in the limit $\hbar \to 0$ and it would play the role of a non homogeneous pressure term in the NS equation.

In this representation it is easier to see that the motion of a BEC has to be irrotational, *i.e.* $\nabla \times \mathbf{v}(\mathbf{x},\mathbf{t}) = 0$, since the velocity is the gradient of a scalar function. Vortices in super-fluids then should not exist because of irrotationality. The only way to save irrotationality of motion and have a vortex at a point $\mathbf{x}_v$, is to have $n(\mathbf{x_v},\mathbf{t}) \to 0$ as $\mathbf{x} \to \mathbf{x}_v$. The vortex will then be outside the system but there will still be clear signature of it that can be translated in mathematical formalism as

$$\int_{\mathcal{C}(\mathbf{x}_v)} \mathbf{v}(\mathbf{x},\mathbf{t}) \cdot d\hat{\mathbf{l}} = n\frac{2\pi\hbar}{m}, \tag{1.17}$$

where $\mathcal{C}(\mathbf{x}_v)$ is any closed path around the point $\mathbf{x}_v$, $d\hat{\mathbf{l}}$ is the infinitesimal tangent vector at the contour at point $\mathbf{x}$ and $n$ is the so called winding number. A vortex is then a singularity in the order parameter, *i.e.* a "tunnel" through the density of the BEC. A similar phenomenon is observed in superconductors of the second type whose properties rely on super-fluidity even though the exact microscopic mechanism is not clear yet. There the system tries to "expel" the magnetic field from the bulk but in some cases (above a threshold value for the external magnetic field) this would require too much energy and hence it prefers to create holes of normal electrons in the bulk of the super-fluid [18]. This similarity offers another good reason to study vortices in ultra-cold gases setups.

We said that vortices are excitations of the BEC; actually they are particular excitations often called topological or homomorphic excitations. These terms comes from the particular shape of the BEC containing vortices: a BEC without vortices cannot be continuously deformed into a BEC with one vortex as a sphere can not be continuously deformed into a torus: they have different topology. We have to introduce a "cut", a shocking event in order to create or destroy a vortex in a BEC and there is an energy gap we have to overcome.

The production of vortices is also interesting from an experimental point of view where an atomic cloud must be set in rotation. The first experiments on liquid $^4$He resembled the

idea for producing vortices in a normal liquid: the rotating bucket. The experimentalists did actually set the bucket in rotation until the vortices appeared. In the classical case the explanation relies on the laminar flow of the liquid and this is what gives rise to the typical $r^{-2}$ dependence of the velocity field. By rotating the bucket we are transferring angular momentum to the whole system through the rotating walls. In the case of liquid $^4$He the situation is a bit different. By rotating the container the experimentalists transferred (through friction) angular momentum to the normal component of the fluid. This normal fluid, interacting with the super-fluid component, transferred angular momentum to it by exciting particular modes. For a super-fluid at this point there are two possible scenarios: either it disappears because of perturbations coming from normal components or it has to "store" this excess of angular momentum somewhere. In the latter case vortices start appearing to store this angular momentum exactly as in the case of a superconductor where in order to deal with the extra flux coming from the external magnetic field the superconducting fluids creates vortices to store it; from here the term fluxons originates.

States with vortices are thus states with non-vanishing angular momentum that in the stationary case has to be conserved on average. We have thus to add this constraint in the minimization of the action [19] exactly as we would do for the average number of particles. This addition is possible by means of a set of three Lagrange multipliers which we will write in vector form as $\mathbf{\Omega}$ and we have to add a term

$$\mathbf{\Omega} \cdot < \hat{\mathbf{L}} > \tag{1.18}$$

to the action.

With this constraint the GP equation for a one mode BEC reads:

$$\frac{\partial}{\partial t}\Phi_0(\mathbf{x}) = \frac{\hat{\mathbf{p}}2}{2m}\Phi_0(\mathbf{x}) + V(\mathbf{x},t)\Phi_0(\mathbf{x}) + 2g\,|\Phi_0(\mathbf{x})|^2\Phi_0(\mathbf{x}) - \mathbf{\Omega}\cdot\hat{\mathbf{L}}\Phi_0(\mathbf{x}). \tag{1.19}$$

For the case of harmonic trapping potential with cylindrical symmetry the stationary states of the above equation for high values of the "angular velocity" $\mathbf{\Omega}$ include vortex lattices. They have been first observed in an experiment at MIT [20] with over 100 vortices. This shows another feature of vortices in super-fluids; vortex lattices formed by many vortices with winding number $n = 1$ are energetically more stable than few vortices with large winding numbers. This comes from the study of local minima of the energy functional in Eq. (1.11). Numerical solutions [21] show that even though a wave function with a vortex with winding number $n > 1$ is a local minimum of the energy functional

it is not a global one. It means that this particular solution is (thermodynamically) unstable and that it would rapidly decay into $n$ vortices with winding number one.

## 1.3 Atom Cooling and Trapping

In this section we briefly review some experimental techniques used to trap and cool alkali atoms. We shall not go deep into details since this overview is only meant to give few notions as a support for the remainder of the thesis. For the interested reader, a more complete exposition on this subject can be found in ref. [22].

Both trapping and cooling are achieved by exploiting the scattering force exerted by a laser beam scattering off the atoms. Cooling of an atomic cloud is achieved combining different techniques, each of which has some limitations. Trapping techniques can be categorized as optical or magnetic. Optical techniques induce a dipole moment on atoms to create a non zero force. Magnetic ones exploit the Zeeman splitting of energy levels to create an inhomogeneous potential for specific hyperfine levels. By combining these two techniques is possible to create a so called *Magneto-Optical Trap (MOT)* that is nowadays the most used setup in the first stages of the trapping and cooling process towards the realization of BECs.

### 1.3.1 Cooling techniques

There are different cooling techniques, each one with its own advantages and disadvantage, but all of them are based on the same physical effect: momentum recoil. The idea is to use the scattering of photons off atoms to apply a force that slows them down. Even though this process is observable in a classical setting (*e.g.* force exerted on small dielectric spheres) in the case of atoms quantum mechanics plays a fundamental role.

The underlying idea is to illuminate an atomic beam with a laser field which is counter propagating with respect to the atoms' average velocity. By properly adjusting the detuning of the laser field to account for the Doppler shift, the atoms will absorb the photons in the laser beam. Due to the conservation of momentum the atoms will also receive a recoil in the opposite direction with respects to their motion which slows them down.

Nevertheless the atom will spontaneously emit a photon in a time interval approximately equal to the lifetime of the excited level it was scattered into by the laser beam. Since spontaneous emission is equally probable for all spatial directions the net recoil for the second emission averages to zero. Moreover, unlike in the classical case, the cross section

of an atom is not its physical cross section, *i.e.* the area of the object exposed to the laser beam, which would be really small for an atom. It is actually the absorption cross section at the resonant frequency of the atom, which is bigger than the physical one.

The absorption cross section at resonance is given by taking into account absorption and stimulated emission of atoms interacting with a monochromatic wave at frequency $\omega_0$ and can be shown to be [22]:

$$\sigma(\omega_0) = \frac{3}{2\pi}\lambda_0^2, \tag{1.20}$$

where $\lambda_0^2 = 2\pi c/\omega_0$ and $c$ is the speed of light in vacuum. Considering the transition at $\lambda_0 = 589nm$ for a sodium atom one finds $\sigma(\omega_0) \approx 2 \times 10^{-13}m^2$ which is orders of magnitude bigger than the kinetic cross section given by the area of the atom $\pi d^2 = 3 \times 10^{-18}m^2$ where $d$ is the sodium radius.

In this approach as the velocity of the atoms changes the laser beam goes off resonant with the atomic transition and thus the absorption cross section diminishes. To overcome this problem different solutions have been proposed and they led to the Nobel Prize that has been award in 1997 to Steven Chu [23], William Phillips [24] and Claude Cohen-Tannoudji [25]. The first two proposed solutions that required an adjustment of the set-up parameters to follow the velocity change. Cohen-Tannoudji proposed a new method to "select" the coldest atoms by transferring them into a dark state. This is the so-called velocity selective coherent population transfer.

Moreover an intrinsic problem of Doppler shift based techniques is that there exist a lower limit to the final momentum of the atoms given by the recoil momentum. Because of the spontaneous emission the atom will always have at least a momentum equal (in modulus) to that of the emitted photon.

### 1.3.2 Zeeman slowing and chirping

The change of the absorption cross section of the atoms as the velocity, and thus the detuning due to Doppler shift changes, can be compensated for by properly adjusting the system parameters. One method is to let the atoms go through a region with a inhomogeous magnetic field. The magnetic field profile is such that the condition $\hbar\omega_0 + \mu_B B(z) = \hbar\omega + \hbar kv$ holds true. Here $\hbar\omega_0$ is the energy difference between the two chosen levels, $\omega$ and $k$ are the laser frequency and wavenumber and $v$ is the atom velocity. Here we have assumed cooling of the atoms along the z direction. This technique exploits the Zeeman shift of atoms in magnetic field to compensate for the change in their velocity due to cooling.

A different technique is the so-called "chirping" method. It amounts to a time variation of the frequency of the cooling laser in order to keep it on resonance with the atomic transition. Since the frequency range to be spanned is usually quite large and the time interval quite short it reminds of the bird-song; from here the name of chirp cooling.

Both these techniques are limited in the lowest velocity achievable by the Doppler limit. This is due to fluctuations in the force of photons on the atoms. This is a purely statistical effect and comes form the mismatch of absorption and spontaneous emission times. The velocity of atoms undergoes a random walk due to the average of these fluctuations and this results in the impossibility of cooling down atoms below a certain threshold temperature: the Doppler temperature $T_D$. The latter is calculated by means of the equipartition theorem as (in one direction):

$$\frac{1}{2}k_B T_D = \frac{1}{2}m\langle v_z^2\rangle, \tag{1.21}$$

where $\langle v_z^2\rangle$ is the average of the square of the recoil velocity in the $z-$ direction as given from the absorption and spontaneous emission of photons. In the case of two level atom the velocity recoil can be expressed in terms of the decay rate from the excited level such that the Doppler temperature reads:

$$\frac{1}{2}k_B T_D = \frac{\hbar}{2}\Gamma. \tag{1.22}$$

This is intuitively what we would expect from quantum mechanics using the relation $\Delta E \Delta t \geq \frac{\hbar}{2}$. The typical time scale error is given by the uncertainty on when the atom will decay and it is given by $\tau = \Gamma^{-1}$, which sets the uncertainty on the energy of the system, *i.e.* $\Delta E \geq \frac{\hbar}{2}\Gamma$.

Special techniques are needed to obtain sub-Doppler cooling. One of this techniques, the so called Sisyphus cooling, relies on the creation of atomic angular momentum dependent energy landscapes to convert kinetic energy into potential energy which is then dissipated by means of spontaneous decay.

### 1.3.3 Optical trapping

An atom under the influence of an external electric field acquires (if it does not already have one) an electric dipole that in turn allows the atom to interact with the electromagnetic field.

This interaction gives rise to a change in energy that in the semiclassical case is given by:

$$V(\mathbf{r},t) = -\hat{\mathbf{d}} \cdot \mathbf{E}(\mathbf{r},t), \tag{1.23}$$

where $\hat{\mathbf{d}}$ is dipole moment operator of the atom and $\mathbf{E}(\mathbf{r},t)$ is the external electric field. Here we are assuming an intense laser beam so that it is well described by the classical field $\mathbf{E}(\mathbf{r},t)$ whereas the atom has to be considered a quantum system.

It is also assumed that the time variation of the electric field is much faster than the typical (unperturbed) time scale of the atom's internal dynamics as given by $\hbar\omega_{0,1} = \epsilon_1 - \epsilon_0$ where $\epsilon_0 < \epsilon_1$ are the energies of the two states involved. In the case of an off-resonant laser beam the above interaction produces a shift in the energy, the Stark shift. By means of time independent perturbation theory this contribution can be evaluated to be [17]

$$U(\mathbf{r}) = -\frac{1}{2}\alpha(\omega)\overline{|\mathbf{E}(\mathbf{r},t)|^2}, \tag{1.24}$$

which is an effective potential acting on the atoms. Here we have assumed that the laser is monochromatic with frequency $\omega$ and $\alpha(\omega)$ is the second order contribution to the dipole moment. The time average is performed in the spirit that the field dynamics occurs on time scales much shorter than the atomic ones.

Because of the spatial dependence of the electric field the effective potential $U(\mathbf{r})$ generates a force

$$F(\mathbf{r}) = \frac{1}{2}\alpha(\omega)\nabla\overline{|\mathbf{E}(\mathbf{r},t)|^2}, \tag{1.25}$$

This force is at the basis of the so called optical tweezers. The type of force depends upon the sign of the coefficient $\alpha(\omega)$: when positive the force is repulsive (with respect to the maximum of the field), whereas when negative the force is attractive. The coefficient $\alpha(\omega)$ can be evaluated from perturbation theory and it reads

$$\alpha(\omega) = \frac{|D|^2}{\hbar}\frac{1}{\omega - \omega_{0,1}}, \tag{1.26}$$

where $D = \langle 1|\hat{\mathbf{d}} \cdot \boldsymbol{\epsilon}|0\rangle$ with $\hat{\mathbf{d}}$ and $\boldsymbol{\epsilon}$ being the dipole moment of the atom and the polarization vector of the light field respectively. In this case the sign of $\alpha(\omega)$ depends

upon the detuning detuning $\delta = \omega_L - \omega_{0,1}$ of the laser fields with respect to the atomic transition and the two cases are also referred to as blue ($\delta > 0$) and red detuned ($\delta < 0$), respectively.

This technique is nowadays exploited for the creation of optical lattices and superlattices that allow for the creation of a clean and controllable setup for the simulation of many-body physics with ultra-cold atoms [26]. These techniques use the possibility of addressing different internal transition of the atoms therefore creating different potentials.

Optical trapping potentials are advantageous in being spin independent; in such a way all atoms of a particular species are trapped regardless of their spin. Electric fields are easier to be "tailored" due to the high level of precision available when manipulating laser fields so that different shapes of traps can be created. In recent years the improvement of the so called spacial light modulators (SLM) promises that in the near future it will be possible to create optical field with any kind of shape and time dependence [27].

Moreover since the trapping does not depend on the spin, and therfore is "magnetically independent", the optical trapping offers the possibility of the addition of external magnetic fields that are used to tune the atom-atom interaction potential via so called Fano-Feshbach resonances [28].

### 1.3.4 Magnetic trapping

A different way of trapping atoms is the possibility of exploiting their magnetic properties. Alkali atoms in particular posses a non-zero spin angular momentum which is given by the sum of the nuclear and electronic spin angular momenta.

As an atom is placed in a region with non-vanishing magnetic field its energy level structure changes due to the Zeeman effect. The energy levels become spin-dependent and they can be grouped in high and low field "seekers" depending on their attitude to minimize their energies in high or low magnetic field regions respectively.

In particular for not too strong fields it can be shown that the energy of an atom in a hyperfine state with total spin $F$ is given by [29]

$$E(B) = \pm \left( E_0 + \frac{1}{2} |\mu_B| m_F B \right), \tag{1.27}$$

where $E_0$ is the energy in the vanishing field $\mu_B$ is the Bohr magneton and $m_F$ is the component of the spin along the magnetic field.

Trapping of the atoms is then achieved by means of a bias field responsible for the Zeeman effect and an inhomogeneous magnetic field $\mathbf{B}(\mathbf{r})$. Since the energy depends on the magnetic field the low(high)-field-seeking states will be driven towards regions with low (high) magnetic field. By properly tailoring the inhomogeneous magnetic field is thus possible to trap the atoms in a localised region. Moreover because of the dependence of the energy on the internal spin it is possible to separate atoms with different spins.

There is another issue to take into account: the Majorana losses. In his seminal paper [30] Majorana showed how the interaction of an atom with an inhomogeneous magnetic field leads to a sudden flip of the atomic spin. This is due to the fact that an inhomogeneous static field as seen from the center of mass of the atom (which is the carrier of the spin) turns out to be a time dependent field. The effect is particularly important if the magnetic field vanishes; in this case the quantization axis is "lost" and as soon as the field goes back to non-zero values the spin direction can be arbitrary. This phenomenon is responsible for losses from the (trapped) low field seekers which undergo a transition to become (untrapped) high field seekers.

There are mainly two setups which avoid Majorana losses: "time-orbiting potentials" and the Ioffe-Pritchard traps. The first method employs a time dependent magnetic field that compensates the change in the magnetic field as seen from the reference frame of the atom. The Ioffe-Pitchard trap solves the problem at the origin: it creates a region where the magnetic field is never zero and it has a harmonic shape.

The Magnetic traps have been used from the early stages of the ultra cold quantum gas era and they have been employed for the realization of the first BEC.

Ioffe-Pitchard traps have some disadvantages: the coils needed to create the magnetic field have to be placed outside the vacuum chamber because of their dimension and this makes the whole apparatus not scalable. Moreover, since the trapping is magnetic in nature, atoms with different component of the spin along the quantization axis will be spatially separated.

On the other hand in recent years a new technology is at our disposal: the atom chips. This are silicon wafers on which it is possible to draw gold wires using lithographic techniques. Current passing to the wires creates a magnetic field right above the chip surface and by adding an external applied bias field it is possible to trap atoms. Different patterns give different magnetic field configurations and thus different trapping potentials. It is possible to have time dependent potential as well in order to be able to transport the atoms. These chips are promising tools, since they make it possible to have a pocket sized lab for ultra-cold atoms and a more stable and controllable setup.

Moreover smaller scales need only smaller currents in order to create the desired trapping thus giving a clear experimental advantage.

# Chapter 2

# Structural change of vortex patterns in 2D BEC

In this chapter we present an analysis of the stability of vortex patterns in 2D BECs as the anisotropy of the trapping potential varies. We shall first show that for a fixed number of vortices there are different geometries of vortex patterns. This result is in agreement with analytical [31] and numerical [32] findings. Nevertheless the patterns are not stable as shown by the analysis of the patterns' modes based on an hydrodynamical approach. This analysis also reveals that the change from different vortex patterns geometries occurs in a discontinuous fashion as the anisotropy varies.

## 2.1 Introduction

Creation of vortices in alkali BECs can be achieved via different methods such as optical phase imprinting techniques [33] or stirring laser fields that allow to excite quadrupole-mode resonances [34]. The study of quantum vortices can also help in understanding related physical phenomena such as the quantum Hall effect [35] and high $T_c$ superconductivity [18]. For this reason from the very beginning the problem of a large number of vortices has been considered. Works on this subject gave us fundamental contribution for the understanding of the properties of vortex lattices. We know that in the limit of a large number of vortices they tend to occupy the sites of the so-called Abrikosov lattice, *i.e.* an hexagonal lattice.

Moreover a seminal work by Tkachenkco[48] shed light on the collective excitation of this lattice. Although these works have been done with superfluid $^4$He in mind, it is useful to recall that their results hold for any superfluid and thus they are applicable to

superconductors as well as to the most recent BECs of excitons [36]. It is thus useful to extend these studies to the case of a small number of vortices to better understand the dynamical properties as well as the possibility to control the dynamics. In the case of ultra-cold atoms it is possible to perturb (and possibly to control) vortex dynamics by acting on the trapping potential, on the scattering properties or adding other species to pin the vortices and drive them.

Here we are interested in the study of the equilibrium properties of vortex patterns in (quasi-) 2D BECs. Numerical evidence has been provided that the vortex pattern of a 2D BEC in an in-plane anisotropic rotating trap can undergo structural changes as a function of the trap anisotropy, *i.e. the ratio between the trapping frequencies in the two directions*. Specifically, in Ref. [32] it has been shown that, for modest changes in the anisotropy, an *off-line* configuration (typical for an Abrikosov lattice) can change into a linear one. While this bears analogies with the case of ionic crystals [37], the characterization of structural changes in anisotropic and rotating BECs remains largely unexplored. Most of the existing literature focuses on the limit of large numbers of vortices for either a symmetric trap [38, 39] or very high angular frequencies, which leads to stripe-shaped vortex patterns [40]. Although the case of medium vorticity has been addressed, the role of external forcing on the dynamics of the vortex structures still awaits a systematic approach [41, 42]. Yet, understanding how vortices behave under external perturbations is a pre-requisite for harnessing the quantum properties of vortex patterns. Yet, in light of the surge of a very broad interest in low-dimensional interacting quantum systems, the study of such structural changes is key both under a statistical mechanics viewpoint and for tasks of understanding coherent many particle quantum dynamics.

Here we present a significant contribution to advance these aims by studying the behavior of finite-sized vortex patterns in 2D BECs confined within a rotating anisotropic trap. In particular we investigate in detail the effects of the eccentricity on the spatial distribution of the vortices. By minimizing the eccentricity-dependent interaction potential between vortices, we show that the vortex configuration undergoes structural changes as the eccentricity parameter is varied. A hydrodynamical approach to the description of the superfluid motion allows us to identify the eigenmodes of the vortex-patterns and connect the appearance of discontinuities with the transition points between different structures. In fact, the modes suggest that the change in the equilibrium positions of the vortices is due to the re-arrangement of the superfluid velocity field.

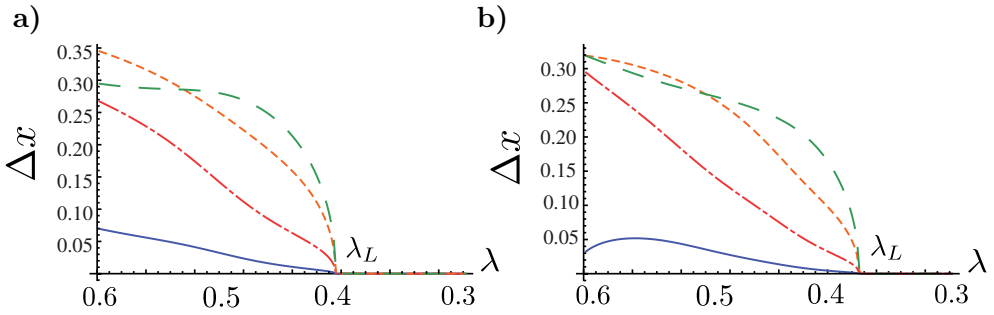



FIGURE 2.1: Distance $\Delta x$ of the vortices from the soft trapping axis (units of $\sqrt{2Ng_{2D}\Omega/\hbar\omega_x}$) against the eccentricity $\lambda$. We show the cases of $N_v = 7$ and 8 (panel **(a)** and **(b)** respectively) and plot only the changes in positions of four vortices in the lattice (the association with the curves is irrelevant). At $\lambda = \lambda_L$ the vortices suddenly align along the y-axis ($\Delta x = 0$). We have used a BEC of $10^6$ $^{87}$Rb atoms with $a = 5.23 \times 10^{-9}$m in a trap with $\omega_z/2\pi = 100$Hz and $\sqrt{\omega_x\omega_y}/2\pi = 50$Hz (regardless of $\lambda$).

## 2.2 Vortex gas

We consider pattern of vortices in the ground state of a BEC held in a rotating trapping potential. The ground state is found by minimizing the energy functional [31]

$$\mathcal{H}[\phi,\phi^*] = \int d\mathbf{x}\left[\frac{\hat{\mathbf{p}}2}{2m}\phi(\mathbf{x}) + V(\mathbf{x})|\phi(\mathbf{x})|^2 + g|\phi(\mathbf{x})|^4 - \phi^*(\mathbf{x})(\mathbf{\Omega}\cdot\hat{\mathbf{L}})\phi(\mathbf{x})\right], \tag{2.1}$$

where $\phi$ is the normalized order parameter of the condensate, $V(\mathbf{x}) = \frac{1}{2}m(\omega_x^2x^2 + \omega_y^2y^2 + \omega_z^2z^2)$ is the trapping potential, $m$ is the atomic mass, $N$ is the number of atoms, $g = 4\pi\hbar^2a/m$ is the inter-atomic interaction energy volume determined by the s-wave scattering length $a$, $\mathbf{\Omega}$ is the rotation frequency vector of the condensate and $\hat{\mathbf{L}}$ is the angular momentum operator. The function $\Phi$ minimizing $\mathcal{H}$ has been studied both numerically and analytically under different working assumptions such as the Thomas-Fermi (TF) and the lowest-Landau-level (LLL) approximation [43]. The first corresponds to the requirement of a very large number of particles, so that the kinetic energy associated with $\nabla|\Phi_{NS}|$ (with $\Phi_{NS}$ representing the non-singular part of the order parameter) can be neglected compared to the boson-boson interaction energy. In the LLL approximation, on the other hand, the main contribution to the energy is the centrifugal term and $\phi$ is well described by a product of single-particle wave-functions.

Here we consider a BEC in a harmonic trap rotating about its $z$-axis, which is also the direction of tight-confinement, *i.e.* $\omega_x, \omega_y \ll \omega_z$. The order parameter $\phi$ can then be factorized into an axial part, which we assume to be the ground state of a harmonic potential, and an in-plane one, $\psi(x, y)$. Moreover we assume that we have control over the trap frequency along the $y$-axis and we define the eccentricity parameter $\lambda = \omega_y/\omega_x$. In what follows $\lambda$ will play the role of a control parameter in our study.

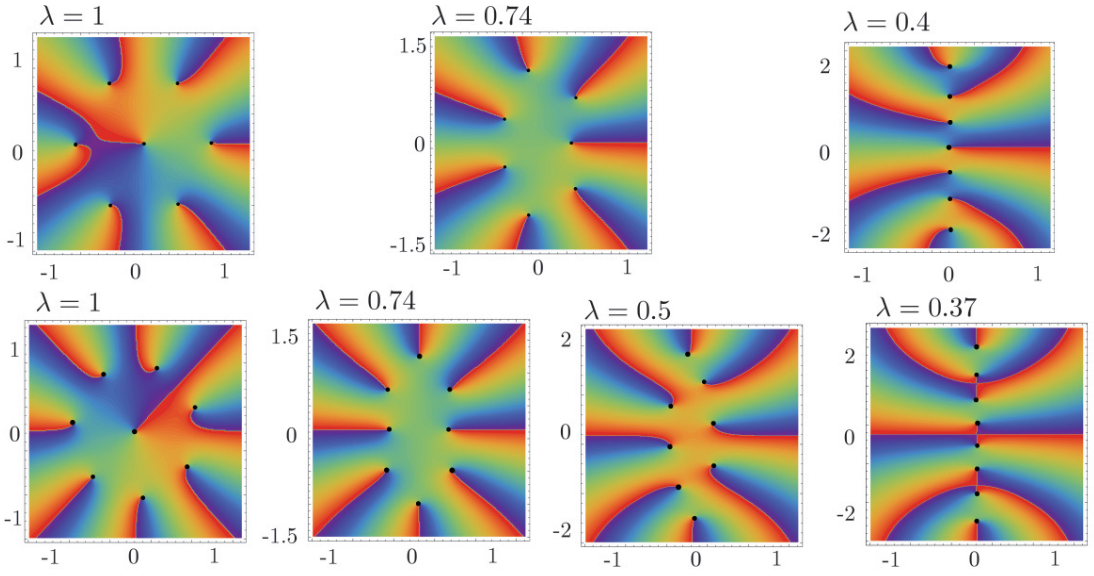



FIGURE 2.2: Phase distribution ($\arg(\psi(\mathbf{x}))$) of a vortex-lattice in the $x-y$ plane with $N_v$=7, 8 (upper and lower row respectively)for different values of $\lambda$. Black dots mark the positions of the vortices (in units of $\sqrt{2Ng_{2D}\Omega/\hbar\omega_x}$).

This allows us to reduce the above problem to a 2D problem by integrating out the axial dimension. The above energy functional reads now

$$\mathcal{H}_{2D}[\psi,\psi^*]=\int d\mathbf{x}\left[\frac{\hat{\mathbf{p}}2}{2m}\psi(\mathbf{x})+V_{2D}(\mathbf{x})|\psi(\mathbf{x})|^2+g_{2D}|\psi(\mathbf{x})|^4-\psi^*(\mathbf{x})(\Omega\hat{L}_z)\psi(\mathbf{x})\right], \quad (2.2)$$

where $V_{2D}(\mathbf{x}) = \frac{1}{2}m\omega^2(x^2+\lambda^2y^2)$ and $g_{2D} = g/\sqrt{2\pi}a_z$. Here $a_z = \sqrt{\hbar/m\omega_z}$ is the harmonic oscillator length in the z-direction. We are now in a position to minimize $\mathcal{H}$ in the TF limit. At a set value of $0<\lambda\leq 1$, we call $\Omega_{N_v}(\lambda)$ the minimum angular frequency of the trap which allows for $N_v$ vortices in the state that minimizes $H[\phi,\phi^*]$, while $\mathbf{r}_i$ is the position of the $i^{\text{th}}$ vortex in the frame rotating with the condensate. By introducing $|\mathbf{r}_i|^2_\lambda = x_i^2+\lambda^2y_i^2$, the energy of the vortex pattern can be written as $U=U_T+U_I$ with [44]

$$\begin{aligned} U_T &= \frac{\pi\rho_0(\lambda)}{(1+\lambda^2)}\sum_{i=1}^{N_v}|\mathbf{r}_i|^2_\lambda, \\ U_I &= -\pi\rho_0(\lambda)\sum_{i=1}^{N_v}\sum_{j\neq i=1}^{N_v}\log(|\mathbf{r}_i-\mathbf{r}_j|). \end{aligned} \quad (2.3)$$

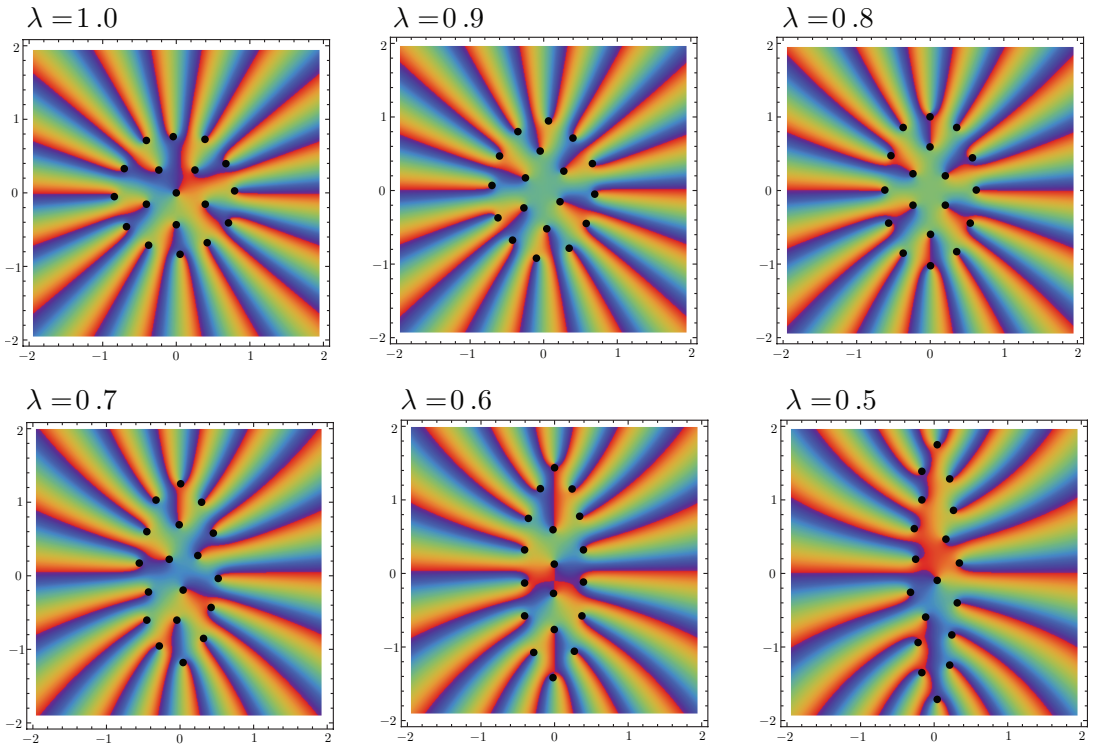



FIGURE 2.3: Phase distribution ($\arg(\psi(\mathbf{x}))$) of a vortex-lattice in the $x-y$ plane with $N_v$=18 for different values of $\lambda$. Black dots mark the positions of the vortices (in units of $\sqrt{2Ng_{2D}\Omega/\hbar\omega_x}$).

Here, $\rho_0(\lambda)=\sqrt{2\lambda/\pi}$ is the density of the condensate at the center of the trapping potential. We note that, beside the well-known logarithmic vortex-vortex interaction, a system with only a finite number of vortices experiences a potential depending on the inhomogeneity of the background *environment*. Eq. (2.3) is our starting point and minimizing this energy with respect to the position of the vortices will determine the vortex pattern's shape as a function of the anisotropy $\lambda$. In doing this, we will assume that the variations of $\lambda$ are accompanied by an adiabatic change of the angular frequency so that $\Omega_{N_v}(\lambda) \leq \Omega \ll \Omega_{N_v+1}(\lambda)$. This ensures that the wave-function minimizing the energy functional allows for exactly $N_v$ vortices and prevents the formation of additional vortices. In order to quantitatively assess the deviations of the vortex pattern from the Abrikosov-like lattice [32], we first show how the distances of the vortices from the tight trapping direction vary against the eccentricity $\lambda$. Fig. 2.1 shows two representative cases ($N_v$=7, 8) of the general trend: the pattern of non-axial vortices corresponding to values of $\lambda$ larger than a *critical* threshold $\lambda_L$ (in general a function of $N_v$) abruptly collapses to an all-aligned configuration. The transition is continuous, thus hinting at a second-order structural change, although the confirmation can only come from an investigation in the thermodynamic limit. In Fig. 2.2 we show the phase $S(\mathbf{x})$ of the BEC where the black dots indicates the presence of vortices as it can be seen from the

discontinuous jump along the lines.

Moreover, as shown in Fig. 2.2, for $1 \geq \lambda > \lambda_L$ one can identify two more structurally distinct configurations. Let us first consider the case of an even number of vortices (bottom row in Fig. 2.2): starting from an Abrikosov-like pattern at zero eccentricity, the first structural change at $\lambda = \lambda_C$ witnesses the central vortex being displaced so as to join the ring formed by the outer ones. A further reduction of $\lambda$ leads to a second threshold value, $\lambda_Z$, at which the axial symmetry is broken and a zig-zag pattern is formed. The situation is different for an odd number of vortices, where a parity effect becomes evident: at odd $N_v$ the Abrikosov-to-ring and ring-to-zig-zag transitions are degenerate and from full isotropy the lattice re-arranges directly into a zig-zag pattern at $\lambda = \lambda_Z$, [see Fig. 2.2 (upper row)]. Regardless of the parity of $N_v$, a further reduction in $\lambda$ makes the vortices align along the weak trapping direction, as already observed in Fig. 2.1. For a larger (but finite) number of vortices the situation is even richer as shown in Fig. 2.3. Let us consider, for instance, a system carrying 18 vortices. At $\lambda = 1$ they arrange in a pattern with a single vortex at the centre of the trap and two concentric rings surrounding it. By decreasing $\lambda$ we first observe an Abrikosov-to-ring change involving the inner ring and the central vortex, similar to the one described above. By further decreasing $\lambda$, the vortices in the newly formed inner ring start joining the outer one. Finally, the ring-to-zig-zag and zig-zag-to-linear transitions occurs.

## 2.3 Hydrodynamic description

We now explore the structural changes in detail by looking at the change in the superfluid motion of the condensate. It is important to stress that, due to the perturbations introduced into the system by the eccentricity, the vortex-lattice configuration found by minimizing Eq. (2.3) does not represent, in general, a *rigid pattern*. By recasting the trapping potential as

$$V_\lambda(\mathbf{x}) \equiv V_s(\mathbf{x}) + V_Q(\lambda, y) = \frac{1}{2} m\omega_x^2 (x^2 + y^2) + \frac{1}{2} m\omega_x^2 (\lambda^2 - 1) y^2, \tag{2.4}$$

one immediately recognizes in $V_Q(\lambda, y)$ a term exciting quadrupole modes *i.e.* non-rotational symmetric modes whose spatial dependence is of the form $f(ax^2 b + xy + cy^2)$. This shows that the background condensate (and thus the vortex pattern) is not stationary. The free energy of the rotating BEC is given by

$$F_{N_v} = E_{N_v}(\Omega, \lambda) + U_T + U_I, \tag{2.5}$$

where $U_{T,I}$ are given by Eq. ((2.3)) and $E_{N_v}(\Omega,\lambda)$ is an energy term that does not depend on the vortex configuration. It represents the energy in the absence of vortices [31]. By calling $\{\mathbf{r}_i^0\}$ $(i=1,..,N_v)$ the vortex positions which minimize Eq. (2.3) for a set number of vortices, we have that

$$\nabla_j F_{N_v}|_{\{\mathbf{r}_i^0\}}=0, \tag{2.6}$$

where $\nabla_j\equiv(\partial_{x_j},\partial_{y_j})$ and where we use the subscript $j$ to represent the coordinates of the $j^{\text{th}}$ vortex. In the rotating frame, a vortex has a velocity $\boldsymbol{v}_j$ such that

$$\nabla_j F_{N_v}|_{\mathbf{r}_j}\cdot\boldsymbol{v}_{\mathbf{r}_j}=0, \tag{2.7}$$

which implies the absence of dissipation, as expected from particles moving in a superfluid. A solution to this equation is given by

$$\boldsymbol{v}_{\mathbf{r}_j}=\alpha(\nabla_j^{\perp}F_{N_v}|_{\mathbf{r}_j}), \tag{2.8}$$

with $\nabla_j^{\perp}\equiv(\partial_{y_j},-\partial_{x_j})$ and $\alpha$ being the amplitude of the velocity field.
Its value $\alpha=a_{ho}\sqrt{\Omega\omega_x}/(\pi\rho_0(\lambda))$ [with $a_{ho}=\sqrt{\hbar/m\omega_x}$] is found by comparing it with the velocity field $(\hbar/m)\nabla S-\boldsymbol{\Omega}\times\mathbf{r}_j$ in the rotating frame. In this expression

$$S(\mathbf{x})=S_0(\mathbf{x})+\sum_{i\neq j}^{N_v}\theta_i(\mathbf{x}), \tag{2.9}$$

is the phase of the order parameter as seen by the $j^{\text{th}}$ vortex,

$$S_0(\mathbf{x})=-\frac{m\Omega(1-\lambda^2)}{\hbar(1+\lambda^2)}xy \tag{2.10}$$

is the vortex-free phase of the BEC at position $(x,y)$ and $\tan\theta_j(\mathbf{x})=(y-y_j)/(x-x_j)$ specifies the polar angle of a reference frame centered on the $j^{\text{th}}$ vortex core [31].

In Fig. 2.4 we show the magnitude of the velocity field for $N_v=8$ in a frame which rotates rigidly with the trap. The value of $\lambda$ decreases from panel **(a)** to **(d)** and the arrows show the flow directions with the magnitude being encoded in the color. In the dark (dark purple) regions the velocity field vanishes, *i.e.* the superfluid moves at the trap angular velocity. For no eccentricity [panel **(a)**] the vortex pattern rotates rigidly with the trap potential since the velocity field at the vortex positions (when the

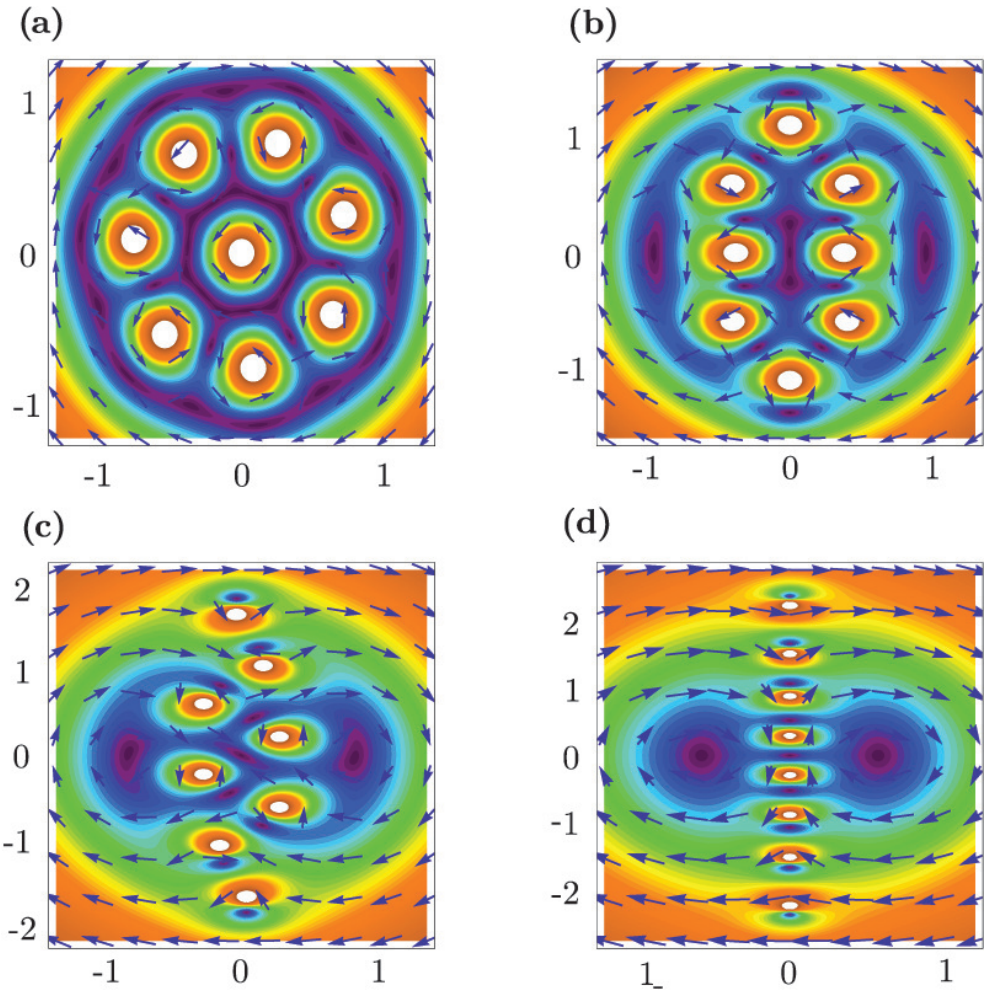



FIGURE 2.4: Superfluid velocity field in the rotating frame for $N_v$=8 (other parameters as in Fig. 2.1). From **(a)** to **(d)** we have $\lambda$=1, 0.76, 0.56, 0.36. Dark purple regions correspond to zero velocity. The velocities close to the cores are not shown on the chosen colourmap.

vortex itself is not present) vanishes in the rotating frame. It is worth noticing that outside the vortex pattern particles flow with a different velocity. This is at the origin of the imperfect rigid-body rotation of finite-sized vortex patterns in isotropic traps. By increasing the eccentricity [panel **(b)-(d)**] the rigid body behavior is lost and the vortex pattern is no longer a steady solution [32]. The continuous rotation of the trap would increase the angular momentum of the system. However, the condition $\Omega \in [\Omega_{N_v}, \Omega_{N_v+1}[$ on the angular velocity fixes the number of vortices in the condensate $N_v$. The only possibility for the system to react is to move the vortex cores to accommodate the angular momentum. In a real system, heating and dissipation would eventually lead to the crystallization of the vortex pattern or the transition to a turbulent regime [45].

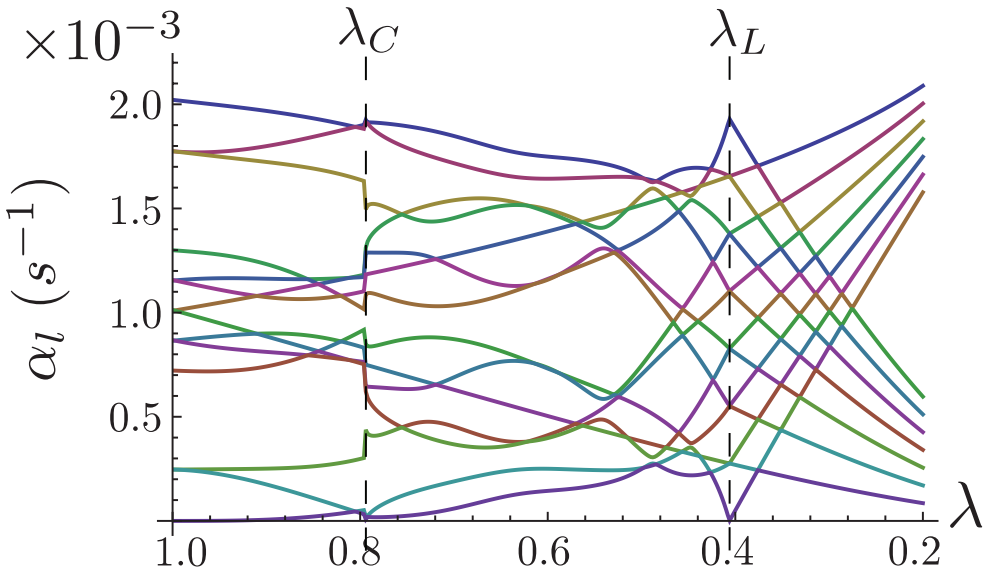



FIGURE 2.5: Spectrum of a BEC with $N_v = 7$ vortices against the eccentricity $\lambda$. The points $\lambda_{C,L}$ where the vortex pattern undergoes a structural change are visible.

## 2.4 Patterns modes

A quantitative confirmation of the abrupt nature of the structural changes can be found by studying the eigenmodes of the vortex pattern [42]. We take a set of small displacements $\{\delta\mathbf{r}_i\}$ from the equilibrium configuration $\{\mathbf{r}_i^0\}$ and write $\delta\boldsymbol{v} = (\delta v^x_{\mathbf{r}_1}, \delta v^y_{\mathbf{r}_1}, .., \delta v^x_{\mathbf{r}_{N_v}}, \delta v^y_{\mathbf{r}_{N_v}})$, so that the vortex cores velocities in the rotating frame become $\delta\boldsymbol{v} \simeq \mathbf{A}\cdot\delta\mathbf{r}$. Here $\mathbf{A}$ is a $2N_v\times 2N_v$ matrix whose $j^{\text{th}}$ row is found by expanding the velocity field $\boldsymbol{v}_{\mathbf{r}_j}=\alpha\nabla_j^{\perp}F_{N_v}|_{\mathbf{r}_j}$ around each $\mathbf{r}_i^0$. This gives

$$\mathbf{A}_j=\alpha\sum_i\left[\partial_{x_i}(\nabla_j^{\perp}F_{N_v})\,\hat{x}_i\;+\;\partial_{y_i}(\nabla_j^{\perp}F_{N_v})\,\hat{y}_i\right]_{\{\mathbf{r}_i^0\}}, \tag{2.11}$$

where $\alpha$ is determined as before. We now numerically diagonalize $\mathbf{A}$ for a set number of vortices. The eigenvalues $\alpha_l$ $(1\leq l\leq 2N_v)$ of $\mathbf{A}$ represent the rate at which vortices start moving from $\{\mathbf{r}_i^0\}$ once they are displaced by the corresponding eigenvector $\delta\mathbf{r}^l$. We note that the eigenmodes are related by $\alpha_n(\lambda)+\alpha_{2N_v-n}(\lambda)=C(\lambda)$ $(0<n\leq N_v)$ and the corresponding eigenvectors are mutually orthogonal. The constant $C(\lambda)$ depends on the system parameters but, remarkably, is independent of the pair of eigenvectors considered. A typical spectrum for $N_v=7$ is shown in Fig. 2.5. At two specific values of $\lambda$ the eigenmodes show non-continuous behavior, beside the appearance of a null eigenvalue. The appearance of a vanishing eigenvalue can be explained with a physical argument as follows. The number of vortices is set by the value of the angular velocity $\Omega$.

As we change the anisotropy we effectively change the total angular momentum of the system. Since we are below the threshold for the creation of a new vortex the system has to "store" this extra amount of angular momentum somewhere else by setting vortices into rotation. Nevertheless there are values of $\lambda$ and configurations of vortices for which all the angular momentum can be stored into a static vortex pattern of the vortices. Thus the appearance of a null eigenvalue as in the symmetric case ($\lambda = 1$) where the eigenvalue corresponding to a rotation around the $z$-axis vanishes because of the circular symmetry of the vortex pattern.

These points can be connected to the structural transition points: $\lambda_C$ signaling the Abrikosov-to-ring transition and $\lambda_L$ the zig-zag-to-linear one. At any other value of $\lambda$ the eigenmodes are positive confirming our previous point on the non-steady nature of the vortex patterns in the rotating frame. However, the exact value of $\lambda$ at which the lowest eigenvalue first deviates from zero is found to grow with the number of vortices. The corresponding eigenvector corresponds to displacements of the vortex positions along the tangent to the vortex ring, *i.e.* a rotation of the vortex pattern produces no effect. In fact, it is not possible to clearly discriminate the eigenmodes of a finite-size lattice with a small number of vortices from the phonon modes of the background condensate: rotating an anisotropic trap excites Bogoliubov modes in the BEC, which have a strong influence on the vortex pattern [46]. The link between Bogoliubov modes and changes in the properties of the *vortex matter* has already been explored in relation to vortex-pattern formation and instability [47].

## 2.5 Conclusions and Outlooks

We have studied the structural transitions induced in a finite vortex-lattice by an increasing degree of eccentricity of a rotating BEC. An Abrikosov-like arrangement undergoes a sequence of symmetry-breaking processes that push it towards a linear arrangement of vortices. Such modifications, witnessed and understood in terms of background superfluid motion, are well signaled by the eigenmodes of the vortex-lattice. By addressing the case of a finite lattice, our work complements and extends the existing literature on vortex instabilities and arrangements in rotating BECs and provides interesting insight into the many-body properties of a mesoscopic quantum system.

Our analysis is not limited to BECs: vortex-like excitations exist in superconducting films, Josephson-junction arrays and dislocation pairs in the theory of 2D melting [49]. Inter-vortex potentials depending logarithmically on the distance between two vortices, similar to Eq. (2.3), have been observed in thin superconducting films [50]. Vortex lattices in thin films under magnetic fields have been shown to take the form of discrete

rows [51]. Strong analogies between the dynamics of vortex lattices and Josephson-junction arrays hold due to the charge-vortex duality [52], thus giving our results a generality and interest that goes beyond the cases addressed here.

Moreover it would be interesting to extend this study to the tree dimensional case and link the instability of the patterns to the generation of Kelvin waves and thus to dissipation of energy. A good model to investigate is a two component BEC because in this way it would be possible to pin vortices generated in one species by means of the second component. Furthermore the presence of the second component would allow for driving of vortices.

The work presented in this chapter has been done in collaboration with Th. Busch and M. Paternostro and it has been published in Phys. Rev. A **83**, 053612 (2011).

# Chapter 3

# Mesoscopic entanglement in BEC

In this chapter we give a very brief overview of the theory of phase space representation for quantum systems. We will focus particularly on the definition of the Wigner function for systems described by the angle and angular momentum variables. The presentation is by no means meant to be complete but it is a useful reference to help the reader in the discussion of the entanglement detection given in sec. 3.7. The interested reader can find a very good and complete treatment of phase space methods in the book by C.W. Gardiner and P. Zoller [53] whereas a good review about the problem of quantization of angular momentum and phase variables can be found in refs. [54]. Next we propose an experimental feasible scheme in order to transfer entanglement from photons to BECs. Experimental assessment of entanglement between the BECs makes use of Wigner function reconstruction.

## 3.1 Introduction

The rich variety of coherently exploitable degrees of freedom with which a photonic system is endowed has been extensively used in recent years in order to demonstrate the building blocks of quantum technology protocols including quantum cryptography [55], quantum repeaters [56], teleportation and quantum computing [57]. In this context, the exploitation of orbital angular momentum (OAM) carried by light is settling as a new and exciting opportunity for coherent manipulation at the classical and quantum level [58]. High density data transmission [59], activation of micro-machines and optical tweezers [60] are among the most prominent applications of optical OAM so far. In addition, the field of quantum information processing has now started exploiting the additional opportunities offered by this photonic degree of freedom for communication

and manipulation purposes. It has been shown that it is possible to create OAM-entangled photons by means of a *routinely used* setup such as spontaneous parametric down conversion (SPDC) [61].

This has triggered a plethora of studies on how to generate, manipulate and detect non-classical states of OAM [64], culminating in the demonstration of Bell's inequality violation by OAM-entangled two-photon states [62], the introduction of so-called hyper-entangled states [65], the design of quantum cryptographic schemes based on higher-dimensional systems [66] and the transfer of OAM states from light to matter-wave systems [67]. In particular, the latter scenario holds the potential for the realization of experimentally feasible long-time quantum memories embodied by superfluid rotational states of Bose-Einstein condensates (BECs) [67–71].

The spatial coherence intrinsic in a BEC allows for a superfluid vortex state in which the bosons in the condensate have a well defined and quantized OAM, which offers a perfect match with rotating photon carriers. Along the seminal lines traced by the experiments in Refs. [67], a few theoretical proposals for the light-to-vortex state transfer have been presented [68–71]. Here we close the circle of these proposals and show that it is possible to create entanglement between two spatially separated BECs by transferring OAM from entangled photon resources to the condensates. We propose a simple and efficient scheme to achieve this goal using experimentally achievable parameters and routinely produced OAM-entangled light resources. On a different level, our study proposes a scheme that is able to transfer (with in principle 100% efficiency) higher-dimensional entanglement between two independent system by means of bilocal interactions, thus contributing to an area that is witnessing theoretical and experimental interest (see Choi *et al.* in [56] and Ref. [72]).

## 3.2 Phase space representation

Phase space representation for classical systems is naturally introduced with the Lagrangian and/or Hamiltonian description. It amounts describing the system, whose degrees of freedom can be labeled as $\mathbf{q}_i$, by means of a probability distribution which is a function of $\mathbf{q}_i$. Moreover the elegant and very powerful formalism which comes from the least action principle turned out to be very flexible due to the possibility of canonical transformation of variables. The right choice of the set of variables can simplify the problem up to the point at which its solution becomes a trivial task. In classical statistical mechanics phase space methods are a natural choice because of their intrinsic probabilistic description for the degrees of freedom are so many that the "equations of motion" loose their meaning. Moreover a description through the probability density

function in phase space greatly simplifies the treatment of noisy systems [53]. In the last thirty years the very same apparatus has been built for quantum system with very good success. Historically the reason why these methods have been introduced and applied to quantum systems is due to the quest for understanding the quantum to classical (and vice-versa) transition. This led to the search for links and anchor points between the two "worlds", something that could create a first bridge to start the investigation across this border. Quantum mechanics introduced the concept of an intrinsic uncertainty in any system. An uncertainty related to the system properties and to its interaction with the rest of the universe. This is translated into the Heisenberg uncertainty relations for pairs of conjugate variables. They state that the product of the root mean squares for two observables $\hat{X}$ and $\hat{Y}$ is

$$\Delta x^2 \Delta y^2 \geq \frac{1}{4}\langle[\hat{X},\hat{Y}]\rangle^2, \tag{3.1}$$

where $\Delta x^2 = \langle \hat{X} - \langle \hat{X}\rangle\rangle^2$ $\Delta y^2 = \langle \hat{Y} - \langle \hat{Y}\rangle\rangle^2$ are the square of the variance for the two observables and $[\hat{X},\hat{Y}] = \hat{X}\hat{Y} - \hat{Y}\hat{X}$ is their commutator. This uncertainty is at the core of the modern formulation of quantum mechanics; the uncertainty relations are a limit to the knowledge we can get about a quantum system. The best possible scenario is when these inequalities saturate, *i.e.* when $\Delta x^2 \Delta y^2 = \frac{1}{4}\langle[\hat{X},\hat{Y}]\rangle^2$. States of a quantum system for which the above equality holds are the so-called coherent states.

The coherent state for the harmonic oscillator turns out to be an eigenstate of the annihilation operator $\hat{a}$. Moreover a harmonic oscillator which is initially in a coherent state will evolve following the classical trajectory for the classical harmonic oscillator. This is the reason why the coherent states are often referred to as the most classical quantum states and which is one of the reasons why they are good choices as starting points to build phase space methods for quantum systems. There are then two approaches for constructing something that can have a connection with the classical theory: either we use the coherent states as a reference or else we start from the "standard" classical description where the important variables are positions and momenta. In the first case one can get the Husimi (or $Q$) and Glauber-Sudarshan (or $P$) functions whereas in the second case one obtains the so called Wigner (or $W$) function.

All of them are the counterpart of the density operator in phase space and all have some advantages and some problems that we shall not discuss in detail since this is far from our purposes. We will only introduce the Wigner function and some of its properties. The Wigner function is probably the most intuitive to approach since it is built on the analogy with the classical case. The Wigner function $W(x,p)$ is built in analogy to the classical probability distribution function in phase space, but it turns out that it lacks

of a very important property: positivity. Nevertheless it is still very useful and helpful in many ways. For the case of a particle moving in one dimension the Wigner function is defined as:

$$W(x,p) = \frac{1}{2\pi}\int_{-\infty}^{\infty} d\xi\; e^{-\imath px/\hbar}\langle x+\xi/2|\hat{\rho}|x-\xi/2\rangle, \tag{3.2}$$

where $\hat{\rho}$ is the density matrix operator describing the system and $x$ and $p$ are the position and the momentum respectively. The Wigner function has some important properties. By integrating out either $q$ or $p$ the resulting function is a proper probability distribution, *i.e.* non-negative with its integral being one. In particular for a pure state $|\Psi(t)\rangle$ it is the square modulus of the wave-function:

$$\begin{aligned}\int_{-\infty}^{\infty} dp\; W(x,p,t) &= |\langle x|\Psi(t)\rangle|^2,\\ \int_{-\infty}^{\infty} dx\; W(x,p,t) &= |\langle p|\Psi(t)\rangle|^2.\end{aligned} \tag{3.3}$$

It is easy to see from its definition that the Wigner function is invariant under any transformation of the Galilean group (translation, position inversion, time reversal and boost at constant velocity). Moreover the transition probability from a state $|\Psi(t)\rangle$ to $|\Phi(t)\rangle$ is given by

$$|\langle\Phi(t)|\Psi(t)\rangle|^2 = 2\pi\hbar\int_{-\infty}^{\infty} dx\int_{-\infty}^{\infty} dp\; W_\Psi(x,p,t)W_\Phi(x,p,t), \tag{3.4}$$

where $W_\Psi(x,p,t)$ and $W_\Phi(x,p,t)$ are the Wigner functions associated with the states $|\Psi(t)\rangle$ and $|\Phi(t)\rangle$ respectively. The knowledge of the Wigner function allows the evaluation of the mean value of any bounded operator $\hat{A}$ acting on the Hilbert space of the system. In particular

$$Tr(\hat{A}\hat{\rho}(t)) = \int_{-\infty}^{\infty} dx\int_{-\infty}^{\infty} dp\; A(x,p)W(x,p,t), \tag{3.5}$$

where $A(x,p)$ is the function associated to the operator $\hat{A}$ in phase space. For the above equality to hold we have to choose

$$A(x,p) = \int_{-\infty}^{\infty} d\xi\; e^{-\imath px/\hbar}\langle x+\xi/2|\hat{A}|x-\xi/2\rangle. \tag{3.6}$$

The above definition of the Wigner function does not really say much about its physical meaning, nevertheless there is an instructive way of interpreting it [73]. We start by noticing that $\langle x^{'}|\hat{\rho}|x^{''}\rangle$ is the coherence between the particle being at position $x^{'}$ and $x^{''}$. In ref. [73] the author talks about a "jump" (Chap. 3) giving to the above term a dynamical interpretation, but here we prefer to talk about the coherence between states. Let us now make a change of variables going from $x^{'}$ and $x^{''}$ to the "center of mass" and "relative position" of the two points defined as usual as $\xi = x^{'} - x^{''}$ and $2x = x^{'} + x^{''}$. Thus we obtain $\langle x + \xi/2|\hat{\rho}|x - \xi/2\rangle$, which can be reinterpreted as follows: given a point $x$ in space, the coherence between two points equally distant from it is given by the above matrix element. Let us assume that the state we want to represent in phase space is a "homogeneous state", where the coherence between two spatial points depends upon their relative distance only. In this case then the Fourier transform of $\langle \xi/2|\hat{\rho}|-\xi/2\rangle$ will give us information on the distribution of the coherences between states with relative momentum $p$. The Wigner function is exactly this: it is a quantification of how spread the correlations between states equally distant from a point $x$ in the momentum representation are.

## 3.3 Wigner function and non-classicality

A very interesting property of the Wigner function is that it can be used to "detect" the (non-)classicality of the state of a system. This property has been exploited to construct different measures of (non-)classicality. One of them, namely the non-classical depth [74], makes uses of the generalized distribution (or Cahill) function $R_\tau$ for pure states. The Cahill function is the convolution of a gaussian with variance proportional to the parameter $\tau$ with the $P$ function of the state. The basic idea of the above criterion is based on the fact that for $\tau = 1$ one gets the always positive (by definition) $Q$ function. Moreover in the limiting case $\tau \to 0$ the $R_\tau$ function obviously tends to the $P$ function, because of the convolution with a delta function. Hence by changing $\tau$ in the interval $[0, 1]$ the $R_\tau$ goes form the $P$ to the $Q$ function. The greatest lower bound $\tau_m$ for which the $R_\tau$ becomes positive, and thus is acceptable as a proper distribution function, is a measure of the depth of the non-classicality of a state. The range of $t_m$ goes from $[0, 1]$ as can be seen as follows. The $Q$ function is always positive so that in the worst case starting from $\tau = 0$ and slowly increasing it we will eventually obtain it for $\tau = 1$ and that is our greatest lower bound. On the other hand a coherent state has a $P$ function which is a delta function and thus it is already a well defined distribution function. Nevertheless the $P$ function is obtained in the limiting case $\tau \to 0$ so that in this case $\tau_m = 0$.

Another measure of non-classicality has been introduced in ref. [75]. The basic idea here is to measure the "volume" of the negative part of the Wigner function.

## 3.4 Angle and angular momentum variables

The first approach to quantum mechanics is probably the quantization of the pair of conjugate variables position and momentum $x$ and $p$ by imposing the commutation relation $[\hat{x}, \hat{p}] = \imath\hbar$ on the two Hermitian operators. Nevertheless depending upon the symmetry of the system sometimes it is more convenient to use another set of variables like the angle and the angular momentum. This happens anytime there is a rotational invariance in the problem for instance. In this section we introduce the quantum mechanical theory for the pair of variables angle and angular momentum. We will then define the phase space and the Wigner function in these variables. We follow the treatment given in refs. [54, 76].

Let us consider a system whose mathematical description is given through the pair of variables azimuthal angle $\theta$ and angular momentum along the $z$-axis $\hat{L}_z$. The angle $\theta$ being defined up to an integer multiple of $2\pi$: $\theta = \tan^{-1}(x/y)$. By analogy with the standard treatment for quantization of position and momentum we can immediately impose the commutation relation $[\hat{\theta}, \hat{L}_z] = \imath\hbar$. Nevertheless it turns out that this is not a good choice. The reason can be easily seen as follows. First we note that the commutator implies that $\hat{L}_z = -\imath\partial/\partial\theta$. This is obvious if we think about the case of the operators $\hat{x}$ and $\hat{p} = -\imath\partial/\partial x$ and the fact that the algebra (commutation relations) we are imposing is the same. From here we can then see that

$$\begin{aligned}
\langle\Psi_1(\theta)|\hat{L}_z\Psi_2(\theta)\rangle &= \int_0^{2\pi} d\theta\, \Psi_1^*(\theta)\left(-\imath\frac{\partial}{\partial\theta}\Psi_2(\theta)\right), \\
&= -\imath\Psi_1^*(\theta)\Psi_2(\theta)\Big|_0^{2\pi} + \int_0^{2\pi} d\theta\, \left(-\imath\frac{\partial}{\partial\theta}\Psi_1(\theta)\right)^* \Psi_2(\theta), \qquad (3.7)\\
&= -\imath\Psi_1^*(\theta)\Psi_2(\theta)\Big|_0^{2\pi} + \langle\hat{L}_z\Psi_1(\theta)|\Psi_2(\theta)\rangle.
\end{aligned}$$

Since the angular momentum is a real variable we have to demand that $\hat{L}_z = \hat{L}_z^\dagger$ or else $\langle\Psi_1(\theta)|\hat{L}_z\Psi_2(\theta)\rangle = \langle\hat{L}_z\Psi_1(\theta)|\Psi_2(\theta)\rangle$. This implies that

$$\Psi_1^*(\theta)\Psi_2(\theta)\Big|_0^{2\pi} = \Psi_1^*(2\pi)\Psi_2(2\pi) - \Psi_1^*(0)\Psi_2(0) = 0. \qquad (3.8)$$

Since it has to hold for any pair of wave-functions $\Psi_1(\theta)$ and $\Psi_2(\theta)$, then among the square integrable functions we have to chose the periodic ones such that $\Psi(2\pi) = \Psi(0)$.

Nevertheless this choice has a problem. Let $|l, m\rangle$ be the the eigenstate of both the total angular momentum operator $\hat{L}^2 = \hat{L}_x^2 + \hat{L}_y^2 + \hat{L}_z^2$ and $\hat{L}_z$ with eigenvalue $\hbar l(l+1)$ and $\hbar m$ respectively. On one hand we have

$$\langle lm|[\hat{\theta}, \hat{L}_z]|lm'\rangle = \langle lm|\hat{\theta}\hat{L}_z|lm'\rangle - \langle lm|\hat{L}_z\hat{\theta}|lm'\rangle = (m' - m)\langle lm|\hat{\theta}|lm'\rangle, \tag{3.9}$$

but on the other hand, because of the imposed commutation relation, $\langle lm|[\hat{\theta}, \hat{L}_z]|lm'\rangle = \imath\hbar\delta_{m,m'}$ so that

$$(m' - m)\langle lm|\hat{\theta}|lm'\rangle = \imath\hbar\delta_{m,m'}, \tag{3.10}$$

which implies $0 = 1$ when $m = m'$.

This inconvenience comes up because in evaluating $\hat{L}_z\hat{\theta}|l, m'\rangle$ we are assuming that the wave-function associated to $\hat{\theta}|l, m'\rangle$ is periodic, so that the "boundary" term vanishes. This is of course not true and we end up with the above paradox. It is therefore not possible to use the pair of operators $\hat{\theta}$ and $\hat{L}_z$ together with the commutation relation $[\hat{\theta}, \hat{L}_z] = \imath\hbar$.

This problem can be overcome by making a different choice for the quantization rules. The use of the functions $\cos\theta$ and $\sin\theta$ has the advantage that they are automatically periodic. The commutation relations then are

$$\begin{aligned} [\cos\hat{\theta}, \hat{L}_z] &= -\imath\hbar\sin\hat{\theta}, \\ [\sin\hat{\theta}, \hat{L}_z] &= \imath\hbar\cos\hat{\theta} \\ &\text{or} \\ [e^{\imath\hat{\theta}}, \hat{L}_z] &= -\hbar e^{\imath\hat{\theta}}. \end{aligned} \tag{3.11}$$

These commutation relations are analogous to the ones involving the operator $\hat{\theta}$ but because of the trigonometric functions they do not suffer from the periodicity problem. Moreover any periodic function can be written in a "Fourier series" using the above functions as basis.

We are now in a position to introduce the Wigner function in a phase space "spanned" by the angular variables. We shall focus on a two dimensional phase space; the extension to

more dimensions is then straightforward. By following the treatment given in ref. [76] we define the Wigner function in an axiomatic way rather than by starting from the position-momentum representation and applying a change of variables. This has the advantage of being completely self-consistent and independent from the particular transformation. We define the Wigner function as a bilinear form that associates to every density matrix operator $\hat{\rho}$ the function $W_m(\theta,t) = Tr(\hat{K}_m(\theta)\hat{\rho})$. The kernel operator $\hat{K}_m(\theta)$ has the the properties:

- it is real: $\langle m''|\hat{K}_m(\theta)|m'\rangle = \Big(\langle m'|\hat{K}_m(\theta)|m''\rangle\Big)^*$;
- invariance under rotation: $\langle m'|\hat{K}_m(\theta+\phi)|m''\rangle = e^{-\imath(m'-m'')\phi}\langle m'|\hat{K}_m(\theta)|m''\rangle$;
- invariance under "boost": $\langle m'+n|\hat{K}_{m+n}(\theta)|m''+n\rangle = \langle m'|\hat{K}_m(\theta)|m''\rangle$;
- invariance under angle inversion: $\langle -m'|\hat{K}_{-m}(\theta)|-m''\rangle = \langle m'|\hat{K}_m(-\theta)|m''\rangle$;
- invariant under "time reversal": $\langle -m'|\hat{K}_{-m}(\theta)|-m''\rangle = \Big(\langle m'|\hat{K}_m(\theta)|m''\rangle\Big)^*$.

These properties are the natural extension of those of the Wigner function $W(x,p,t)$ in the position and linear momentum variables. All together they define in a unique way the Wigner function in the angle and angular momentum variable. The actual form of the kernel operator $\hat{K}_m(\theta)$ is determined [76] by means of the above properties and the relation $\langle\theta|m\rangle = e^{\imath m\theta}/\sqrt{2\pi}$.

## 3.5 The model

Let us start by presenting the model used in order to describe the light-to-BEC transfer of entanglement. We shall see that a key point in this mechanism resides in the collective coupling of the atoms belonging to one of the BECs to the respective light field. Together with the indistinguishability of the resource photons, this permits us to entangle the two BECs. We consider two spatially separated and trapped BECs, each with $N_0^I$ ($I = A, B$) $^{87}$Rb atoms and let each of them interact with one of the field modes of an OAM-entangled two-photon state (see the sketch in Fig. 3.1). Such a photonic resource can be produced, for instance, by type-I parametric down conversion of a Gaussian laser beam which is an OAM-preserving process: the sum of the OAM carried by the entangled signal and idler mode produced by a laser-pumped non-linear crystal equals the OAM initially carried by the pump [61, 62]. In this paper we shall consider a two-photon state produced by SPDC of a laser beam with no-OAM (*i.e.* prepared in a Gaussian spatial mode). This implies that the output modes, here labeled as $\alpha$ and $\beta$, carry opposite OAM and enter the state

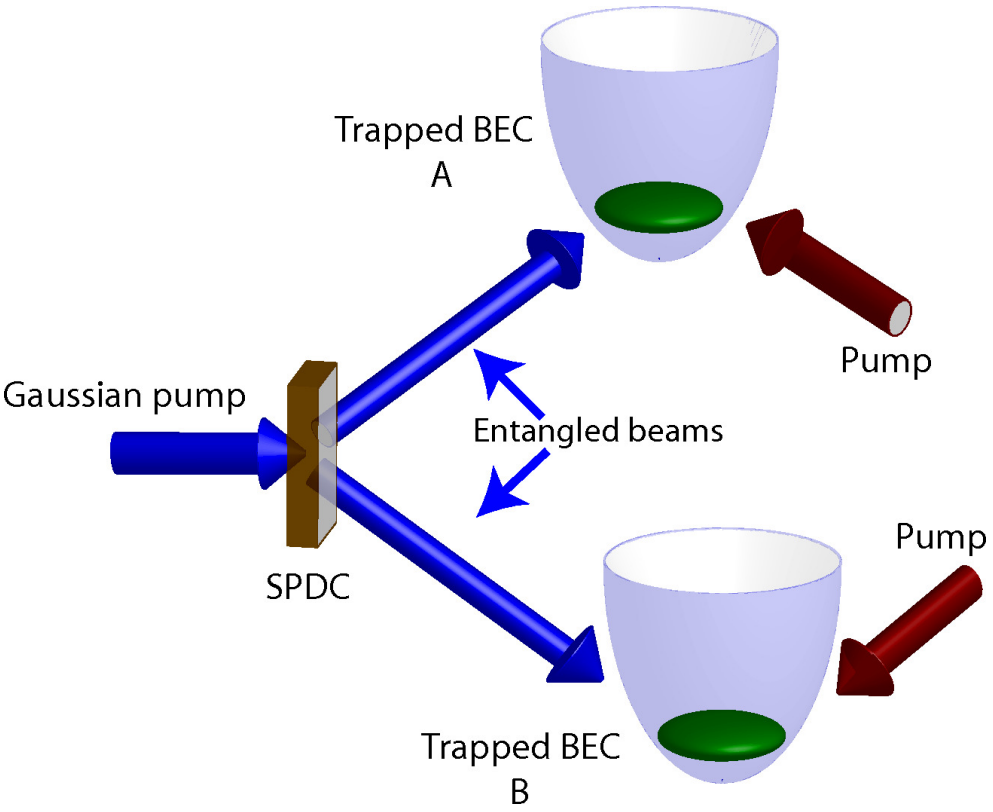



FIGURE 3.1: Sketch of the proposed setup. An OAM-entangled two-photon state is produced by spontaneus parametric down conversion (SPDC) of a Gaussian pump. Each output mode interacts with a respective trapped Bose-Einstein condensate (BEC), which is also pumped by an intense field with no OAM. The local matter-light interaction transfers the OAM entanglement from the field modes to the condensates rotational degree of freedom.

$$|\Phi\rangle_{\alpha\beta} = C|0\rangle_\alpha|0\rangle_\beta + \sum_{l=-\infty}^{\infty} C_{l,-l}|1_l\rangle_\alpha|1_{-l}\rangle_\beta. \tag{3.12}$$

Here, $|n_k\rangle_\alpha$ indicates an $n$-photon state populating mode $\alpha$ and carrying OAM equal to $\hbar k$ and $|C|^2 + \sum_{l=-\infty}^{\infty} |C_{l,-l}|^2 = 1$. The main idea behind our proposal is that the arrangement of a locally-assisted OAM-transfer from a light mode to the respective BEC would also allow for the transfer of quantum correlations, therefore constructing an effective entangled channel involving remote matter systems.

The basic building block for the transfer is an off-resonant double Raman scattering process. We consider each individual atom as a six-level system, shown in Fig. 3.2. The energy scheme comprises a ground-state triplet made out of a non-rotating state $|0\rangle$ and two other states, indicated as $|\pm 1\rangle$, having angular momentum $\pm\hbar$. The elements of excited-state triplet $|e\rangle$ and $|e^{'}\rangle$ are linked to $|\pm 1\rangle$ by two classical pumps, while the field modes in $|\Phi\rangle_{\alpha\beta}$ drive the $|0\rangle \leftrightarrow |E, e, e'\rangle$ transitions. In what follows, $\Delta$ and $\Delta_0$ indicate the one-photon Raman detunings which are set by appropriate chosing the frequencies

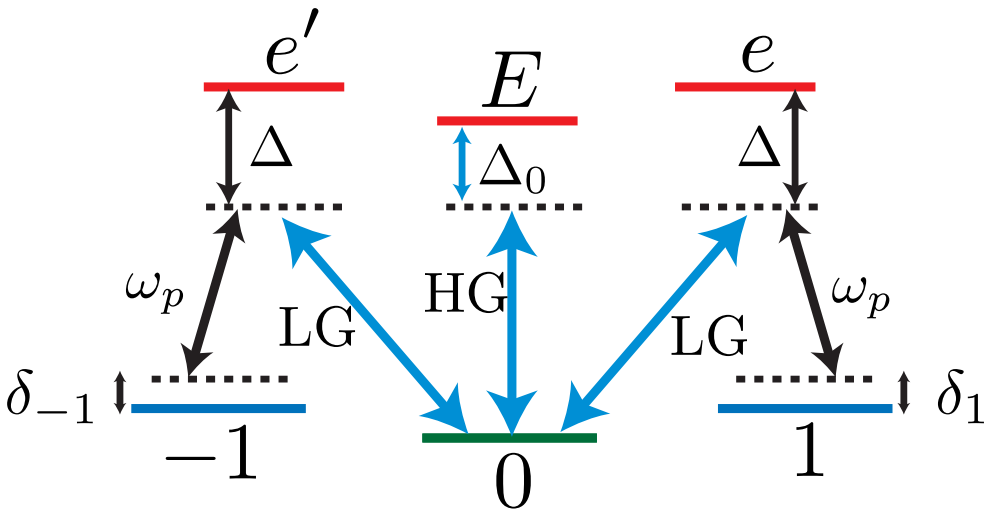



FIGURE 3.2: Six-level configuration for OAM transfer. We show a schematic representation of the relevant energy levels of a single $^{87}$Rb atom interacting with Laguerre-Gauss (LG) driving fields and classical Gaussian pumps with frequency $\omega_p$. The ground-state triplet comprises states having angular momentum 0 and $\pm\hbar l$. The excited-state triplet is adiabatically eliminated from the dynamics by a double off-resonant Raman transition with the one-photon detunings $\Delta$ and $\Delta_0$. Two-photon detunings $\delta_{\pm l}$ are also introduced for the stabilization of the entanglement-transfer process. The component in Eq. 3.12 carrying zero OAM [being in a Hermite-Gauss (HG) spatial mode] drives off-resonantly the $|0\rangle \leftrightarrow |E\rangle$ transition.

of the driving fields. The classical pumps are taken to have a Gaussian spatial profile so that photons scattered in the $|e\rangle \leftrightarrow |1\rangle$ and $|e'\rangle \leftrightarrow |-1\rangle$ transitions carry no OAM. Together with the conditions on the OAM properties of Eq. (3.12), this ensures that an atom undergoing the two-photon Raman transition from state $|0\rangle$ to $|\pm 1\rangle$ (as shown in Fig. 3.2) acquires an OAM exactly equal to $\pm\hbar$. We now introduce the second-quantized matter field operators $\hat{\psi}_{I,j}(\mathbf{r})$ obeying the bosonic commutation rules

$$[\hat{\psi}_{I,i}(\mathbf{r}), \hat{\psi}^{\dagger}_{J,j}(\mathbf{r}')] = \delta_{I,J}\delta_{i,j}\delta(\mathbf{r}-\mathbf{r}'), \tag{3.13}$$

where $I, J = A, B$ are labels for the BECs while $i, j = 0, \pm l, E, e, e'$ refer to the atomic states. As for the photonic part of our system, standard commutation relations

$$[\hat{c}_{n_I,k}, \hat{c}^{\dagger}_{n_J,k'}] = \delta_{n_I,n_J}\delta_{k,k'}, \tag{3.14}$$

involving the creation (annihilation) operator $\hat{c}^{\dagger}_{n_I,k}$ ( $\hat{c}_{n_I,k}$) hold. Here $n_A = \alpha$ ($n_B = \beta$) refers to the photonic mode $\alpha$ ($\beta$) that interacts with condensate $A$ ($B$). Finally, $k, k' = \pm l, 0$ refers to the OAM degree of freedom of the photon. Besides the term describing the energy of the free photonic fields, the Hamiltonian of the system consists of the

following four terms

$$\hat{H} = \hat{H}_a + \hat{H}_{aa} + \hat{H}_{ad} + \hat{H}_{ap}, \tag{3.15}$$

which we now address in detail.

The first two terms describe the properties of the trapped BECs and are given by

$$\hat{H}_a = \sum_{I,j} \int_{\mathcal{V}_I} d\mathbf{r}\ \hat{\psi}^\dagger_{I,j}(\mathbf{r}) \left( -\frac{\hbar^2}{2m}\nabla^2_I + V_{I,j}(\mathbf{r}) \right) \hat{\psi}_{I,j}(\mathbf{r}), \tag{3.16}$$

$$\hat{H}_{aa} = \frac{1}{2} \sum_{I,j,j'} \eta^I_{j,j'} \int_{\mathcal{V}_I} d\mathbf{r}\ \hat{\psi}^\dagger_{I,j}(\mathbf{r})\ \hat{\psi}^\dagger_{I,j'}(\mathbf{r})\ \hat{\psi}_{I,j'}(\mathbf{r})\ \hat{\psi}_{I,j}(\mathbf{r}). \tag{3.17}$$

In all the above, $\mathcal{V}_I$ is the quantization volume for the light-matter interaction involving condensate $I$. The $V_{I,j}(\mathbf{r})$s are the state-dependent atomic trapping potentials, $\eta^I_{j,j'} = (4\pi\hbar^2/m)a^I_{j,j'}$ accounts for the collisional energy between two atoms (of mass $m$) in states $j$ and $j'$ and $a^I_{j,j'}$ is the corresponding s-wave scattering length. As it will be clarified later on, the excited triplet $\{E, e, e'\}$ can be adiabatically eliminated from the dynamics of the atomic system. Therefore, by assuming no initial population of these states, we can simplify our treatment and take $a^I_{j,E} = a^I_{j,e} = a^I_{j,e'} = 0$ for $j = 0, \pm l$. The third term in Eq. (3.15) describes the interaction between BEC $I$ and the quantized field mode $n_I$ and can be written as

$$\begin{aligned} \hat{H}_{ad} = \sum_{I=A,B} \Bigg( & \chi_{I,0}\ \hat{c}_{n_I,0} \int_{\mathcal{V}_I} d\mathbf{r}\ \hat{\psi}^\dagger_{I,E}(\mathbf{r}) \hat{\psi}_{I,0}(\mathbf{r}) \mathscr{A}_{n_I,0}(\mathbf{r}) \\ & + \chi_{I,l}\ \hat{c}_{n_I,l} \int_{\mathcal{V}_I} d\mathbf{r}\ \hat{\psi}^\dagger_{I,e}(\mathbf{r}) \hat{\psi}_{I,0}(\mathbf{r}) \mathscr{A}_{I,l}(\mathbf{r}) \\ & + \chi_{I,-l}\ \hat{c}_{n_I,-l} \int_{\mathcal{V}_I} d\mathbf{r}\ \hat{\psi}^\dagger_{I,e'}(\mathbf{r}) \hat{\psi}_{I,0}(\mathbf{r}) \mathscr{A}_{I,-l}(\mathbf{r}) \Bigg) + h.c.\ . \end{aligned} \tag{3.18}$$

The coefficients $\chi_{I,k}$ $(k = 0, \pm l)$ are the effective dipole moments associated with the transitions depicted in Fig. 3.2. The functions $\mathscr{A}_{n_I,k}(\mathbf{r})$ describe the spatial shape of the states entering $|\Phi\rangle_{\alpha\beta}$ and we choose them to be

$$\begin{aligned} \mathscr{A}_{n_I,0}(\mathbf{r}) &= i\sqrt{\frac{\hbar\omega_0}{2\epsilon_0\mathcal{V}_I}} e^{ik_z z} e^{-\frac{r^2}{\mathcal{W}^2}}, \\ \mathscr{A}_{n_I,\pm l}(\mathbf{r}) &= i\sqrt{\frac{\hbar\omega_{\pm l}}{2\epsilon_0\mathcal{V}_I}} \left( \frac{\sqrt{2}r}{\mathcal{W}} \right)^{|l|} e^{\pm il\phi} e^{ik_z z} e^{-\frac{r^2}{\mathcal{W}^2}}, \end{aligned} \tag{3.19}$$

where $\epsilon_0$ is the vacuum permeability. While the first of these equations refers to a field mode having a Gaussian spatial profile, the second describes OAM-carrying Laguerre-Gauss beams. We assume that the beam-waist $\mathcal{W}$ is larger than any linear dimension

of the BECs so that the Gaussian part of the function reduces to a constant. This approximation also ensures the collective nature of the interaction between the fields and the atoms belonging to a given BEC. The last term in $\hat{H}$ describes the coupling between the classical pumps and the BECs

$$\begin{aligned}\hat{H}_{ap} = \sum_{I=A,B} \Bigg( & \hbar\Omega_I e^{-i\omega_I t} \int_{\mathcal{V}_I} d\mathbf{r}\, \hat{\psi}^{\dagger}_{I,e}(\mathbf{r}) \hat{\psi}_{I,l}(\mathbf{r}) e^{i\mathbf{k}_I\cdot\mathbf{r}} \\ & + \hbar\Omega_I e^{-i\omega_I t} \int_{\mathcal{V}_I} d\mathbf{r}\, \hat{\psi}^{\dagger}_{I,e'}(\mathbf{r}) \hat{\psi}_{I,-l}(\mathbf{r}) e^{i\mathbf{k}_I\cdot\mathbf{r}} \Bigg) + h.c.\,.\end{aligned} \tag{3.20}$$

The coefficients $\Omega_I$ are the Rabi frequencies for the matter-pump interactions. Moreover, we initially prepare each condensate in the atomic state $|0\rangle$ by means of optical pumping techniques, for instance, in such a way that the excited triplet can be considered as empty.

We now proceed with the adiabatic elimination of the excited states under the assumption of large single-photon detunings $\Delta$ and $\Delta_0$ (with respect to the typical coupling rates entering $\hat{H}_{aa}$, $\hat{H}_{ad}$ and $\hat{H}_{ap}$). We take the time evolution due to the fields as faster than the center of mass motion of the atom when in one of the excited levels, so that we can neglect the free atomic Hamiltonian for these states. We move to a proper rotating frame where we redefine the excited-state (ground-state) matter field operators as $\hat{\psi}_{I,e} = \hat{\tilde{\psi}}_{I,e} e^{-i\omega_l t}$, $\hat{\psi}_{I,e'} = \hat{\tilde{\psi}}_{I,e'} e^{-i\omega_{-l} t}$ and $\hat{\psi}_{I,E} = \hat{\tilde{\psi}}_{I,E} e^{-i\omega_0 t}$ ($\hat{\tilde{\psi}}_{I,k} = e^{-i\omega_I t}\hat{\psi}_{I,k}$) and the photonic operators as $\hat{\tilde{c}}_{I,k}(t) = e^{i\omega_I t}\hat{c}_{I,k}$ (with $k = 0, \pm l$). Following the works by Marzlin et al. [68] and Kapale and Dowling [70], we explicitly allow for two-photon Raman detunings $\delta_{\pm l}(t) = \omega_l - \omega_p(t) - \tilde{\omega}_{\pm l}$ (see Fig. 3.2), which help in the stabilization of the transfer process (see also Ref. [69]). Here $\hbar\tilde{\omega}_{\pm l}$ are the actual energies of the rotating atomic states. In fact, one can intuitively understand the necessity for a time-dependent two-photon detuning as a result of the adiabatic elimination of the excited triplet and the existence of inter-atomic collisions, which change the energies of the atom in time. Therefore, in order to achieve efficient transfer of OAM entanglement, we need a "chirped" frequency of the pump fields that allows to track and compensate the change of the energy levels. The field operators are given by:

$$\begin{aligned}
\hat{\tilde{\psi}}_{I,E}(\mathbf{r}) &= \frac{\chi_{I,0}\mathscr{A}_{n_I,0}(\mathbf{r})}{\hbar\Delta_{I,0}}\, e^{i\omega_0 t}\, \hat{c}_{n_I,0}\, \hat{\psi}_{I,0}(\mathbf{r}), \\
\hat{\tilde{\psi}}_{I,e}(\mathbf{r}) &= \frac{\Omega_I}{\Delta_I}\, e^{i\mathbf{k}_I\cdot\mathbf{r}} e^{-i(\omega_I-\omega_l)t}\, \hat{\psi}_{I,l}(\mathbf{r}) + \frac{\chi_{I,l}\mathscr{A}_{n_I,l}(\mathbf{r})}{\hbar\Delta_I}\, e^{i\omega_l t}\, \hat{c}_{n_I,l}\, \hat{\psi}_{I,0}(\mathbf{r}), \\
\hat{\tilde{\psi}}_{I,e'}(\mathbf{r}) &= \frac{\Omega_I}{\Delta_I}\, e^{i\mathbf{k}_I\cdot\mathbf{r}}\, e^{-i(\omega_I-\omega_{-l})t}\, \hat{\psi}_{I,-l}(\mathbf{r}) + \frac{\chi_{I,-l}\mathscr{A}_{n_I,-l}(\mathbf{r})}{\hbar\Delta_I}\, e^{i\omega_{-l} t}\, \hat{c}_{n_I,-l}\, \hat{\psi}_{I,0}(\mathbf{r}),
\end{aligned} \tag{3.21}$$

where we have defined the single photon detunings $\Delta_{I,0} = \omega_0 - \omega_{I,E}$, $\Delta_I = \omega_l - \omega_{I,e}$. In order to explicitly include the chirped two-photon Raman detunings, which are crucial in the stabilization of the transfer process, we define new field operators in a rotating frame defined by the Hermitian operator $\hat{O} = \sum_{I,k} \omega_I \left( \hat{\psi}^\dagger_{I,k}(\mathbf{r},t)\hat{\psi}_{I,k}(\mathbf{r},t) - \hat{c}^\dagger_{n_I,k}\hat{c}_{n_I,k} \right)$. Explicitly $\hat{\tilde{\psi}}_{I,k}(\mathbf{r},t) = e^{i\hat{O}t}\hat{\psi}_{I,k}(\mathbf{r},t)e^{-i\hat{O}t} = e^{-i\omega_I t}\hat{\psi}_{I,k}(\mathbf{r},t)$, while the photonic operators become $\hat{\tilde{c}}_{n_I,k} = e^{i\hat{O}t}\hat{c}_{n_I,k}e^{-i\hat{O}t} = e^{i\omega_I t}\hat{c}_{n_I,k}$.

Defining the free Hamiltonians $H_0^{I,k} = -\hbar^2\nabla_I^2/(2m) + V_{I,k}(\mathbf{r})$ and with the help of Eqs. (3.21) we finally get

$$
\begin{aligned}
i\hbar\frac{d}{dt}\hat{\tilde{\psi}}_{I,0}(\mathbf{r}) \;=\; & \Bigg[\hat{H}_0^{I,0} + \hbar\omega_I + \sum_j \eta^I_{j,0}\hat{\tilde{\psi}}^\dagger_{I,j}(\mathbf{r})\hat{\tilde{\psi}}_{I,j}(\mathbf{r}) + \frac{\chi^2_{I,0}|\mathscr{A}_{n_I,0}(\mathbf{r})|^2}{\hbar\Delta_{I,0}}\hat{\tilde{c}}^\dagger_{n_I,0}\hat{\tilde{c}}_{n_I,0} \\
& + \frac{\chi^2_{I,l}|\mathscr{A}_{n_I,l}(\mathbf{r})|^2}{\hbar\Delta_I}\hat{\tilde{c}}^\dagger_{n_I,l}\hat{\tilde{c}}_{n_I,l} + \frac{\chi^2_{I,-l}|\mathscr{A}_{n_I,-l}(\mathbf{r})|^2}{\hbar\Delta_I}\hat{\tilde{c}}^\dagger_{n_I,-l}\hat{\tilde{c}}_{n_I,-l}\Bigg]\hat{\tilde{\psi}}_{I,0}(\mathbf{r}) \\
& + \frac{\Omega_{I,l}\chi^*_{I,0}}{\Delta_I}\mathscr{A}^*_{n_I,l}(\mathbf{r})e^{i\mathbf{k}_I\cdot\mathbf{r}}\hat{\tilde{c}}^\dagger_{n_I,l}\hat{\tilde{\psi}}_{I,l}(\mathbf{r}) + \frac{\Omega_I\chi^*_{I,-l}}{\Delta_I}\mathscr{A}^*_{n_I,-l}(\mathbf{r})e^{i\mathbf{k}_I\cdot\mathbf{r}}\hat{\tilde{c}}^\dagger_{n_I,-l}\hat{\tilde{\psi}}_{I,-l}(\mathbf{r}),
\end{aligned}
$$

$$
\begin{aligned}
i\hbar\frac{d}{dt}\hat{\tilde{\psi}}_{I,l}(\mathbf{r}) \;=\; & \Bigg[\hat{H}_0^{I,l} + \hbar(\omega_l - \delta_l - \tilde{\omega}_l) + \frac{\hbar|\Omega_I|^2}{\Delta_I} + \sum_j \eta^I_{j,l}\hat{\tilde{\psi}}^\dagger_{I,j}(\mathbf{r})\hat{\tilde{\psi}}_{I,j}(\mathbf{r})\Bigg]\hat{\tilde{\psi}}_{I,l}(\mathbf{r}) \\
& + \frac{\Omega^*_I\chi_{I,l}}{\Delta_I}\mathscr{A}_{n_I,l}(\mathbf{r})e^{-i\mathbf{k}_I\cdot\mathbf{r}}\hat{\tilde{c}}_{n_I,l}\hat{\tilde{\psi}}_{I,0}(\mathbf{r})
\end{aligned}
\tag{3.22}
$$

and

$$
i\hbar\frac{d}{dt}\hat{\tilde{c}}_{n_I,0} \;=\; \Bigg[ -\hbar\omega_I + \int_{\mathcal{V}_I} d\mathbf{r}\frac{\chi^2_{I,0}|\mathscr{A}_{n_I,0}(\mathbf{r})|^2}{\hbar\Delta_{I,0}}\hat{\tilde{\psi}}^\dagger_{I,0}(\mathbf{r})\hat{\tilde{\psi}}_{I,0}(\mathbf{r})\Bigg]\hat{\tilde{c}}_{n_I,0},
$$

$$
\begin{aligned}
i\hbar\frac{d}{dt}\hat{\tilde{c}}_{n_I,l} \;=\; & \Bigg[ -\hbar\omega_I + \int_{\mathcal{V}_I} d\mathbf{r}\frac{\chi^2_{I,l}|\mathscr{A}_{n_I,l}(\mathbf{r})|^2}{\hbar\Delta_I}\hat{\psi}^\dagger_{I,0}(\mathbf{r})\hat{\psi}_{I,0}(\mathbf{r})\Bigg]\hat{\tilde{c}}_{n_I,l} \\
& + \int_{\mathcal{V}_I} d\mathbf{r}\quad\frac{\Omega_I\chi^*_{I,l}}{\Delta_I}\mathscr{A}^*_{n_I,l}(\mathbf{r})e^{i\mathbf{k}_I\cdot\mathbf{r}}\hat{\tilde{\psi}}^\dagger_{I,0}(\mathbf{r})\hat{\tilde{\psi}}_{I,l}(\mathbf{r}).
\end{aligned}
\tag{3.23}
$$

From these expressions it is straightforward to define the effective interaction Hamiltonian

$$
\hat{H}_{eff} = \hat{\tilde{H}}_a + \hat{H}_{aa} + \hat{\tilde{H}}_{int} \tag{3.24}
$$

for the description of the adiabatic interaction between light and BECs, where

$$
\hat{\tilde{H}}_a = \sum_{I,j}\int_{\mathcal{V}_I} d\mathbf{r}\,\hat{\tilde{\psi}}^\dagger_{I,j}(\mathbf{r})\left(-\frac{\hbar^2}{2m}\nabla_I^2 + V_{I,j}(\mathbf{r}) + \epsilon_j(t)\right)\hat{\tilde{\psi}}_{I,j}(\mathbf{r}), \tag{3.25}
$$

$$\begin{aligned}\hat{\tilde{H}}_{int}=\sum_{I,k}\Bigg[&\hat{\tilde{c}}_{n_I,k}\int_{\mathcal{V}_I}d\mathbf{r}\mathscr{C}_{n_I,k}(\mathbf{r})\hat{\tilde{\psi}}^{\dagger}_{I,k}(\mathbf{r})\hat{\tilde{\psi}}_{I,0}(\mathbf{r})+h.c.\\&+\hat{\tilde{c}}^{\dagger}_{n_I,k}\hat{\tilde{c}}_{n_I,k}\int_{\mathcal{V}_I}d\mathbf{r}\frac{\chi^2_{I,l}|\mathscr{A}_{n_I,k}(\mathbf{r})|^2}{\Delta_I}\hat{\tilde{\psi}}^{\dagger}_{I,0}(\mathbf{r})\hat{\tilde{\psi}}_{I,0}(\mathbf{r})\Bigg]\\&+\sum_I\hat{c}^{\dagger}_{n_I,0}\hat{\tilde{c}}_{n_I,0}\int_{\mathcal{V}_I}d\mathbf{r}\frac{\chi^2_{I,0}|\mathscr{A}_{n_I,0}(\mathbf{r})|^2}{\Delta_{I,0}}\hat{\tilde{\psi}}^{\dagger}_{I,0}(\mathbf{r})\hat{\tilde{\psi}}_{I,0}(\mathbf{r}).\end{aligned}\tag{3.26}$$

In Eq. (3.25) $j=0,\pm l$ should be taken, while in Eq. (3.26) it is $k=\pm l$. Moreover, we have introduced the coupling coefficient $\mathscr{C}_{n_I,k}(\mathbf{r})=(\hbar\Omega^*_I\chi_{I,k}/\Delta_I)\mathscr{A}_{n_I,k}(\mathbf{r})e^{-i\mathbf{k}_I\cdot\mathbf{r}}$ and the energies $\epsilon_j(t)$ such that $\epsilon_0(t)=\hbar\omega_I$ and $\epsilon_{\pm l}(t)=\hbar(\omega_{\pm l}-\delta_{\pm l}(t)-\tilde{\omega}_{\pm l})$. The term describing inter-particle collisions $\hat{H}_{aa}$ remains identical to Eq. (3.17). The interpretation of the form taken by $\hat{H}_{eff}$ is straightforward. While Eq. (3.25) describes the energy of non-interacting matter part of the system, modified by the introduction of $\delta_{\pm}$-related terms, Eq. (3.26) accounts for the light-matter interaction and includes the dynamical a.c. Stark shift effect arising from the adiabatic elimination. In particular, the first term in $\hat{\tilde{H}}_{int}$ describes a three-mode interaction where photonic excitations are used in order to perform an atomic transition between ground-triplet states. This is the key to our analysis on OAM entanglement transfer and the starting point of our quantitative study.

## 3.6 Three-mode expansion and light-induced transfer of OAM entanglement

### 3.6.1 Bosonic-mode expansion

In order to detail the ideas and discuss an experimentally relevant case, we consider the anisotropic harmonic trap potential $V_I(r,z)=(m/2)(\omega_r^2r^2+\omega_z^2z^2)$ for each of the BECs used in our proposal. Here $\omega_z$ ($\omega_r$) is the frequency of the trap along the longitudinal (radial) direction. In order to be able to neglect any longitudinal excitations, we assume $\omega_z\gg\omega_r$, so that each BEC is confined in a pancake-like structure. In the limit where the inter-atomic collisions are very small, the cylindrical symmetry of the problem allows us to describe the centre-of-mass of one atom in a BEC by means of the set of eigenstates ($\theta$ is the angular coordinate of a cylindrical reference frame)

$$\begin{aligned}\phi_{I,0}(r,z)&=\frac{1}{\pi^{\frac{3}{4}}a_r\sqrt{a_z}}e^{-\frac{1}{2}\left(\frac{r^2}{a_t^2}+\frac{z^2}{a_z^2}\right)},\\\phi_{I,\pm l}(r,z,\theta)&=\frac{1}{\sqrt{|l|!a_r^{|l|}}}r^{|l|}e^{\pm il\theta}\phi_{I,0}(r,z),\end{aligned}\tag{3.27}$$

with associated eigenvalues $E_l = \hbar\omega_z/2 + \hbar(|l|+1)\omega_r$. Here $a_{z,r}$ are the characteristic lengths of the harmonic ground state motion along the longitudinal and radial direction. The description provided by the eigenfunctions (3.27) remains valid under the assumption of dilute BECs, so that their ground states result from the simple tensor product of the single-particle states $\phi_{I,0}(r,z)$. This is a good approximation as long as $N^I a^I_{j,j'} \ll a_z$ [17], implying that the scattered part of the single-particle wavefunction contributes with only a small correction to the wave-function of the non-interacting case.

In order to provide a better picture of the anticipated three-mode interaction depicted in Eq. (3.26), we now define new bosonic operators $\hat{b}_{I,j}$ and $\hat{b}^\dagger_{I,j}$ for the matter-like part of our system as (omitting the tilde on the field operators for readability) $\hat{\psi}_{I,j}(\mathbf{r}) = \phi_{I,j}(\mathbf{r})\hat{b}_{I,j}$. By using the orthogonality of the $\phi_{I,j}(\mathbf{r})$ and the commutation relations valid for the $\hat{\psi}(\mathbf{r})$'s, it is straightforward to find that $[\hat{b}_{I,i}, \hat{b}^\dagger_{I,j}] = \delta_{i,j}$. Inserting these definitions into the effective Hamiltonian we obtain a much simplified and self-evident picture of the process through

$$\begin{aligned}
\hat{H}_a &= \sum_{I,k}(E_{I,0} + |k|\hbar\omega_r + \epsilon_k(t))\hat{b}^\dagger_{I,k}\hat{b}_{I,k}, \\
\hat{H}_{aa} &= \frac{1}{2}\sum_{I,j,j'}\xi^I_{j,j'}\hat{b}^\dagger_{I,j}\hat{b}^\dagger_{I,j'}\hat{b}_{I,j'}\hat{b}_{I,j}, \\
\hat{H}_{int} &= \sum_{I,k=l,-l}\left(g_{I,k}\hat{b}^\dagger_{I,k}\hat{b}_{I,0}\hat{c}_{n_I,k} + h.c.\right) \\
&\quad + \hat{b}^\dagger_{I,0}\hat{b}_{I,0}\sum_{I,k}\rho_{I,k}\hat{c}^\dagger_{n_I,k}\hat{c}_{n_I,k},
\end{aligned} \tag{3.28}$$

where each coefficient can be expressed in terms of the non-interacting wave-functions as shown in Table 3.1. The effect of the light-matter coupling is now manifest: besides the a.c. Stark shifts proportional to $\rho_{I,j}$, $\hat{H}_{int}$ consists of a scattering process at a rate $g_{I,k}$ where the annihilation (creation) of a photon of angular momentum $k$ is accompanied by the Raman transition $|0\rangle_I \to |k\rangle_I$ ($|k\rangle_I \to |0\rangle_I$). Such a mechanism, which would determine a perfect transfer of OAM from the light resource to the BECs, is *disturbed*

TABLE 3.1: Coupling rates in the effective Hamiltonian after the introduction of the effective matter-like bosonic operators [see Eqs. (3.28)] and their expressions in terms of the non-interacting atomic wave-function for a pancake-like potential.

| Coefficients | Corresponding expression |
|---|---|
| $E_{I,0}$ | $\int_{\mathcal{V}_I} d\mathbf{r}\phi^*_{I,0}(\mathbf{r})(-\frac{\hbar^2}{2m}\nabla^2_I + V_{I,j}(\mathbf{r}))\phi_{I,0}(\mathbf{r})$ |
| $g_{I,k}$ | $\int_{\mathcal{V}_I} d\mathbf{r}\mathscr{C}_{n_I,k}(\mathbf{r})\phi^*_{I,k}(\mathbf{r})\phi_{I,0}(\mathbf{r})$ |
| $\rho_{I,0}$ | $\int_{\mathcal{V}_I} d\mathbf{r}\frac{\chi^2_{I,0}\lvert\mathscr{A}_{n_I,0}(\mathbf{r})\rvert^2}{\Delta_{I,0}}\lvert\phi_{I,0}(\mathbf{r})\rvert^2$ |
| $\rho_{I,l}$ | $\int_{\mathcal{V}_I} d\mathbf{r}\frac{\chi^2_{I,l}\lvert\mathscr{A}_{n_I,l}(\mathbf{r})\rvert^2}{\Delta_I}\lvert\phi_{I,0}(\mathbf{r})\rvert^2$ |
| $\xi^I_{j,j'}$ | $\eta^I_{j,j'}\int_{\mathcal{V}_\mathcal{I}} d\mathbf{r}\lvert\phi_{I,j}(\mathbf{r})\rvert^2\lvert\phi_{I,j'}(\mathbf{r})\rvert^2$ |

by the inter-atomic collisions in $\hat{H}_{aa}$ and should also take into account the modifications induced by the dynamical shifts in $\hat{H}_{a,int}$. The creation of inter-BEC OAM entanglement is thus a trade-off between these various processes. The task of the next Subsection is precisely the quantitative assessment of such a trade-off. It is worth remarking here that, in virtue of the definitions of $\epsilon_k(t)$ the term $|k|\hbar\omega_r + \epsilon_k(t)$ appearing in the energy of the rotating states with $j = \pm l$ is explicitly dependent on the two-photon Raman detunings $\delta_k(t)$ and takes the form $\hbar(\omega_k - \delta_k - \tilde{\omega}_k + |k|\omega_r)$. When the interactions considered in our scheme are included, the energy levels are shifted so that the shift $\tilde{\omega}_k - |k|\omega_r \neq 0$ is in general non-zero and, possibly, time-dependent. In what follows, we shall assume that such shift occurs linearly in time.

### 3.6.2 Entanglement transfer process

As discussed in Sec. 3.5, we assume an initial preparation where the atomic excited triplet is empty and all atoms in each BEC populate $|0\rangle_I$. We indicate such a collective atomic state as $|N_0^I\rangle_I$, which condenses information on the population of level $|0\rangle_I$ and $|\pm 1\rangle_I$. On the other hand, the OAM-entangled photonic resource is assumed to be prepared in the state $|\Phi_Z\rangle_{\alpha\beta} = (1/\sqrt{3})(|1_0, 1_0\rangle_{\alpha\beta} + |1_1, 1_{-1}\rangle_{\alpha\beta} + |1_{-1}, 1_1\rangle_{\alpha\beta})$. In Refs. [61, 62] it was shown that two-photon multidimensional OAM-entangled states generated by means of SPDC can be effectively distilled into states very close to $|\Phi_Z\rangle_{\alpha\beta}$, thus making the contributions coming from states having higher OAM negligible. Moreover in ref. [63] it has been shown that entangled photon pairs can be produced in an heralded way. By means of continuously pumped cavity-enhanced SPDC, which is a customary method for the generation of photonic resources for atomic memories and quantum repeaters, one can have highly-monochromatic twin-beam states in spatially distinct single-photon wave-packets carrying the desired value of angular momentum. Such states can be treated, for all practical purposes, as plane waves in our calculations. However, it is straightforward to adapt our formalism to the case of pulsed SPDC by making the Rabi frequencies appearing in $\hat{H}_{eff}$ explicitly time dependent, so as to incorporate the form of the photonic wave-packet. This effectively makes the Hilbert space spanned by photonic OAM states isomorphic to that of a spin$-1$ particle, or *qutrit*, so that $|\Phi_Z\rangle_{\alpha\beta}$ describes a maximally entangled two-qutrit state. The initial state is thus taken to be $|\Psi(0)\rangle_{AB\alpha\beta} = |N_0^A, N_0^B\rangle_{AB}|\Phi_Z\rangle_{\alpha\beta}$, whose dynamics under Eqs. (3.28) is now evaluated in a rotating frame defined according to Eqs. (3.22),(3.23). It is straightforward to verify that, when starting from $|\Psi(0)\rangle_{AB\alpha\beta}$ as given above, the evolved state $|\Psi(t)\rangle_{AB\alpha\beta}$

obtained upon use of the effective Hamiltonian in Eq. (3.28) lies entirely in a nine-dimensional sector of the Hilbert space spanned by the states

$$
\begin{aligned}
|\Psi_0\rangle &= |N_0^A\rangle_A|N_0^B\rangle_B|1_0\rangle_\alpha|1_0\rangle_\beta,\\
|\Psi_1\rangle &= |N_0^A\rangle_A|N_0^B\rangle_B|1_1\rangle_\alpha|1_{-1}\rangle_\beta,\\
|\Psi_2\rangle &= |N_0^A\rangle_A|N_0^B\rangle_B|1_{-1}\rangle_\alpha|1_1\rangle_\beta,\\
|\Psi_3\rangle &= |N_0^A-1,1_1\rangle_A|N_0^B\rangle_B|0\rangle_\alpha|1_{-1}\rangle_\beta,\\
|\Psi_4\rangle &= |N_0^A-1,1_{-1}\rangle_A|N_0^B\rangle_B|0\rangle_\alpha|1_1\rangle_\beta,\\
|\Psi_5\rangle &= |N_0^A\rangle_A|N_0^B-1,1_1\rangle_B|1_{-1}\rangle_\alpha|0\rangle_\beta,\\
|\Psi_6\rangle &= |N_0^A\rangle_A|N_0^B-1,1_{-1}\rangle_B|1_1\rangle_\alpha|0\rangle_\beta,\\
|\Psi_7\rangle &= |N_0^A-1,1_1\rangle_A|N_0^B-1,1_{-1}\rangle_B|0\rangle_\alpha|0\rangle_\beta,\\
|\Psi_8\rangle &= |N_0^A-1,1_{-1}\rangle_A|N_0^B-1,1_1\rangle_B|0\rangle_\alpha|0\rangle_\beta.
\end{aligned}
\tag{3.29}
$$

The notation used here is such that $|N_0^I - s, s_k\rangle_I$ indicates a state where $s$ atoms populate an atomic eigenstate of the angular momentum with eigenvalue $k\hbar$ while $N_0^I - s$ atoms populate the state $|0\rangle_I$ having zero OAM. It is worth stressing that the number and structure of the states involved in the evolution of a given initial state strongly depends on the total initial angular momentum carried by the latter. In fact, our effective Hamiltonian preserves the total light-matter OAM. This property implies that the dynamically evolved state of the system should be written as

$$
|\Psi(t)\rangle_{AB\alpha\beta} = \sum_{i=0}^{8} f_i(t)|\Psi_i\rangle \tag{3.30}
$$

with numerical coefficients $f_i(t)$ such that $\sum_i |f_i(t)|^2 = 1$.

The analytic solution of such a dynamics is a formidable problem and we thus resort to a numerical investigation in order to infer the behavior of $f_i(t)$'s. To find the coefficients $\{f_i(t)\}$, we have numerically solved the Schrödinger equation using the Hamiltonian in Eqs. (3.28). We have explored a wide range of parameters, including the case where the system is symmetric under the exchange of the two BECs, finding qualitatively similar results. In the following, we concentrate on the symmetric case and use the parameters listed in the caption of Fig. (3.3), which shows that a complete transfer of OAM from the photonic state to the BECs is possible, in analogy with the semiclassical case approached in Refs. [68–70].

The (dashed) green curve shows the temporal dynamics of the probabilities $|f_{1,2}(t)|^2$ whereas the (solid) yellow ones depict $|f_{7,8}(t)|^2$ for a given set of the relevant physical

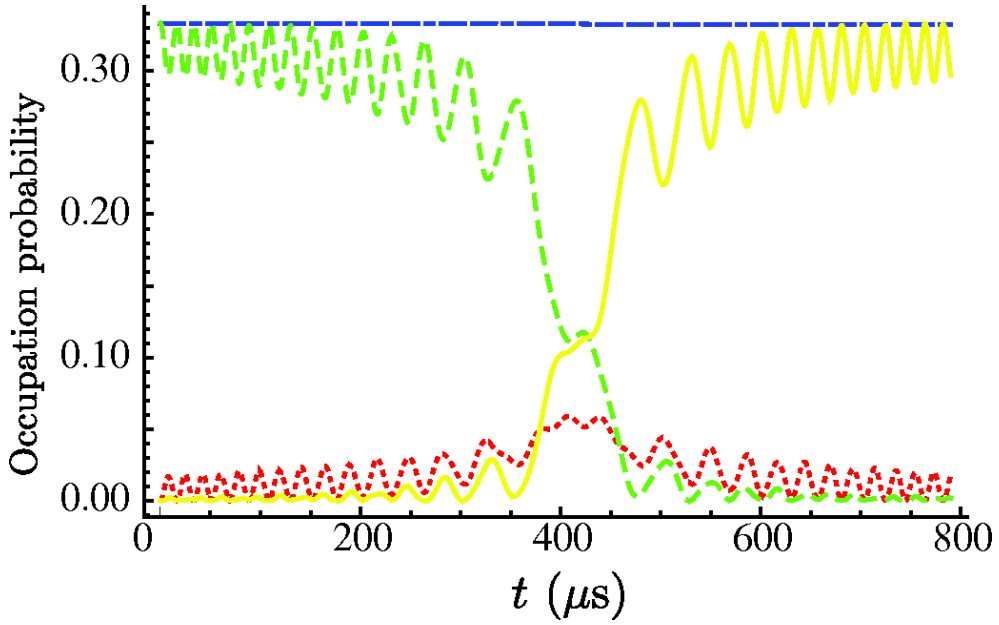



FIGURE 3.3: Evolution of the state probabilities $|f_i(t)|^2$ against the interaction time $t$ (in $\mu$s) for $N_0^I = 10^5$ atoms per condensate. Here $f^I_{j,j'} = 5nm$, $\Omega_I = 27.5$kHz, $\chi_{I,\pm l} = 1.18$kHz, $\Delta = 90$kHz and the two-photon detunings having the functional form $\delta_{\pm l}(t) = 2\Omega_I(1 - \Omega_I t/2) - \omega_t$. The trap frequencies are $\omega_t = 70$Hz and $\omega_z = 500$Hz. The photonic resource is tailored at a wavelength of 702nm at an angle of $4^o$ off the initial pumping gaussian beam's axis

parameters and a specific choice for the functional form of the chirped two-photon detunings. These two sets of probabilities are almost mutually mirror symmetric. Damped oscillations are superimposed to a monotonic behavior induced by the compensation arising from the chirped detunings (in our case $\delta_{\pm l}(t) = 2\Omega_I(1 - \Omega_I t/2) - \omega_t$). The low-lying (dotted) red curve is for $|f_{3,4,5,6}|^2$, whose corresponding states only marginally contribute to the evolution of the system. Finally, the (dot-dashed) horizontal blue line shows the probability $|f_0(t)|^2$, which does not change in time as $|\Psi_0\rangle$ is an eigenstate of the effective Hamiltonian. As we shall see this gives a lower limit for the population of the ground state of the reduced density matrix for the two BECs. In fact a plot of the populations of the BECs reduced density matrix, $\rho_{AB}(t) = \mathrm{Tr}_{\alpha\beta}(|\Psi(t)\rangle_{AB\alpha\beta}\langle\Psi(t)|)$ shows that the state $|N_0^A\rangle_A|N_0^B\rangle_B$ has always a finite occupation probability. This is due to the unavoidable presence of photons carrying no OAM that continuously project the two BECs onto their ground states. The (solid) yellow curve in Fig. 3.4 shows the population of the state $|B\rangle = (|N_0^A{-}1, 1_1\rangle|N_0^B{-}1, 1_{-1}\rangle + |N_0^A{-}1, 1_{-1}\rangle|N_0^B{-}1, 1_1\rangle)/\sqrt{2}$ (we have omitted the BEC label as no ambiguity exists) which shows OAM entanglement between the BECs. Clearly, the OAM entanglement transfer generates quite a large component of $|B\rangle$ in the reduced two-BEC state. This arises from the OAM-carrying components in the photonic resource and the efficiency of the population-transfer process. The introduction of this state allows us to draw a clear and compact picture of the asymptotic form of the map $\hat{\mathcal{M}}_t$ transforming photonic OAM entanglement into

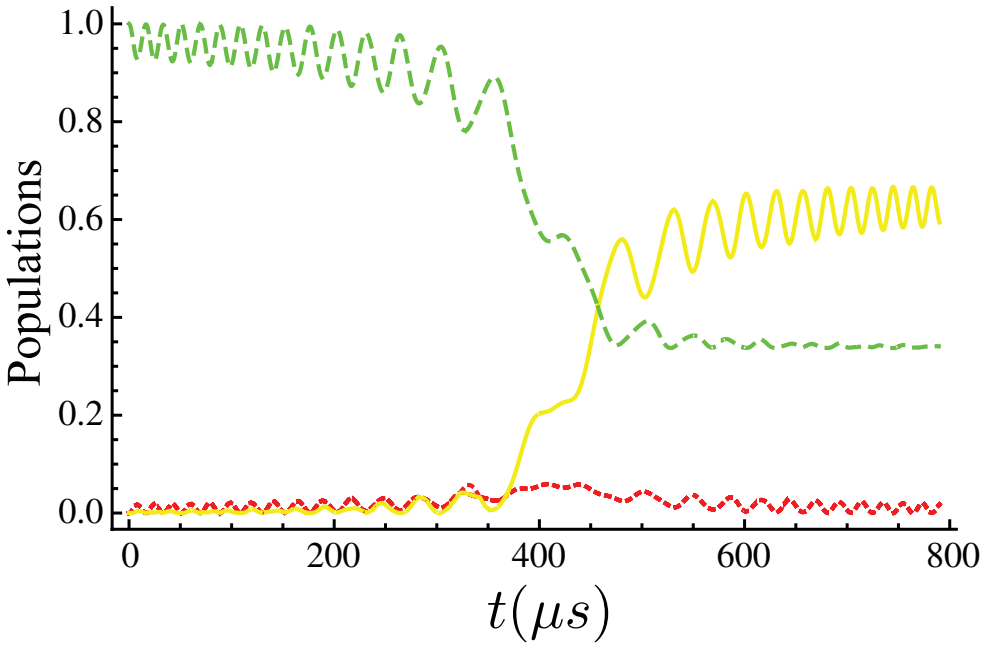



FIGURE 3.4: Time behavior of the populations of the atomic states in $\rho_{AB}(t) = \mathrm{Tr}_{\alpha\beta}(|\Psi(t)\rangle_{AB\alpha\beta}\langle\Psi(t)|)$. The same parameters as in Fig. 3.3 have been used here. The (dashed) green curve is for $|N_0^A, N_0^B\rangle_{AB}$, the (solid) yellow one is for state $|B\rangle$. The low-lying (dotted) red curves represent the probability that the remaining two-BEC basis states are excited. The incomplete population transfer from $|0\rangle_I$ to $|\pm l\rangle_I$ $(I = A, B)$ is due to the zero-OAM terms in $|\Phi_Z\rangle_{\alpha\beta}$.

matter-like one via bi-local far off-resonant double Raman coupling. By neglecting the very small components associated with the remaining excited two BEC states ((dotted) red line in Fig. 3.4) and collecting the remaining terms into a diagonal density matrix, this is approximately given by

$$\begin{aligned} &\lim_{t\to\infty} \hat{\mathcal{M}}_t(|N_0^A, N_0^B\rangle_{AB}\langle N_0^A, N_0^B|) \\ &\simeq \frac{1}{3}(2|B\rangle_{AB}\langle B| + |N_0^A, N_0^B\rangle_{AB}\langle N_0^A, N_0^B|), \end{aligned} \tag{3.31}$$

Such a formal asymptotic map also explains that we can formally infer the properties of the reduced two-vortex density matrix by treating it as the state of two (in general entangled) qutrits.

### 3.6.3 Assessment of entanglement

We are now in a position to quantitatively estimate the amount of vortex entanglement set between the BECs. In order to tackle this point, our approach will be twofold. First, we study the time evolution of the *linearized entropy* [77]

$$S_L(\rho_{AB}(t)) = (9/8)[1 - \mathrm{Tr}(\rho_{AB}(t))], \tag{3.32}$$

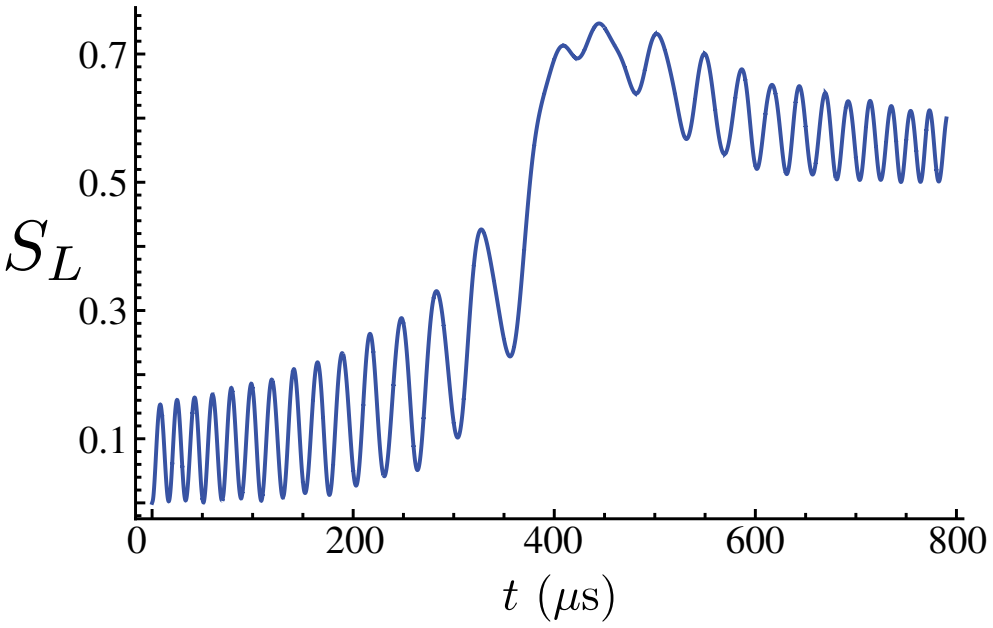



FIGURE 3.5: Linear entropy $S_L(\rho_{AB})$ against time $t$ (units of $\mu$s). The same parameters as in Fig. 3.3 have been used here.

of the BEC density matrix. As $S_L$ is a good measure of the purity of a state (it achieves 0 for perfectly pure states and 1 for statistical mixtures), this will give us an indication of the residual entanglement set between the photonic and matter-like part of the system: as the dynamics set by $\hat{H}_{eff}$ is unitary, the entanglement initially present in the photonic state has to be conserved when the whole state of the matter-light system is considered. Needless to say, such entanglement can be transferred from the photonic subsystem to the atomic one and/or vice versa and a transient can well exist where the two are almost separable. Such a situation would be witnessed by a small value of $S_L$ and correspond to either large or small values of BEC entanglement, with minimal photon-atom quantum correlations. We have determined the form of $S_L$ as a function of time, which is shown in Fig. 3.5. As expected, at exactly the time when the populations of the OAM carrying atomic system become non-zero, the linear entropy changes its behavior, signaling a maximum of mixedness of the light-matter state. This simply implies that for $t \in [400, 500]\mu$s the two subsystems are correlated in a nonclassical sense. If time increases further, $S_L$ evidently decreases, witnessing a reduction in the light-matter entanglement. Because of the conservation of entanglement discussed above, this is the region we are interested in, as it could well be the case that in this long-time window significant inter-vortex entanglement is set at the expenses of the initial all-optical one and the transient matter-light correlations highlighted here.

We quantitatively confirm our expectations by studying the *negativity* [78, 79], an entanglement measure based on the violation of the "positivity of partial transposition"

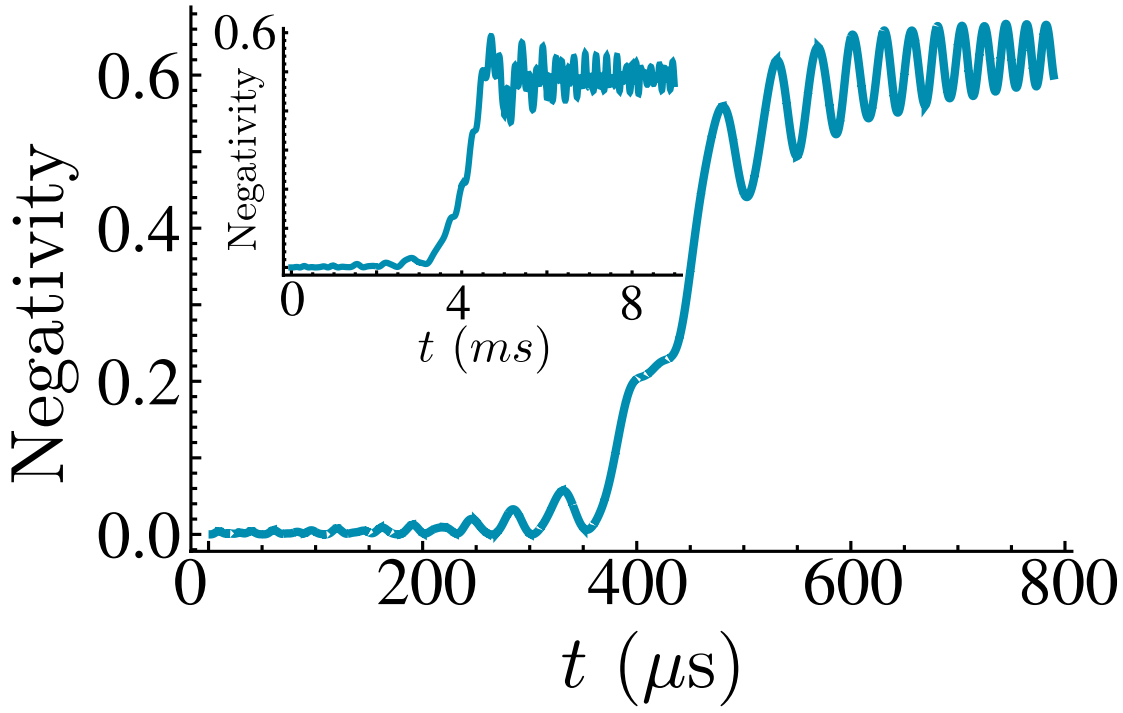



FIGURE 3.6: Negativity $N(\rho_{AB})$ against the interaction time $t$ (units of $\mu$s). The same parameters as in Fig. 3.3 have been used here. We obtain a maximum of entanglement in correspondence of the range of decreasing trend of $S_L(\rho_{AB}(t))$, which witnesses a larger purity of the two-vortex state and smaller quantum correlations between light and matter. Inset: Negativity against $t$ for $N_0^A = 10N_0^B = 10^4$ and $\Omega_B = 10\ \Omega_A = 27.5$ kHz. Other parameters as in Fig. 3.3.

(PPT) criterion for separability of a state. Negativity is defined as [79]

$$N(\rho_{AB}(t)) = -2\sum_k \lambda_k^-, \tag{3.33}$$

where $\lambda_k^-$ are the negative eigenvalues of the partially transposed density matrix with respect to one of the BEC systems. The results are shown in Fig. 3.6. As expected, the region of large inter-vortex entanglement corresponds to the range of interaction times where the linearized entropy decreases towards a steady-state value.

We point out that the wavy behaviour of the curve in Fig. 3.6, as well as in the other plots of the paper, is due to the inter-atomic scattering. This is confirmed by the plot shown in the inset of the figure, where an asymmetric case has been studied. The comparison between symmetric and asymmetric case shows that a mismatched number of atoms in the two BECs results in a change in the oscillatory behavior of the curve describing the time evolution of the transferred entanglement. On the other hand, mismatched Rabi frequencies only determine a change in the temporal scale of the entanglement dynamics.

The degree of transferred entanglement is only mildly affected, which demonstrates the robustness of our protocol to such effects. The efficiency of our protocol does not depend

on the assumption of symmetry under the exchange of the condensates and is retained in a wide range of the relevant parameters. Therefore, for the sake of convenience and without affecting the generality of our results, in what follows we restrict our attention to the symmetric case. As discussed above, quite a large value of entanglement is set between the vortex states of the two condensates, although a maximally entangled state [achieving $N(\rho_{AB}) = 1$] is not reached. We stress that this is not a limitation of our scheme but, on the contrary, an effect of the zero-OAM component in the photonic resource $|\Phi_Z\rangle_{\alpha\beta}$. Such a detrimental contribution can be removed from the BECs reduced state (and its properties) by resorting to an "active" approach where, instead of discarding the state of light after the interaction with the condensates, we properly *post-select* its state. Upon inspection of $|\Psi_{7,8}\rangle$ in Eqs. (3.29), it is straightforward to see that state $|B\rangle_{AB}$ is associated with modes 1 and 2 in the vacuum state. On the other hand, the *entanglement-spoiling* component $|n_0^A, n_0^B\rangle_{AB}$ would bring about photons in both the modes. It is therefore sufficient to use a standard Geiger-like avalanche photo-detector per mode, which discriminate the vacuum from the presence of any non-zero number of photons in a field, in order to operate the optimal post-selection of the BECs state: by registering no click at both the photo-detectors, we project the state of $A$ and $B$ onto the maximally entangled state $|B\rangle$. It is in fact worth stressing that, by effectively excluding the possibility that the atoms occupy state $|0\rangle_I$, the post-selection procedure further reduces the dimension of the relevant Hilbert space spanned by each vortex state to a bidimensional one, thus leaving us with two effective qubits.

## 3.7 Detection of vortex entanglement

In this Section we describe a method for the detection of the vortex entanglement created by the process above. Given the low-excitation level of our protocol, the usual matter-wave interference is not helpful and we instead propose an approach based on the inversion of the process addressed here for light-to-BEC entanglement transfer. After generation of a two-vortex entangled state (as described in Sec. 3.6), the OAM-transferring interaction should be stopped. We thus assume that the pump fields have been turned off (or set far off-resonant with respect to the frequency of the transitions they guide) so as not to perturb the entangled states of the vortices. The time-reversal nature of our protocol makes it intuitive to understand that, if we now reinstate such pumps, photons will be scattered into two Laguerre-Gauss modes at the frequency of the $|0\rangle_I \leftrightarrow |e, e'\rangle$ transition, thus *writing back* the two-vortex state onto light fields. One can then apply state-property reconstruction techniques, including testing Bell's inequality violation for bipartite states of effective three-level particles [81].

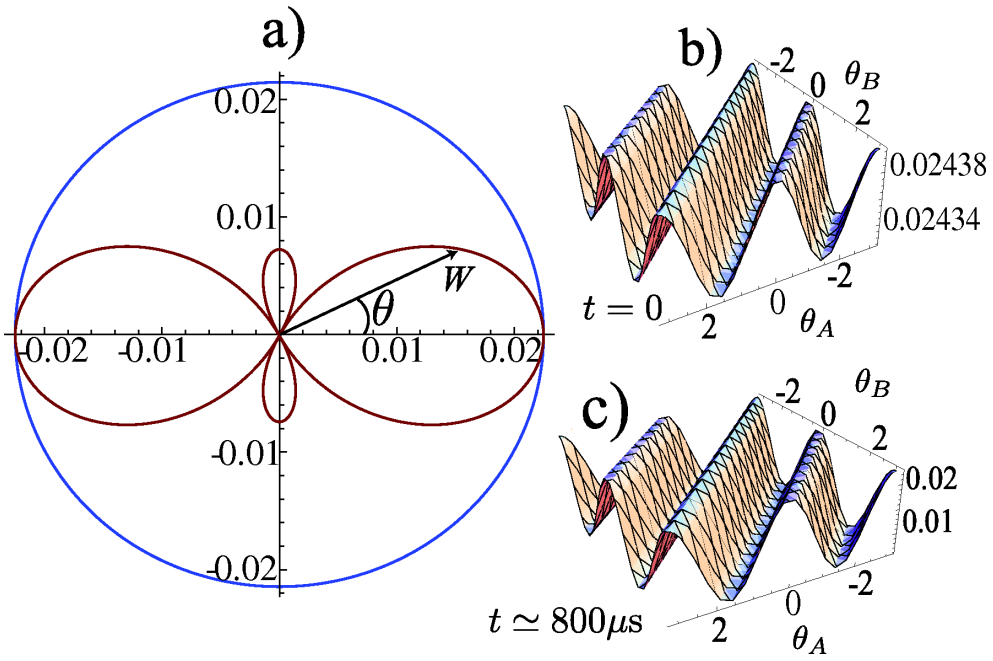



FIGURE 3.7: Analysis of the Wigner function for $\rho_{AB}(t)$. **(a)**: The blue circle shows a projection the Wigner function on the unit circle for $t = 0$, while the red butterfly structure is associated with $t \simeq 800\mu$s, where OAM entanglement has been transferred. **(b)** and **(c)**: We plot $W_{0,0}(\theta_A, \theta_B)$ at the two instants of time considered for panel **(a)**. Notice the different vertical-axis scales in the two plots. The visibility of the fringes of interference in the Wigner function is an indication of quantum correlations.

However, the success of such tests is usually very sensitive to the form of the state under scrutiny and the level of non-ideality affecting it. We thus resort to a specific and quite promising way to infer the properties of the state we have generated based on Wigner function reconstruction, which is possible by using computer generated holograms [61] and homodyne-like measurements [82]. Theoretically, the Wigner function for the OAM state of a photon has been defined in the discrete cylinder $\mathbb{Z} \times C_1$ ($C_1$ is the unitary circle) representing the phase space for the OAM operator and its canonically conjugate operator $\hat{\theta}$. In Ref. [80] it has been shown that the study of the Wigner function for an OAM state gives information both on the various OAM eigenstates involved in the description of the state and on their relative phase. We define the two-mode Wigner function as

$$W_{l_A,l_B}(\theta_A, \theta_B) = \mathrm{Tr}[\hat{K}_{l_A}(\theta_A) \otimes \hat{K}_{l_B}(\theta_B)\rho_{AB}], \tag{3.34}$$

where we have introduced the kernel $\hat{K}_{l_I}(\theta_I)$ ($I = A, B$) mapping quantum states in phase space [80] in a way completely analogous to the continuous position-momentum phase space. In Fig. 3.7 **a)** we compare the Wigner function $W_{0,0}(\theta, 0)$ associated with $\rho_{AB}(t)$ when the entanglement transfer has not occurred [wide blue circle] to what is achieved at long-enough $t$, where the map $\hat{\mathcal{M}}_t$ has been implemented [inner (red) butterfly-like structure]. The difference due to the coherence established between two-mode orthogonal eigenstates of the OAM operator in the entangled state $\rho_{AB}$ is striking.

Moreover, from Fig. 3.7 **b)** and **c)**, we find that $W_{0,0}(\theta_A, \theta_B)$ exhibits oscillations whose amplitude depends on the relative phase between the states $|B\rangle$ and $|D\rangle$. The curves shown in panels **b)** and **c)** are associated with the same interaction time as in the circular and burtterfly-like structures shown in panel **a)**, respectively, which demonstrates that the oscillation amplitudes depend on the populations of these states. Remarkably, the analysis of $W_{l_A,l_B}(\theta_A, \theta_B)$ for incoherent superpositions of OAM eigenstates results in a flat distribution. Therefore, by experimentally reconstructing the Wigner function, one can determine the inference of entanglement in the associated OAM state. Any deviation from flat distributions typical of incoherent superpositions implies coherence in the bipartite state, although not entanglement. Methods based on the inverse Radon transform [83] could then be used in order to achieve full information on the state and, eventually, the entanglement set by the transfer mechanism. It is thus possible to know if the two BECs are entangled by comparing their Wigner function with the one of an inchoerent states which turn out to be a simple flat distribution.

## 3.8 Conclusions and outlook

We have shown that vortex states of spatially remote, non-isotropically trapped BECs can be entangled by means of bilocal OAM-transfer processes and quantum correlated photonic resources. The amount of vortex entanglement set by our scheme can be quite considerable and appears to be limited only by the zero-OAM carrying component in the photonic resource. While such a bottleneck can be actively bypassed by means of post-selection, as described in Sec. 3.6, we are currently working on a modification of our protocol based on the use of other forms of the entangled photon-pair [84]. The difference between the two-vortex state achieved by our scheme and a classical admixture of OAM eigenstates (without coherence and, thus, entanglement) can be revealed by a straigthforward *state-retrieval* process and the reconstruction of the OAM-state Wigner function. We believe that the superfluid phase of a BEC, together with virtually frictionless rotational states of light-induced vortices, can be reliably exploited in order to set a promising scenario for the storage of quantum information and the distribution of quantum correlated channels for communication.

The work presented in this chapter has been done in collaboration with S. McEndoo, Th. Busch and M. Paternostro and it has been published in Phys. Rev. A **81**, 053625 (2010).

# Chapter 4

# Detection of quantum coherence by means of a BEC

In this chapter we address the problem of revealing quantum coherences in the dynamics of a (micro/nano) mechanical oscillator. The motivation behind this work are to be found in the recent efforts of reaching the quantum regime for mechanical oscillators in both the opto-mechanical and electromechanical framework. It is then of great importance to be able to detect quantum coherence in the state of the oscillator in order to assess whether the quantum regime has been reached. We start by giving a brief overview of the physics of mechanical oscillators. As the topic is quite wide and since it is not the purpose of this chapter to cover it all, we shall focus on the aspects relevant for our discussion. In particular we focus on the fabrication methods and discuss the basic concepts behind techniques to "cool down" a micro/nano oscillator. We then present our contribution to the topic of coherence detection by considering a particular experimental set up. We propose a scheme which exploits all available and well tested techniques, therefore making our proposal a feasible one.

## 4.1 Introduction

The start of the era of miniaturization can be traced back to the invention of the transistor. From then on we pushed our technology to smaller and smaller scales; we went from room-sized computers to current notebooks that are smaller in dimension and many times faster in computation. Nevertheless there are physical impediments to a further reduction of the dimensions of the components. The most important comes from quantum effects becoming manifest at those scales. On the other hand the need for micro and nano devices helps us in understanding the "small" world and in particular about its

counter intuitive behavior as described by quantum mechanics. We also want to know how our classical world emerges from the quantum realm. One way of doing it is to increase the size of current quantum objects and investigate them to the border of the classical realm.

The two approaches, top-bottom and bottom-up, have an intersection: the micro/nano mechanical oscillators. Mechanical oscillators play a key role in science having a broad range of applicability: from detection and analysis of molecular dynamics [85] to elements of atom chips for ultra cold gases trapping [86], from the imaging of surface [87] to being part of "quantum circuits" [88]. The geometry of these objects is quite wide; there are cantilevers, single and double clamped [89], drums [90], membranes [91], pianos [92]. Each of them is designed to accomplish a particular task.

Recently, a considerable research effort has been put in achieving quantum control of micro and nano-scale mechanical systems [93, 114, 115]. The role played by such objects in the current quest for demonstrating quantum behavior at the mesoscopic scale has changed in time, and these systems are now at the center of an extensive experimental and theoretical research effort.

Being three dimensional objects, mechanical oscillators support different "modes" exactly as their macroscopic counterparts. So that a (micro/nano) mechanical oscillator can bend, twist, breath or perform any other movement its design allows it. Addressing and controlling these modes is the first step towards making these systems useful for quantum technologies. New techniques have been developed and the old ones have been improved such as electron beam lithography, chemical etching, optical lithography, vapor deposition, and many more.

To manipulate, control and extract information out of these mechanical oscillators electrical and optical means are usually used. In the first case the oscillators are part of an electric circuit through which it is possible to control or read out its state. They are called micro/nano electro mechanical systems (MEMS/NEMS). In the case of optical interfaces the control and the read out are accomplished via exerting radiation pressure and measuring the phase shift of scattered light. They are referred to as opto-mechanical systems. A beautiful example of an opto-mechanical system is the atomic force microscope (AFM) [94] which is able to "take pictures" of single atoms on surfaces. A light beam scatters off the free standing edge of a cantilever which is displaced by the repulsion of the scanned surface. The displacement turns into a phase shift of the reflected light; the amount of the shift is related to the strength of the repulsion and thus to the distance from the surface. In this way it is possible to reconstruct the surface profile and get an image of it. Nevertheless as interesting and promising as they could be, such systems are in general very difficult to probe and measure directly. The reason is that

in the quantum regime there is a dynamical back action of the controlling device onto the system we want to probe. As we will see this effect has been used for the cooling process of a mechanical mode.

The necessity of isolating their fragile dynamics from the influences of the outside world and the need for low operating temperatures that allow for the magnification of the quantum mechanical features of their motion often imply that no direct access to such devices is possible. By today several schemes exist that use the interaction with light to extract information from the mechanical structures [95]. However, such methods are certainly not exhaustive and a more systematic approach to measure the quantum features of micro/nano mechanical devices is highly desirable.

In this sense, a considerable step forward has been the design of interfaces between mechanical systems and ancillae such as superconducting systems and (ultra-)cold atomic ensembles [96, 97], which can be used to efficiently monitor, measure, and prepare the inaccessible mechanical counterparts. Most interestingly, some of these hybridization strategies are already mature enough to have found interesting preliminary implementations [89]. In this chapter we present a new strategy by demonstrating that the interaction between an ultra-cold atomic system and a mechanical oscillator can be exploited for effective diagnostics of mechanical quantum coherences. A similar approach has been used in a recent work [98] for different purposes. Along the lines of Ref. [96], where it was shown that a similar system can mimic the strong coupling regime of cavity quantum electrodynamics, we consider a setup composed of a mechanical oscillator placed on an atom chip and coupled to a spinor BEC through a magnetic tip. In our scheme, the magnetic tip acts as a transducer turning the mechanical oscillations into a magnetic field experienced by the atomic spins. The motion of the latter in turn results in a driving force for the mechanical oscillator. A physically transparent description of the mechanism underlying our proposal is provided by the formal mapping of the spinor BEC onto a three dimensional rotor: the magnetic-like coupling between the atoms of the BEC and the mechanical system results in the interaction between a harmonic oscillator and one of the components of the rotor. This allows one to "write" signatures of the coherences present in the cantilever state onto the state of the rotor, which can then be read out using a technique based on the optical Faraday effect. Our work provides a fully analytical framework for the proposed protocol and discusses a number of relevant cases showing the effectiveness of the scheme. The complexity of the problem requires the management of a very large sector of the Hilbert space of the cantilever-BEC system and demands the development of appropriate methods to include the relevant sources of noise affecting the device. One way of extending this work including noise is by exploiting phase space methods.

## 4.2 "Cooling" of a mechanical oscillator

The mechanical oscillators dynamics is fully characterized by the knowledge of the mechanical modes dynamics which in turn depend upon the oscillator's geometry. The oscillators have to be designed in such a way that it is possible to address each of these modes independently so to make their control easier. The information on how easy it is to distinguish one mode from another is given by the so called quality factor $Q$. The $Q$ factor is actually a measure of the motion damping of an harmonic oscillator. The higher the $Q$ factor the lower is the damping thus giving a very sharp response of the oscillator at the resonance frequency of the mode. For a free oscillator, each resonance corresponds to one of its natural modes and a high $Q$ factor implies a good resolution of each of this modes. This is of fundamental importance since coupling one of these mode to another system we can assume that the dynamics involves only the addressed mode whereas the others can be neglected or treated as noise.

In this picture "cooling of a mechanical oscillator" means to reduce the amplitude of the oscillation of a particular mode at frequency $\omega_h$ and thus its energy. Many efforts have been devoted to introducing efficient schemes to cool down a mechanical oscillator. Most of them involve the coupling of the oscillator to a laser beam in analogy with the cooling of atoms and molecules. The idea behind all these schemes is to create a "viscous medium" that damps the motion.

### 4.2.1 Resolved sideband cooling

This technique is borrowed from cooling of ions in harmonic traps. In the ions' case the cooling mechanism relies on the presence of side-bands in the spectrum of the ion. The latter has both internal (electronic energy levels) and external (center of mass motion) degrees of freedom. Hence if $\omega_0$ is the resonance frequency between two internal energy levels and $\omega_h$ is the frequency of the harmonic potential the ion has resonances at $\omega_n = \omega_0 + n\omega_h$ where $n \in \mathbb{Z}$. This can be seen as a modulation of emitted light resulting from the ion's motion. By making use of a laser with frequency $\omega_{-1} = \omega_n = \omega_0 - \omega_h$ it is possible to excite the atom to a higher electronic level but a lower vibrational motion. The most probable channel of decay is the one for which the vibrational state does not change and the final internal state is the electronic ground state. The difference between the final and initial vibrational state will be $-\hbar\omega_h$ giving us the cooling of the ion. By repeating this process further it is possible to transfer more and more ions in the lowest vibrational state thus achieving the cooling.

In the case of a micro/nano mechanical oscillator the process is exactly the same. In the opto-mechanical setting light with frequency $\omega_0$ is reflected off the surface of the oscillator that has an oscillation frequency $\omega_h$. The reflected light it is thus modulated and peaks at all sidebands with frequencies $\omega_n = \omega_0 + n\omega_h$ appear. Again, light at $\omega_{-1} = \omega_0 - \omega_h$ is used to cool down the oscillator. The detuning $\Delta$ ensures that the number of photons $N_{-1}$ and $N_1$ scattered at frequency $\omega_{-1} = \omega_0 - \omega_h$ and $\omega_1 = \omega_0 + \omega_h$ respectively are such that $N_{-1} < N_1$. The conservation of energy thus implies that the oscillator loses energy at any cycle and cooling is achieved.

## 4.3 The set up and the Hamiltonian

We consider the setup sketched in Fig. 4.1, which consists of an on-chip single-clamped cantilever and a spinor BEC trapped in close proximity to the chip and the cantilever. The latter is assumed to be manufactured so as to accommodate at its free-standing end a magnetic molecule (or *tip*). Technical details on the fabrication methods of similar devices can be found in Refs. [89, 96], which have also been found to have very large quality factors, which guarantee a good resolution of the rich variety of modes in the cantilever's spectrum. At room temperature, thermal fluctuations are able to (incoherently) excite all flexural and torsional modes and in the following we assume that a filtering process is put in place, restricting our observation to a narrow frequency window, so as to select only a single mechanical mode.

The second key element of our setup is a BEC of $^{87}$Rb atoms held in a (tight) optical trap and prepared in the hyperfine level $|F = 1\rangle$. As we assume the trapping to be optical, there is no distinction between atoms with different quantum numbers $m_F = 0, \pm 1$ of the projections of the total spin along the quantization axis. Moreover, for a moderate number of atoms in the condensate and a tight trap, we can invoke the so-called single-mode approximation (SMA) [99], which amounts to considering the same spatial distribution for all spin states. These approximations will be made rigorous and formal in the next Subsections.

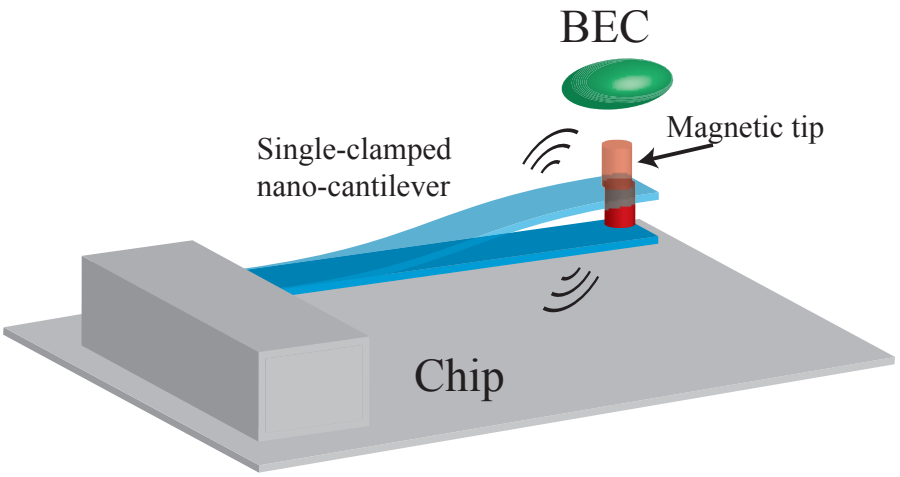



FIGURE 4.1: Sketch of the set-up for BEC-based probing of mechanical coherences. A BEC is placed in close proximity to a nano-mechanical cantilever endowed with a magnetic tip. The coupling between the magnetic field generated by the mechanical *quantum antenna* and the ultra-cold atoms embodies a mechanism for the effective probing of coherences in the state of the mechanical system.

### 4.3.1 Hamiltonian of the system

In the following we will briefly review the mapping of a spinor BEC into a rotor [100]. The Hamiltonian of a BEC in second quantization reads [101]

$$\begin{aligned}\hat{H} =&\sum_{\alpha}\int d\mathbf{x}\hat{\Psi}^{\dagger}_{\alpha}(\mathbf{x})\hat{H}^{0}_{\alpha}\hat{\Psi}_{\alpha}(\mathbf{x})\\ &+\sum_{\alpha,\beta,\mu,\nu}G_{\alpha,\beta,\mu,\nu}\int d\mathbf{x}\hat{\Psi}^{\dagger}_{\alpha}(\mathbf{x})\hat{\Psi}^{\dagger}_{\beta}(\mathbf{x})\hat{\Psi}_{\mu}(\mathbf{x})\hat{\Psi}_{\nu}(\mathbf{x}),\end{aligned} \tag{4.1}$$

where the second line of equation describes the particle-particle scattering mechanism and $\hat{H}^{0}_{\alpha}= -(\hbar^2/2m)\nabla^2 + m(\omega^2(x^2+y^2)+\omega_z^2 z^2)/2$, $m$ is the mass of the Rb atoms and $\omega$ and $\omega_z$ are the in-plane and axial trapping frequencies respectively. The subscripts $\alpha,\beta,\mu,\nu$ refer to different z-components of the single-atom spin states. As the scattering between two particles does neither change the total spin nor its z-component, we can link the coefficients $G_{\alpha,\beta,\mu,\nu}$ to the scattering lengths for the channels with total angular momentum $F_T = 0, 2$. The absence of the channel with $F_T = 1$ is due to the fact that in this case the spinor component of the wave function is anti-symmetric. Since the total wave-function has to be symmetric it turns out that the spatial wave-function of the two bosons has to be anti-symmetric too. This gives us a vanishing s-wave scattering length.

Thus, by making use of the Clebsch-Gordan coefficients, the full BEC Hamiltonian can be re-written as

$$\begin{aligned}\hat{H} =& \sum_{\alpha} \int d\mathbf{x}\ \hat{\Psi}^{\dagger}_{\alpha}(\mathbf{x}) \hat{H}^{0}_{\alpha} \hat{\Psi}_{\alpha}(\mathbf{x}) \\ &+ \frac{c_s}{2} \sum_{\alpha,\beta} \int d\mathbf{x}\ \hat{\Psi}^{\dagger}_{\alpha}(\mathbf{x}) \hat{\Psi}^{\dagger}_{\beta}(\mathbf{x}) \hat{\Psi}_{\alpha}(\mathbf{x}) \hat{\Psi}_{\beta}(\mathbf{x}) \\ &+ \frac{c_a}{2} \sum_{\alpha,\beta,\alpha',\beta'} \int d\mathbf{x}\ \hat{\Psi}^{\dagger}_{\alpha}(\mathbf{x}) \hat{\Psi}^{\dagger}_{\beta}(\mathbf{x}) (\mathbf{F}_{\alpha,\beta} \cdot \mathbf{F}_{\alpha',\beta}) \hat{\Psi}_{\alpha'}(\mathbf{x}) \hat{\Psi}_{\beta'}(\mathbf{x})\end{aligned} \tag{4.2}$$

where $c_s{=}(g_0{+}2g_2)/3$ and $c_a{=}(g_2{-}g_0)/3$ with $g_{2j}{=}4\pi\hbar^2 a_{2j}/m$ ($j{=}0,1$) and $a_{2j}$ being the scattering length for the $F_T = 2j$ channel [102]. Here $\mathbf{F}$ is the vector of the spin-1 matrices obeying the commutation relation $[\mathbf{F}^i, \mathbf{F}^j] = i\ \epsilon_{ijk} \mathbf{F}^k$ with $\epsilon_{ijk}$ being the Levi-Civita tensor.

As one can see from Eq. (4.2), if $c_a \approx 0$ (*i.e.* if $g_0 \approx g_2$) and/or the number of atoms is not too large, the total Hamiltonian is symmetric in the three spin components. By assuming a strong enough optical confinement and a BEC of a few thousand atoms, one can therefore think of the order parameter as having a constant spatial distribution for all the three species $m_F = 0, \pm 1$ and write $\hat{\Psi}_{\alpha}(\mathbf{x}){=}\phi(\mathbf{x})\hat{a}_{\alpha}$. This is the so called single-mode approximation (SMA) [99, 103] which leaves the Hamiltonian in the form

$$\begin{aligned}\hat{H} =& \sum_{\alpha} \hat{a}^{\dagger}_{\alpha} \hat{a}_{\alpha} + \frac{c'_s}{2} \sum_{\alpha,\beta} \hat{a}^{\dagger}_{\alpha} \hat{a}^{\dagger}_{\beta} \hat{a}_{\alpha} \hat{a}_{\beta} \\ &+ \frac{c'_a}{2} \sum_{\alpha,\beta,\alpha',\beta'} (\mathbf{F}_{\alpha,\beta} \cdot \mathbf{F}_{\alpha',\beta'})\, \hat{a}^{\dagger}_{\alpha} \hat{a}^{\dagger}_{\alpha'} \hat{a}_{\beta} \hat{a}_{\beta'},\end{aligned} \tag{4.3}$$

where we have defined $c'_i{=}c_i \int d\mathbf{x}\ |\phi(\mathbf{x})|^4$. As the distance $z_0$ between the BEC and the magnetic tip can be in the range of a few $\mu$m (we take $z_0 = 1.5\mu$m in what follows) and the spatial dimensions of the BEC are typically between tenths and hundredths of $\mu$m (we considered $a_z = 0.25\mu$m and $a_r = 0.09\mu$m), the relative correction to the magnetic field across the sample is small enough to justify the SMA (of the order of 0.2) Moreover, in the configuration assumed here, the system will be mounted on an atomic chip, where the static magnetic field can be tuned by adding magnets and/or flowing currents passing through side wires. Such a design can compensate any distortions to the trapping potential induced by the tip.

By introducing $\hat{N}{=}\sum_{\alpha} \hat{a}^{\dagger}_{\alpha}\hat{a}_{\alpha}$ and the angular momentum operators $\hat{L}^{+}{=}\sqrt{2}(\hat{a}^{\dagger}_{0}\hat{a}_{-1} + \hat{a}^{\dagger}_{1}\hat{a}_{0})$ and $\hat{L}_z{=}(\hat{a}^{\dagger}_{1}\hat{a}^{-}_{1}\hat{a}^{\dagger}_{-1}\hat{a}_{-1})$, we can rewrite Eq. (4.3) as $\hat{H}{=}\hat{H}_A + \hat{H}_S$, where we have explicitly identified a symmetric part $\hat{H}_S = \mu\hat{N} - c'_s\hat{N}(\hat{N}-1)$ and an antisymmetric one $\hat{H}_A = c'_a(\hat{L}^2 - 2\hat{N})$.

It is important to remember that such a mapping is possible due to the assumption of a common spatial wave function for the three spin components. As long as the anti-symmetric term is small enough, this is not a strict constraint. By exploiting Feshbach resonances [104], it is possible to adjust the couplings $g_0$ and $g_2$ in such a way that $g_0 \approx g_2$, which allows for the possibility to increase the number of atoms in the BEC, still remaining within the validity of the SMA.

We now consider the BEC interaction Hamiltonian when an external magnetic field is present. Due to its magnetic tip, the cantilever produces a magnetic field and the cantilever can be modeled as a single quantum harmonic oscillator whose annihilation (creation) operator we call $\hat{b}_c$ ($\hat{b}_c^\dagger$). By allowing the tip to have an intrinsic magnetization, we can split the magnetic field into a static contribution $\mathbf{B}^0$ and an oscillating one $\delta\hat{\mathbf{B}}$ that arises from the oscillatory behavior of the mechanical mode. The physical mechanism of interaction is Zeeman-like, *i.e.* each atom experiences a torque which tends to align its total magnetic moment to the external magnetic field. The Hamiltonian for a single atom can be written as

$$\hat{H}_Z^{(1)} = -\boldsymbol{\mu}\cdot\mathbf{B} = (g\mu_B/\hbar)\hat{\mathbf{S}}^{(1)}\cdot\mathbf{B}, \tag{4.4}$$

where $\mu_B$ is the Bohr magneton, $\hat{\mathbf{S}}^{(1)}$ is the spin operator vector for a single atom and $g$ is the gyromagnetic ratio. In line with Ref. [105], we adopt the convention that $g$ and $\mu$ have opposite signs. The total interaction Hamiltonian is then given by the sum over all the atoms. By taking the direction of $\mathbf{B}^0$ as the quantization axis (z-axis) and the x-axis in the direction of $\langle\delta\hat{\mathbf{B}}\rangle$, the magnetic Zeeman-like Hamiltonian is

$$\hat{H}_Z = g\mu_B B_z^0 \hat{L}_z + g\mu_B G_c a_c(\hat{b}_c^\dagger + \hat{b}_c)\hat{L}_x, \tag{4.5}$$

where we have used $\delta\hat{\mathbf{B}} = G_c a_c(\hat{b}_c^\dagger + \hat{b}_c)\overline{\mathbf{x}}$ with $G_c = 3\mu_0|\boldsymbol{\mu}_c|/(4\pi z_0^4)$ being the gradient of the magnetic field produced by the tip at a distance $z_0$, $\overline{\mathbf{x}}$ the unit vector along the x-axis, $a_c = \sqrt{\hbar/(2m_e\omega_c)}$ and $m_e$ the effective mass of the cantilever, which represents the mass involved in the oscillation of the mode considered and it might be different from the total mass of the cantilever.

The full Hamiltonian of the BEC-cantilever system is thus $\hat{H} = \hat{H}_{BEC}^0 + \hat{H}_c^0 + \hat{H}_I$ with

$$\begin{aligned}
\hat{H}_{BEC}^0 &= \mu\hat{N} - c_s'\hat{N}(\hat{N}-1) + c_a'(\hat{L}^2 - 2\hat{N}) + g\mu_B B_z^0\hat{L}_z,\\
\hat{H}_c^0 &= \hbar\omega_c\hat{b}_c^\dagger\hat{b}_c,\\
\hat{H}_I &= g\mu_B G_c a_c(\hat{b}_c^\dagger + \hat{b}_c)\hat{L}_x.
\end{aligned} \tag{4.6}$$

It has been shown in Refs. [101, 103] that $\hat{H}_{BEC}^0$ with $B_z^0 = 0$ allows for interesting dynamics of the populations of the three spin states, which undergo Rabi-like oscillations,

thus witnessing the coherence properties of the BEC.

### 4.3.2 Mapping into a rotor

While the Hamiltonian above is rather appealing, it is not yet in a form that is of use for our application. In fact, let us consider the natural basis to describe the system, *i.e.* the one spanned by $|L, L_z\rangle$, which are the common eigenstates of $\hat{L}$ and $\hat{L}_z$. Due to the coherence in the state of the BEC, we cannot fix the quantum number $L$, since, for instance, if the BEC is in an eigenstate of $\hat{L}_z$ with $L_z = 0$, then the state has the form $\sum_{L=0}^{N} c_L|L, 0\rangle$. Tracking the evolution induced by Eq. (4.6) on such a superposition is a non trivial problem since for $N \gg 1$ the accessible region of the Hilbert space becomes quite large. Nevertheless, the problem can be tackled by the formal mapping of the BEC into a quantum rotor. In the following, we briefly discuss the basic ideas of this mapping as given in Ref. [100]. Since we work with a fixed number of particles, the state of the BEC can be decomposed as

$$\sum_{n'_{0,\pm1}} C_{n'_{0,\pm1}} (\hat{a}_1^\dagger)^{n'_1} (\hat{a}_0^\dagger)^{n'_0} (\hat{a}_{-1}^\dagger)^{n'_{-1}} |0\rangle, \tag{4.7}$$

where the sum is performed over all sets of labels $\{n'_{0,\pm1}\}$ such that $n'_0{+}n'_{-1}{+}n'_1{=}N$. Let us now introduce the Schwinger-like operators $\hat{b}_x{=}(\hat{a}_{-1}{-}\hat{a}_1)/\sqrt{2}$, $\hat{b}_y{=}(\hat{a}_1{+}\hat{a}_{-1})/(i\sqrt{2})$, $\hat{b}_z{=}\hat{a}_0$ such that $[\hat{b}_\alpha, \hat{b}_\beta]{=}0$, $[\hat{b}_\alpha, \hat{b}_\beta^\dagger]{=}\delta_{\alpha,\beta}$ [100]. The generic BEC state in Eq. (4.7) can now be written as $|\Omega_N\rangle{=}\frac{1}{\sqrt{N!}}(\mathbf{\Omega}{\cdot}\hat{\mathbf{b}}^\dagger)^N|0\rangle$ with $\mathbf{\Omega}{=}(\cos\phi\sin\theta, \sin\phi\sin\theta, \cos\theta)$. By varying $(\theta, \phi)$ and thus the position vector $|\mathbf{\Omega}\rangle$ on the unit sphere, it is possible to recover any superposition for the state of a single atom among the states with $m_z = 0, \pm1$. A state with a fixed number of particles with same spin in the bosonic Hilbert space can then be written as $|\Psi\rangle = \int d\Omega\ |\mathbf{\Omega}_N\rangle\psi(\mathbf{\Omega})$ where $\psi(\mathbf{\Omega})$ is the wave function of the rotor we are looking for to complete the mapping. The next step is to find the form of the Hamiltonian in this space. According to Ref. [100], a sufficient criterion for the two dynamics to be equivalent is the existence of a Hamiltonian operator $\hat{\mathcal{H}}$ in the Hilbert space of the rotor such that $\hat{H}|\Psi\rangle = \int d\Omega|\mathbf{\Omega}_N\rangle\hat{\mathcal{H}}\psi(\mathbf{\Omega})$. The explicit form of $\hat{\mathcal{H}}$ can in fact be found by a straightforward calculation that leads to the expressions of the $z$ and $x$ components of the angular momentum operator of the form

$$\begin{aligned}
\hat{L}_z &= -i(\hat{b}_x^\dagger\hat{b}_y - \hat{b}_y^\dagger\hat{b}_x) = -i\overline{\mathbf{z}}\cdot(\mathbf{\Omega}\times\nabla) = \frac{1}{\hbar}\overline{\mathbf{z}}\cdot\hat{\mathcal{L}} = -i\partial_\phi, \\
\hat{L}_x &= \frac{1}{2}(\hat{b}_z^\dagger\hat{b}_x - \hat{b}_x^\dagger\hat{b}_z) + \frac{i}{2}(\hat{b}_z^\dagger\hat{b}_y - \hat{b}_y^\dagger\hat{b}_z) = -i\overline{\mathbf{x}}\cdot(\mathbf{\Omega}\times\nabla) \\
&= \frac{1}{\hbar}\overline{\mathbf{x}}\cdot\hat{\mathcal{L}} = i(\sin\phi\ \partial_\theta + \cot\theta\cos\phi\partial_\phi).
\end{aligned} \tag{4.8}$$

After discarding an inessential constant term, the Hamiltonian that we are looking for reads $\hat{\mathcal{H}} = \hat{\mathcal{H}}_R^0 + \hat{\mathcal{H}}_c^0 + \hat{\mathcal{H}}_I$ with

$$\begin{aligned} \hat{\mathcal{H}}_R^0 &= c_a' \hat{\mathcal{L}}^2 + (g\mu_B/\hbar) B_z^0 \, \hat{\mathcal{L}}_z, \\ \hat{\mathcal{H}}_c^0 &= \hat{p}_c^2/2m_e + m_e \omega_c^2 \hat{q}_c^2/2, \\ \hat{\mathcal{H}}_I &= (g\mu_B/\hbar) G_c \hat{q}_c \hat{\mathcal{L}}_x. \end{aligned} \tag{4.9}$$

In Eq. (4.9) we have introduced, for convenience, the cantilever's position and momentum operators $\hat{q}_c = \sqrt{\hbar/(2m\omega_c)}(\hat{b}_c + \hat{b}_c^\dagger)$ and $\hat{p}_c = i\sqrt{\hbar m\omega_c/2}(\hat{b}_c^\dagger - \hat{b}_c)$. We are now in a position to look at BEC-cantilever joint dynamics. In particular we will focus on the detection of the cantilever properties by looking at the BEC spin dynamics.

## 4.4 Probing quantum coherences

### 4.4.1 Dynamics

The form of the interaction Hamiltonian $\hat{\mathcal{H}}_I$ allows for the measurement of any observable whose corresponding operator on the Hilbert space can be expressed as a function of $\hat{q}_c$ and $\hat{p}_c$ with, as we shall see, negligible back action on the cantilever dynamics. Moreover, when there is no magnetic field, the ground state of a "ferromagnetic" (*i.e.* $c_2 < 0$) spinor BEC is such that all the atomic spins are aligned along a direction resulting from a spontaneous symmetry breaking process [101]. Under the effects of the cantilever antenna, two preferred directions are introduced in the system: the $z$-direction along which we have the static magnetic field and the $x$-direction defined by the oscillatory component. The interplay between these two competing magnetic fields is responsible for a "gyroscopic" motion of the rotor about the $z$-axis, exactly as in a classical spinning top. By looking at the way the rotor undergoes such a gyromagnetic motion, we can gather information about the properties of the cantilever state. We notice that a similar approach has been used to show the resonant coupling of an atomic sample of $^{87}$Rb atoms with a magnetic tip similar to the one considered here [106].

In order to understand the mechanism, let us look at the time evolution of the operator $\hat{\mathcal{L}}_x(t)$. We take an initial state of the form

$$|\Psi(0)\rangle = \sum_n C_n |E_n\rangle \int_{\Sigma_1} d\Omega \; \psi(\Omega) |\Omega_N\rangle, \tag{4.10}$$

where $\Sigma_1$ is the unit sphere and $|E_n\rangle$ are the energy eigenvalues for the harmonic oscillator such that $\hat{\mathcal{H}}_c^0|E_n\rangle = E_n|E_n\rangle$. In the Heisenberg picture, the mean value of the x-component of the angular momentum is

$$\langle\hat{\mathcal{L}}_x(t)\rangle = \langle\Psi(0)|e^{i\frac{\hat{\mathcal{H}}}{\hbar}t}\hat{\mathcal{L}}_x(0)e^{-i\frac{\hat{\mathcal{H}}}{\hbar}t}|\Psi(0)\rangle$$

$$\begin{aligned}
&= \int_{\Sigma_1,q,q'} d\Omega dq dq' \left(\sum_{n,m} C_m^* C_n e^{-i\omega_{n,m}t}\phi_m^*(q')\phi_n(q)\langle q'|q\rangle\right) \\
&\quad \times \psi^*(\Omega)\left(e^{i\frac{\hat{\mathcal{H}}_I+\hat{\mathcal{H}}_R^0}{\hbar}t}\hat{\mathcal{L}}_x(0)e^{-i\frac{\hat{\mathcal{H}}_I+\hat{\mathcal{H}}_R^0}{\hbar}t}\right)\psi(\Omega) \qquad (4.11)
\end{aligned}$$

$$\begin{aligned}
&= \int_q dq \sum_{n,m} C_m^* C_n e^{-i\omega_{n,m}t}\phi_m^*(q)\phi_n(q) \\
&\quad \times \int_{\Sigma_1} d\Omega\ \psi^*(\Omega)\left(e^{i\frac{\hat{\mathcal{H}}_I+\hat{\mathcal{H}}_R^0}{\hbar}t}\hat{\mathcal{L}}_x(0)e^{-i\frac{\hat{\mathcal{H}}_I+\hat{\mathcal{H}}_R^0}{\hbar}t}\right)[\psi(\Omega)]
\end{aligned}$$

where we have used the closure relation $\int_q |q\rangle\langle q| = \hat{1}$ twice and introduced $\phi_n(q)=\langle q|E_n\rangle$ and $\omega_{n,m}=\omega_c(n-m)$. By setting $\Omega_q=\sqrt{(g\mu_B/\hbar)^2[(B_z^0)^2+G_c^2q^2]}$, the time-evolved x-component of the angular momentum operator is

$$\begin{aligned}
\hat{\mathcal{L}}_x(t) =& \frac{g^2\mu_B^2}{\hbar^2\Omega^2(q)}\left[(B_z^0)^2\cos(\Omega_q t)+G_c^2q^2\right]\hat{\mathcal{L}}_x(0) \\
&+\frac{g\mu_B B_z^0}{\hbar\Omega_q}\sin(\Omega_q t)\hat{\mathcal{L}}_y(0) \\
&+\frac{g^2\mu_B^2 B_z^0 G_c q}{\hbar^2\Omega^2(q)}\left[1-\cos(\Omega_q t)\right]\hat{\mathcal{L}}_z(0) \qquad (4.12)
\end{aligned}$$

$$= a_1(q,t)\hat{\mathcal{L}}_x(0)+a_2(q,t)\hat{\mathcal{L}}_y(0)+a_3(q,t)\hat{\mathcal{L}}_z(0).$$

Comparing Eqs. (4.11) and (4.12) we find $\langle\hat{\mathcal{L}}_x(t)\rangle=\sum_{j=x,y,z}A_j(t)L_j^0$, where

$$\begin{aligned}
L_j^0 &= \int_{\Sigma_1} d\Omega\ \psi^*(\Omega)\hat{\mathcal{L}}_j(0)[\psi(\Omega)], \\
A_j(t) &= \sum_{n,m} C_m^* C_n e^{-i\omega_{n,m}t}\int_q dq\phi_m^*(q)\phi_n(q)a_j(q,t). \qquad (4.13)
\end{aligned}$$

If the cantilever is initially prepared in the general mixed state $\rho_c(0)=\sum_n C_{n,m}|E_n\rangle\langle E_m|$, a similar expression for the mean value of $\hat{\mathcal{L}}_x(t)$ is found, where now

$$A_j = \sum_{n,m} e^{-i\omega_{n,m}t}C_{n,m}\int_q dq\ \phi_m^*(q)\phi_n(q)a_j(q,t). \qquad (4.14)$$

As the qualitative conclusions of our analysis do not depend upon the initial value of the angular momentum component of the spinor, in what follows we shall concentrate on an illustrative example that allows us to clearly display our results. We thus consider,

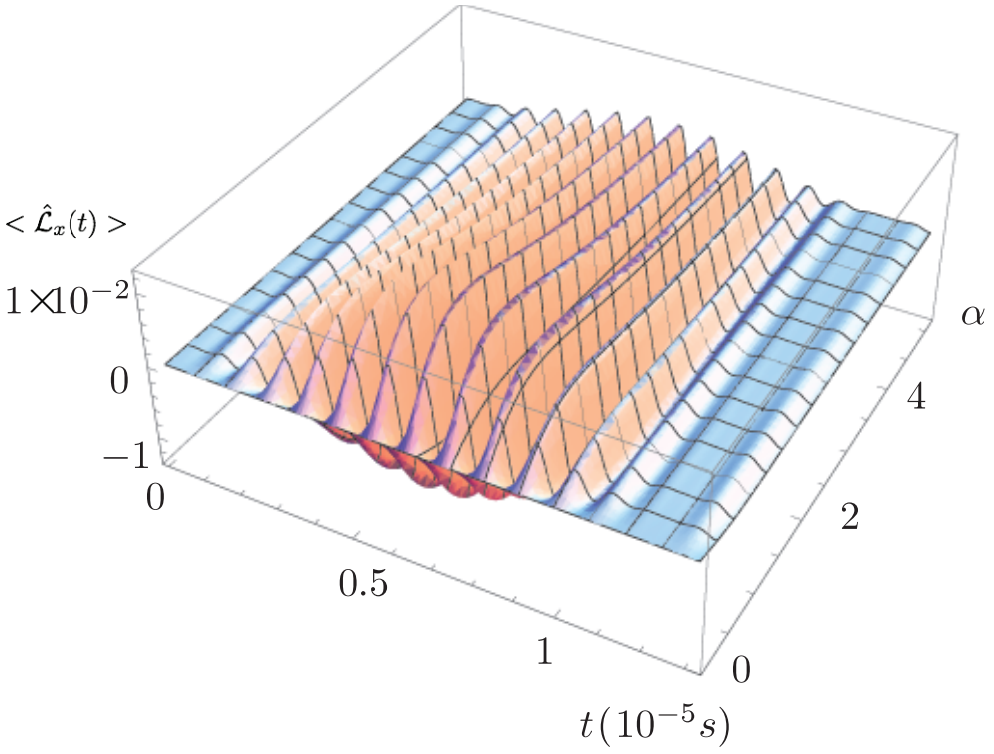



FIGURE 4.2: Mean value of $\hat{\mathcal{L}}_x(t)$ for a cantilever in the initial state as given by Eq. (4.10) with $C_0$=$C_1/\alpha$=$1/\sqrt{1+\alpha^2}$and $C_n = 0$ otherwise. The BEC consists of $N$=$10^3$ $^{87}$Rb atoms and $\langle\hat{\mathcal{L}}_{x,y}(0)\rangle = 0$, $\langle\hat{\mathcal{L}}_z(0)\rangle = 100$. We have used $B_z^0$=$3\times10^{-6}\mu T$ and $G_c \approx 1.8\times10^3\mu T/\mu$m.

without affecting the generality of our discussions, $\langle\hat{\mathcal{L}}_{x,y}(0)\rangle = 0$ and $\langle\hat{\mathcal{L}}_z(0)\rangle = 100$. When the cantilever and the BEC are uncoupled, we should expect $\langle\hat{\mathcal{L}}_x(t)\rangle$ to oscillate at the Larmor frequency $\omega_L = g\mu_B B_z^0$ and with an amplitude independent of $\langle\hat{\mathcal{L}}_x(0)\rangle$. The BEC-cantilever coupling introduces a modulation of such oscillations and in the following we will demonstrate that the analysis of such oscillatory behavior is indeed useful to extract information on the state of the cantilever.

We first consider the case of a cantilever initially prepared in a superposition of a few eigenstates of the free Hamiltonian $\hat{\mathcal{H}}_c^0$, as in Eq. (4.10). In Fig. 4.2 we show the mean value of $\hat{\mathcal{L}}_x(t)$ as a function of the coherence between the states with quantum number $n = 0$ and $n = 1$, *i.e.* a state having $C_0 = C_1/\alpha = 1/\sqrt{1+\alpha^2}$ and $C_n = 0$ otherwise. One can see a clear modulation of the behavior of $\langle\hat{\mathcal{L}}_x(t)\rangle$: a close inspection reveals that the carrier frequency $\omega_L$ is modulated by the frequency $\omega_{0,1}$. In reality, the Larmor frequency is renormalized as can be seen by the expression for $\Omega_q$. However, as we have taken $G_c a_c \ll B_z^0$, one can safely assume that the carrier frequency is very close to $\omega_L$. Moreover, the maximum of the function is found at $C_{0,1} = 1/\sqrt{2}$, which maximizes the coherence between the two states and thus the effect of the modulation. For symmetry reasons, the modulation described is not visible if the cantilever is prepared in a superposition of phonon eigenstates whose quantum numbers are all of the the same parity

(such as a single-mode squeezed state). In this case, in fact, the function entering the integral over $q$ in $A_3$ is antisymmetric, thus making it vanish. In Fig. 4.3, $\langle\hat{\mathcal{L}}_x(t)\rangle$ is shown for an initial state of the cantilever having $C_{0,1} = C_2/\alpha = 1/\sqrt{2+\alpha^2}$ and $C_n = 0$ otherwise. It is worth noticing that one can identify two regions of oscillations separated by the line of nodes at $\alpha = 1$ where $C_0 = C_1 = C_2$. We can understand this behavior by studying the amplitudes of oscillation in three $\alpha$-dependent regions. For $\alpha < 1$, the main modulation frequency is given by $\omega_{0,1}$ and the role of the third state is to modify the amplitude of the oscillations [see Fig. (4.3)]. At $\alpha = 1$ a destructive interference takes place and the amplitude drops down. For $\alpha > 1$ the frequency $\omega_{1,2}$ enters into the evolution of $\langle\hat{\mathcal{L}}_x(t)\rangle$ (for parity reasons, the term with frequency $\omega_{0,2}$ has no role) and determines a phase shift of the oscillation fringes. It is interesting to observe that if the initial state of the cantilever is purely thermal, $\langle\hat{\mathcal{L}}_x(t)\rangle$ does not oscillate: only quantum coherence in the state of the mechanical system give rise to oscillatory behaviors and their presence is well signaled by the pattern followed by the angular momentum of the spinor-BEC. Although the examples considered so far have been instrumental in explaining the connections between the properties of the cantilever and the dynamics of the spinor's degrees of freedom, they are unfortunately currently far from being realistic. We will therefore now consider a closer-to-reality example of a pure state that is likely to be achieved soon. Given the impressive advances in the control and state-engineering of micro and nano-mechanical systems, we will consider the cantilever to be prepared in a coherent state with an average phonon number $n_{ph}$. Such a coherent state can be generated by displacing, with an intense laser field, the ground state of a cantilever. This is a realistic expectation: current state of the art experiments are only a few quanta away from such an achievement [115]. In Fig. 4.4 we show the time evolution of $\hat{\mathcal{L}}_x(t)$ for $|\alpha|^2 = 1$ [panel **(a)**], 5 [panel **(b)**], 15 [panel **(c)**], and 20 [panel **(d)**]. One can see that, depending on the mean number of phonons initially present in the mechanical state, new frequencies are introduced in the dynamics of the device: the larger $|\alpha|^2$, the larger the number of frequencies involved due to the Poissonian nature of the occupation probability distribution of a coherent state. In Fig. 4.4 **(e)**, which addresses the case of $|\alpha|^2 = 20$, the study of the dynamics at long evolution times reveals that the carrier frequency is unaffected, for all practical purposes, while the large number of frequencies entering in the evolution gives rise to series of beats occurring at different time scales.

### 4.4.2 Detection scheme

To read out the information imprinted on the rotor, one can make use of the Faraday-rotation effect, which allows one to measure one component of the the angular momentum of the BEC with only a negligible back action on the condensate itself. It is

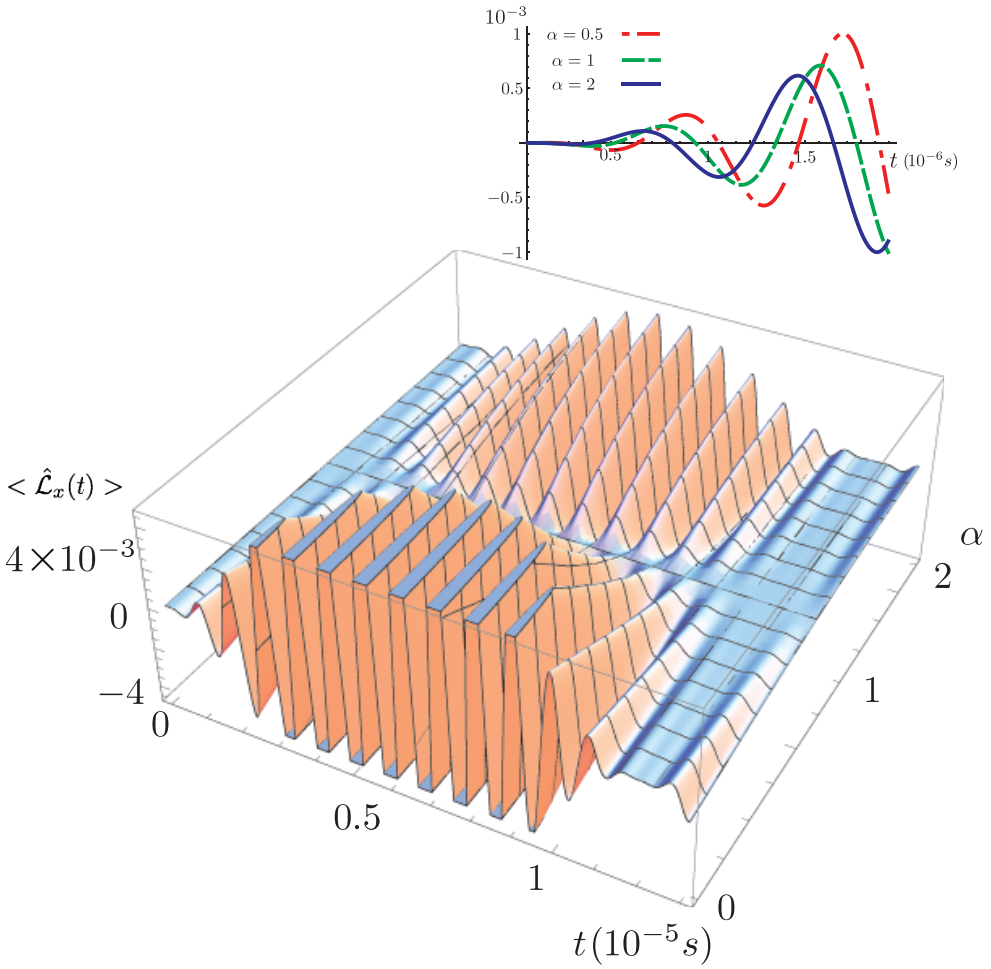



FIGURE 4.3: Mean value of $\hat{\mathcal{L}}_x(t)$ for a cantilever in the initial state as given by Eq. (4.10) with $C_0 = C_1 = C_2/\alpha = 1/\sqrt{2+\alpha^2}$ and $C_n = 0$ otherwise. The BEC parameters are the same as in Fig. 4.2. The inset shows that the change in $|\alpha|$ amounts to a shift of the oscillations [we have taken $= e^{i\pi/6}(0.5, 1, 2)$].

well-known from classical optics that the linear polarization of an electromagnetic field propagating across an active medium rotates with respect to the direction it had when entering the medium itself. This is the essence of the Faraday-rotation effect, which can be understood by decomposing the initial polarization in terms of two opposite circularly-polarized components experiencing different refractive indices [107]: by going through the medium, the two components acquire different phases, thus tilting the resulting polarization.

In the case of an ultra-cold gas, an analogous rotation of the polarization of a laser field propagating across the BEC is due to the interaction of light with the atomic spins. If the spins are randomly oriented the net effect is null, while for spins organized in clusters, the effect can indeed be measured. It has been shown in Refs. [108, 109] that the back-action on the BEC induced by these sorts of measurements is rather negligible. In recent experiments non-destructive measurements on a single BEC of $^{23}$Na atoms

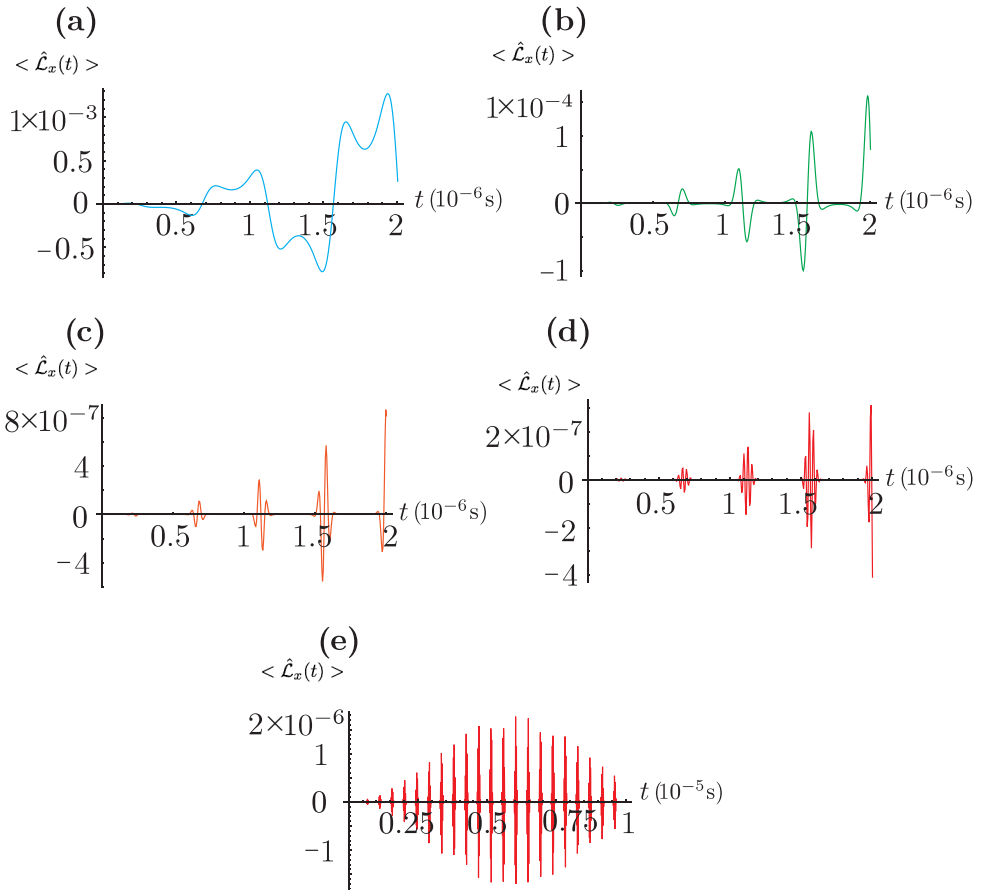



FIGURE 4.4: Time evolution of $\hat{\mathcal{L}}_x$ for a coherent initial state of the cantilever with $|\alpha|^2 = 1$ **(a)**, 5 **(b)**, 15 **(c)**, 20 **(d)**. For the same parameter as in **(d)**, the plot **(e)** shows that the carrier frequency $\omega_L$ is not significantly affected.

have been used to show the dynamical transition between two different regions of the stability diagram of the system [110]. This method can thus be effectively used to determine the dynamics of the angular momentum components of the rotor BEC and thus indirectly witness the presence of coherences in the state of the cantilever. The measurement can be performed by means of homodyne detection schemes. Moreover, as shown in Ref. [109], the signal to noise ratio (SNR) is proportional to $\sqrt{\tau_{pd}/\tau_s}$ where $\tau_{pd}$ is the characteristic time for the response of the photo-detector and $\tau_s$ is the average time between consecutive photon-scattering events. In order to be able to detect two distinct events on a time scale $\tau$ we thus need $\tau_{pd} < \tau < \tau_s$ to hold. This condition states that the number of scattered photons has to be small enough during the time $\tau$ over which the dynamics we want to resolve occurs. On the other hand the detector "dead time" should be smaller than the typical evolution time. While $\tau_s$ can be easily tuned by adjusting the experimental working point, ultrafast photo-detectors of the latest generation have response time $\tau_{pd}$ of a few $ps$. As in our scheme we have $\tau \in [10^{-8}, 10^{-5}]$s, the proposed coherence-probing method appears to be within reach.

## 4.5 Conclusions

We have considered a mechanical cantilever equipped with a magnetic tip interacting with a spinor Bose-Einstein condensate (BEC) held in an optical trap. The tip produces a magnetic field made up of two components, namely a static one along the tip's natural anisotropic axes and one perpendicular to it due to the cantilever's oscillations. By exploiting the mapping of a spinor BEC into a rotor model [100] it is possible to take into account its quantum properties, which would have been missed in a mean field theory approach. The BEC is thus mapped onto a quantum gyroscope undergoing a precession about the direction of the magnetic tip's static field. We have assumed that the cantilever has been cooled down [114, 115] to a quantum regime and described it as a quantum harmonic oscillator. We have shown that it is possible to detect the presence of quantumness in the cantilever state in the form of superposition of different eigenstate of the harmonic oscillator. The way to do this is to look at the gyroscopic precession by using Faraday spectroscopy, which in turn only minimally disturbs the BEC dynamics, thus allowing for a continuous probing of the system. Even though we have restricted our analysis to a cantilever equipped with a magnetic molecule it is possible to generalize this scheme to other sorts of mesoscopic magnetic system such as nanotubes.

The work presented in this chapter has been done in collaboration with Th. Busch, G. M. Palma and M. Paternostro and it has been published in Phys. Rev. A **84**, 063815 (2011).

# Chapter 5

# Markov regime for open quantum dynamics

In this chapter we address a recently very debated problem: definition of Markov regime for quantum systems. We will first review the basics for mathematical treatment of stochastic classical variables' dynamics. We then discuss the standard mathematical description for open quantum system dynamics. Once we have the basic ingredients we shall turn to give a different definition of Markov regime in analogy with the classical case.

## 5.1 Introduction

The quest for the mathematical description of open quantum system dynamics has lately intensified. A milestone in this field is the theory developed in the 70s, which is based on the Gorini-Kossakowski-Sudarshan-Lindblad (GKSL) equation [116, 117]. This equation is often associated to the Markov assumption for classical systems for it reduces to the Pauli equation in the case of a diagonal density matrix in an orthonormal basis [118]. The solution to the Pauli equation respects the Markov assumption and this is assumed to be enough to justify the notion Markov process in the quantum realm. Nevertheless the GKSL equation is derived under two assumptions: a) boundness of the operators and b) complete positivity for the dynamical map. The first one is a strong assumption as Lindblad himself states in his original paper [117] and could not hold for many systems, whereas the second one is not necessary [119]. A review of certain concepts in quantum open system theory is desirable if we want it to follow the most recent studies in different fields; it has applications in problems such as thermalization [120], transport in non-equilibrium settings [121], dynamics of quantum systems in noisy environments [122] and

emerging irreversibility from a microscopic description as first spotted by Lindblad[123]. The description of classical stochastic systems has a large number of applications ranging from motion of particles under stochastic forcing [124], to financial markets [125] and models of biological evolution [126]. They all share the fact that the system under study is in contact with an external "environment" which is replaced by stochastic "forces" acting on it. In this framework a special class of systems are those for which the Markov assumption holds true. Its power comes from the simplicity of the resulting mathematical description for these systems.

Such a simplicity is even more desirable in the case of quantum open systems and in fact the GKSL equation is an example of such a simple but very powerful description. Nevertheless in dealing with real systems the role of the external environment has to be taken into account properly and the GKSL does not encompass a realistic treatment. For this reason the study of the so called non-Markovian (meaning not of the GKSL form) master equations is an hot topic nowadays. At the same time characterization of Markov (and consequently non-Markov) regimes in the dynamics of a quantum system has recently received an increasing attention [127–132]. In contrast to the classical theory of open quantum systems, however, there is apparently no clear definition of Markov processes. In the quantum case the Markov property is often linked with the the quantum regression theorem [133, 134]. In this chapter we first review the Markov assumption and its implications for classical stochastic processes. We then move to analyze the quantum case and define the Markov *regime* for a quantum system's dynamics in analogy with the original Markov assumption for classical stochastic processes. We shall show that by using the "physical" implications of the classical Markov assumption it is possible to define the Markov regime for a quantum system regardless of the differences between the classical and quantum mathematical objects used to describe the system (*i.e.* the probability density and the density operator).

## 5.2 Classical stochastic systems

There are phenomena such as turbulent motion at the bottom of a waterfall, city traffic, diffusion of a perfume in air, electric conduction through a copper wire and many others whose mathematical description is made by means of random variables. It sounds amazing as soon as we realize that at the microscopic level all the equations are deterministic. In the case of water flow for instance it is possible to write Newton equations for each molecule. Nevertheless this is not at all a reasonable idea because of the number of variables we will end up dealing with. It is thus often better to replace the microscopic variables with macroscopic ones obtained from coarse graining over some characteristic

temporal and/or spatial scales. The details of the coarse graining process however are important since these complex systems can show multi-scale behavior; a good example is fully developed and homogeneous turbulence where one can identify the injection and dissipation scales, *i.e.* scales on which the energy is injected into the system and then is dissipated through friction respectively. These coarse grained variables turn out to be random and their time evolution is given by stochastic dynamics. Given a random variable $X$ that takes on values $x \in \mathbb{K}$ where $\mathbb{K} = \mathbb{N}, \mathbb{Z}, \mathbb{R}$ or $\mathbb{C}$ (for the sake of simplicity we assume that our system is characterized by one variable only; the extension to more than one variable is then straightforward) a stochastic process can be regarded as a set of maps (for different $n's$)

$$\mathbb{R}_+^n \to \mathcal{D}_n : (t_n, \cdots, t_1) \to p^{(n)}(x_n, \cdots, x_1), \tag{5.1}$$

where $\mathcal{D}_n$ is the space of distributions defined on $\mathbb{K}^n$ and $\mathbb{R}_+ \equiv [0, \infty)$.

These distributions allow to calculate different quantities to characterize the system. Let us consider a generic function $f(X)$ of the stochastic variable $X$ (energy, temperature, etc.); its average at time $t$ is then

$$\langle f(X) \rangle(t) = \int dx \; f(x)\, p(x,t), \tag{5.2}$$

where we have defined $p^{(1)}(x,t) \equiv p(x,t)$ and included the time dependence in the function; $p(x,t)dx$ is the probability that the random variable $X$ takes on value $x$ at time $t$. This shows the importance of the time dependent probability density: it allows the evaluation of the mean value of any function of the stochastic variable. Nevertheless the mean values of the observables do not fully characterize the system; taken any two functions $f_1(X)$ and $f_2(X)$ one could be interested in correlation functions such as $\langle f_2(X) f_1(X) \rangle(t_2, t_1) = \int dx_2 dx_1 \; f_2(x_2)\, f_1(x_1)\, p^{(2)}(x_2, t_2; x_1, t_1)$ $(t_2 \geq t_1)$. The mean value is the integral of the product of the two functions at $X = x_1$ and $X = x_2$ respectively multiplied by the probability that the stochastic variable $X$ takes on the value $x_2$ at $t_2$ **and** the value $x_1$ at time $t_1$. This introduces a new quantity, namely $p^{(2)}(x_2, t_2; x_1, t_1)$ which in general cannot be derived from $p(x,t)$. In the special case $p^{(2)}(x_2, t_2; x_1, t_1) = p(x_2, t_2) p(x_1, t_1)$ then $\langle f_2(X) f_1(X) \rangle(t_2, t_1) = \langle f_2(X) \rangle(t_2)\; \langle f_1(X) \rangle(t_1)$ which amount to say that the two quantities are not correlated. Note here that the above property holds for *any* pair of functions and it only depends on whether or not the two-point probability density is factorized. Similarly one can define the n-point (in time) correlation functions as

$$\langle f_n(X)\cdots f_1(X)\rangle(t_n,\cdots,t_1)=\int dx_n\cdots dx_1\; p^{(n)}(x_n,t_n;\;\cdots\;;\;x_1,t_1)\; f_n(x_n)\cdots f_1(x_1), \tag{5.3}$$

where $(t_n\geq\cdots\geq t_1)$.

Again in this case the n-point probability density $p^{(n)}(x_n,t_n;\;\cdots\;;\;x_1,t_1)$ cannot, in general, be recast in terms of $p^{(1)}(x,t)$ only. It is useful at this point to introduce the relative probabilities

$$p^{(n)}(\mathbf{x}_{k,1})\,p_{n|k}(\mathbf{x}_{n+k,k+1}\mid\mathbf{x}_{k,1})=p^{(n+k)}(\mathbf{x}_{n+k,1}), \tag{5.4}$$

where $\mathbf{x}_{i,j}=\{x_j,t_j;\;\cdots\;;\;x_i,t_i\}$. The $p_{n|k}$ are the probability densities for the stochastic variable $X$ to take on the values $x_{n+k}$ at $t_{n+k}$ **and** $x_{n+k-1}$ at $t_{n+k-1}$ **and** $\cdots$ **and** $x_{k+1}$ at $t_{k+1}$ **whenever** it took the values $x_k$ at $t_k$ **and** $x_{k-1}$ at $t_{k-1}$ **and** $\cdots$ **and** $x_1$ at $t_1$. In particular we have $p^{(2)}(x_2,t_2;x_1,t_1)=p_{1|1}(x_2,t_2|x_1,t_1)\,p^{(1)}(x_1,t_1)$. Let now consider a set of time steps $\{t_k\}$ such that $t_n>t_m\;\;\forall n>m$.

The equation governing the time evolution of the above probability distribution can be quite difficult to solve due to the dependence of lower order probability densities on higher order ones and vice versa. We do not discuss this problem here since it is not our aim.

There is a particular case in which the dynamics is greatly simplified and that is whenever the Markov assumption holds. This assumption is expressed as

$$p_{n|k}(\mathbf{x}_{n+k,k+1}\mid\mathbf{x}_{k,1})=p_{n|1}(\mathbf{x}_{n+k,k+1}|\mathbf{x}_{k,k}). \tag{5.5}$$

It means that the probability at later times do not depend on the past history of the system. This has different consequences with one of them being a change in the regime of the validity of the Chapman-Kolmogorov equation for the probability distribution density:

$$p_{1|1}(x,t\mid x_1,t_1)=\int\; dy\; p_{1|1}(x,t\mid y,s)p_{1|1}(y,s\mid x_1,t_1), \tag{5.6}$$

where $t_1\leq s\leq t$ and $t_1\geq t_0$ in general. The Chapman-Kolmogorov equation shows that the relative probability densities form a semi-group with $t$ as parameter. This property is important because it guarantees the existence of an infinitesimal generator from which the semi-group can be derived [136]. The physical implication of the Markov assumption

is that once $p_{1|1}(x_2, t_2|x_1, t_1)$ and the initial distribution $p_0(x_0, t_0)$ are known we have access to **any** quantity of the system. The system then is fully described by these two objects only.

For a generic system the following relation holds

$$p_{1|1}(x, t \mid x_1, t_1) = \int dy\, p_{1|1}(x, t \mid y, s; x_1, t_1) p_{1|1}(y, s \mid x_1, t_1), \tag{5.7}$$

where $t_1 \leq s \leq t$. This relation can be proven by means of the definition of relative probability densities. It is easy to see that when the Markov assumption is valid Eq. (5.7) reduces to the Chapman-Kolmogorov equation.

Moreover this equation shows that the two-point relative probability density $p_{1|1}(x, t \mid x_1, t_1)$ is related to higher order probability densities making the problem highly non trivial.

Let us now call $p_0(x_0, t_0)$ the initial probability density. We can then formally write [137]

$$p^{(n)}(\mathbf{x}_{n,1}) = \int d\tilde{x}\, G^{(n)}(\mathbf{x}_{n,1}|\tilde{x}, \tilde{t})\, p(\tilde{x}, \tilde{t}), \tag{5.8}$$

where the $G^{(n)}(\mathbf{x}_{n,1}|\tilde{x}, \tilde{t})$ are the Green's functions that solve the initial problem.

Hänggi showed [137, 138] that it is always possible (Markov and non-Markov case), to find a class of propagators $G^{(n)}(\mathbf{x}_{n,1}|\tilde{x}, \tilde{t})$ (for each $n$) with the semi-group property and which are independent of the initial conditions by construction.

These Green's functions have nevertheless a different meaning than the relative probability distribution densities. In this respect Hänggi says [137]: "The propagators $G(t|t_1)$ of each semi-group are the conditional probabilities of a Markov process which has the same single-event probabilities $p(t)$ (*but different multivariate probabilities* $p^{(n)}$) as the non-Markov process under consideration". This again is to stress that the mean values alone do not fully characterize the system as two processes can have same mean values but different correlation functions.

## 5.3 Open quantum systems' dynamics

The dynamics of a closed and isolated quantum system is given by a unitary evolution operator $\hat{U}(t, t_0) = e^{-\imath \hat{H}(t-t_0)}$ where $\hat{H}$ is the Hamiltonian operator. Let us assume that the total system is made up of two parts whose temporal scales differ by several order of magnitudes and we are only interested in the dynamics of the "slower" one: the

system. The reduced density operator of the subsystem we are interested in is given by $\hat{\rho}_S = Tr_E\big[\hat{U}(t,t_0)\hat{\rho}(t_0)\hat{U}^\dagger(t,t_0)\big]$ where $\hat{\rho}(t_0)$ is the initial density operator of the total system and the labels $S$ and $E$ refer to the system and to the "environment" (*i.e.* the collection of fast degrees of freedom) respectively. It is common to consider the weak system-environment coupling limit for which it is possible to find an effective *master equation* for the reduced density matrix of the system only [135]. Let us call $\hat{H}_I$ the system - environment interaction Hamiltonian; in the interaction picture the evolution equation for the density matrix operator is given by

$$\frac{d}{dt}\hat{\rho}(t) = -\imath[\hat{H}_I(t), \hat{\rho}(t)]. \tag{5.9}$$

By assuming weak coupling and the fact that the environment has usually a larger Hilbert space than the system we are interested in we can make the replacement

$$\hat{\rho}(t) \approx \hat{\rho}_S(t) \otimes \hat{\rho}_E(0). \tag{5.10}$$

This comes from perturbation theory in analogy with the Born-Oppenheimer approximation made in atomic physics when the motion of electrons is separated from the motion of the nuclei. It simply states that on the time scale of the system's dynamics the state of the environment does not appreciably change. By formally integrating Eq. (5.9) and reinserting it into Eq. (5.9) with the above assumption we obtain:

$$\frac{d}{dt}\hat{\rho}(t) = -\int_0^t ds\ [\hat{H}_I(t), [\hat{H}_I(s), \hat{\rho}_S(s) \otimes \hat{\rho}_E(0)]]. \tag{5.11}$$

By tracing over the environment's degrees of freedom the equation governing the evolution of $\hat{\rho}_S(t)$ is obtained

$$\frac{d}{dt}\hat{\rho}_S(t) = -\int_0^t ds\ Tr_E([\hat{H}_I(t), [\hat{H}_I(s), \hat{\rho}_S(s) \otimes \hat{\rho}_E(0)]]), \tag{5.12}$$

which is known as the Redfield equation. Nevertheless it is usually difficult to solve it because it is an integro-differential equation for the reduced density matrix operator $\hat{\rho}_S(t)$; it is possible to further simplify it by assuming locality in time for the effect of the system - environment interaction. It means that the effects of the environment on the system only depends on the state of the system at that time and not on its previous states. This amounts to replace $\hat{\rho}_S(s)$ with $\hat{\rho}_S(t)$ in the above equation. But this is still not enough because of the integral ranging from the initial time up to $t$. To further simplify the resulting equation separation of time scales enters the discussion. Because of

the difference in time scales we assume correlations between environment's observables go to zero on *any time scale of the system*, *i.e.* environment's dynamics is faster than system's one. This means that we can extend the integral from zero up to infinity after a change of variables:

$$\frac{d}{dt}\hat{\rho}_S(t) = -\int_0^\infty ds\, Tr_E([\hat{H}_I(t),[\hat{H}_I(t-s),\hat{\rho}_S(t)\otimes\hat{\rho}_E(0)]]). \tag{5.13}$$

This is what is usually referred to as the Markov approximation because of the local character of the equation and thus the so called absence of *memory*. Nevertheless it can be noticed that this has nothing to do with classical Markov assumption as introduced above. The link it is not clear apart for the memoryless character of both, which has not been justified mathematically in the quantum case.

Starting from Eq. (5.13) it is possible to show that the equation of motion is given by [135]

$$\begin{aligned}\frac{d}{dt}\hat{\rho}_S(t) &= -\imath[\hat{H}_{LS},\hat{\rho}_S(t)] + \mathcal{D}(\hat{\rho}_S(t))),\\ \mathcal{D}(\bullet) &= \sum_\omega\sum_\alpha \gamma_\alpha(\omega)\left(\hat{A}_\alpha(\omega)\bullet\hat{A}^\dagger_\alpha(\omega) - \frac{1}{2}\left\{\hat{A}^\dagger_\alpha(\omega)\hat{A}_\alpha(\omega),\bullet\right\}\right),\end{aligned} \tag{5.14}$$

where $\hat{H}_{LS}$ is a residual unitary dynamics that is often called the Lamb shift contribution in analogy with the Lamb shift of the energy levels of an atom resulting from the interaction with the electromagnetic vacuum. The so called super-operator $\mathcal{D}$ is responsible for the non-unitary dynamics of the reduced density matrix of the system.

## 5.4 The dynamical map

At this point it is useful to define the dynamical map $\Phi_{t,t_0}$ as:

$$\Phi_{t,t_0} \;:\; \hat{\rho}_S(t_0) = Tr_E\big[\hat{\rho}(t_0)\big] \;\rightarrow\; \hat{\rho}_S(t) = Tr_E\big[\hat{U}(t,t_0)\hat{\rho}(t_0)\hat{U}^\dagger(t,t_0)\big]. \tag{5.15}$$

In the following it will be useful to consider expressions such as

$$Tr_E\big[\hat{U}(t,t_0)\;\hat{o}\otimes\hat{\rho}_E\;\hat{U}^\dagger(t,t_0)\big], \tag{5.16}$$

where $\hat{o}$ is an operator acting *only* on the Hilbert space $\mathcal{H}_S$ of the system whereas $\rho_E$ is the density operator of the environment. It is possible to show that the algebra of

operators acting on a Hilbert space $\mathcal{H}$ can always be written as a linear combination of the identity operator plus a set of $N^2-1$ ($N=\dim(\mathcal{H})$) operators $\{\hat{F}_j\}$ such that $Tr[\hat{F}_j]=0$ and $Tr[\check{F}^i\hat{F}_j]=\delta_{i,j}$ where the last identity defines the dual operators $\{\check{F}^i\}$. Furthermore these operators are characterized by the relations $[\hat{F}_i,\hat{F}_j]=d_{ij}^k\ \hat{F}_k$ and $\{\hat{F}_i,\hat{F}_j\}=2\delta_{i,j}/N+s_{ij}^k\ \hat{F}_k$ where the structure factors $d_{ij}^k$ and $s_{ij}^k$ have been defined.

It is then possible to write *any* operator acting on the whole Hilbert space $\mathcal{H}=\mathcal{H}_S\otimes\mathcal{H}_E$ as a linear superposition of the operators $\{\hat{f}_i\otimes\hat{F}_j;\ 0\leq i\leq N_S^2-1, 0\leq j\leq N_E^2-1\}$ where $\{\hat{f}_i\}$ and $\{\hat{F}_j\}$ act on the Hilbert spaces $\mathcal{H}_S$ and $\mathcal{H}_E$ respectively and $\hat{f}_0=\hat{1}_S/N_S,\ \hat{F}_0=\hat{1}_E/N_E$.

By writing both $\hat{U}(t,0)$ and $\hat{o}\otimes\hat{\rho}_E$ in the basis $\{\hat{f}_i\otimes\hat{F}_j;\ 0\leq i\leq N_S^2-1, 0\leq j\leq N_E^2-1\}$ with the help of the dual operators and by making use of the commutation and anti-commutation relations one can prove that the time evolution of the operator $\hat{o}$ is given by

$$\Phi_{t,t_0}\ :\ \sum_{i=0}^{N_S^2-1} c^i(t_0)\,\hat{f}_i\ \rightarrow\ \sum_{i,j=0}^{N_S^2-1} D_i^j(t)c^i(t_0)\,\hat{f}_j, \tag{5.17}$$

where $c^i(t_0)=Tr[\check{f}^i\hat{o}]$ and the $D_i^j(t)$ are coefficient which depend upon the evolution operator $\hat{U}(t,0)$ and the environmental state $\hat{\rho}_E$.

As it can be noted we used the same symbol for the density operator and the above functional that maps the operator $\hat{o}$ into its evolved. This is true whenever the initial operator is separable such as $\hat{o}\otimes\hat{\rho}_E$ because the resulting operator $\Phi_{t,t_0}$ depends only on the state $\hat{\rho}_E$ and not on system and environment correlations. This property is very important for the definition of Markov regimes as we shall see in the following.

## 5.5 Multivariate time correlation functions

Let us now consider a system interacting with its environment. We assume that the interaction does not change significantly the state of the bath, *i.e.* $Tr_S[\hat{\rho}(t)]\approx\hat{\rho}_E$ where $\hat{\rho}(t)$ is the total density matrix at time $t$. The validity assumption relies on the physical problem under study and if the state of the environment sensibly changes during the time interval we are considering it will not be possible to separate the two dynamics but they will have to be considered as a joint one. We then define two functionals $\mathcal{P}$ and $\mathcal{Q}$ acting on the algebra of operators of the total system such that

$$\mathcal{P}[\hat{O}]=Tr_E[\hat{O}]\otimes\hat{\rho}_E, \tag{5.18}$$

and

$$\mathcal{Q} = \mathcal{I} - \mathcal{P}, \tag{5.19}$$

where $\hat{O}$ is an operator acting on the total Hilbert space and $\mathcal{I}[\hat{O}] = \hat{O}$ is the identity functional. Let us first consider the expression $\langle \hat{o}_1(t+\tau)\hat{o}_2(t)\rangle$ where the operators $\hat{o}_i$ only act on the system's Hilbert space. By means of the definition $T(\tau_1,\tau_0)[\bullet] = e^{-\imath\hat{H}(\tau_1-\tau_0)}\bullet e^{\imath\hat{H}(\tau_1-\tau_0)}$ where $\hat{H}$ is the (total) Hamiltonian of the system and $\hat{o}_i(t) = e^{\imath\hat{H}t}\hat{o}_i e^{-\imath\hat{H}t}$ it is possible to show that

$$\langle \hat{o}_1(t+\tau)\hat{o}_2(t)\rangle \;=\; Tr_S\Big[\hat{o}_1 Tr_E\Big[T(\tau,t_0)\big[\,\hat{o}_2 T(t,t_0)[\rho(t_0)]\,\big]\,\Big]\Big]. \tag{5.20}$$

By making use of identity functionals $\mathcal{I} = \mathcal{P} + \mathcal{Q}$ the above expression reads:

$$\begin{aligned} &Tr_S\Big[\hat{o}_1\, Tr_E\Big[T(\tau,0)\,\hat{o}_2\,T(t,t_0)\,\rho(t_0)\;\Big]\Big] \\ &= \sum_{i,j,k=1}^{2} Tr_S\Big[\hat{o}_1\, Tr_E\Big[\;\mathcal{K}_k\,T(\tau,t_0)\,\hat{o}_2\,\mathcal{K}_j\,T(t,t_0)\,\mathcal{K}_i\,\rho(t_0)\;\Big]\Big], \end{aligned} \tag{5.21}$$

where $\mathcal{K}_1 = \mathcal{P}$ and $\mathcal{K}_2 = \mathcal{Q}$ (for readability we dropped square brackets and we assume that every functional does act on *everything* on its right side). The relation derived in the previous section allows us to prove that

$$\begin{aligned} &Tr_S\left[\hat{o}_1\, Tr_E\left[\mathcal{P}\,T(\tau,0)\,\hat{o}_2\,\mathcal{P}\,T(t,t_0)\mathcal{P}\rho(t_0)\right]\right] \\ &= Tr_S\left[\hat{o}_1\,\Phi_{\tau,0}\,\hat{o}_2\,\Phi_{t,t_0}\,\rho_S(t_0)\right]. \end{aligned} \tag{5.22}$$

This expression can be easily obtained by assuming that the infinitesimal generator of the system's dynamics is of the Lindbland form [53, 135]. In fact in this case the relation $\langle \hat{o}_1(t+\tau)\hat{o}_2(t)\rangle \;= Tr_S\Big[\hat{o}_1\,\Phi_{\tau,0}\,\hat{o}_2\,\Phi_{t,0}\,\rho_S(0)\;\Big]$ holds because other terms in the sum on the right hand side of Eq. (5.21) vanish. It is easy to see that expressions analogous to Eq. (5.21) hold for generic n-point (in time) correlation functions.

Thus if the infinitesimal generator of the dynamics of a system is of the Lindbland form the knowledge of the propagator $\Phi_{t,t_0}$ and the initial state of the system is enough to fully characterize the system dynamics. This is a crucial point for our discussion and we will therefore discuss it in more detail. The fact that the knowledge of both the propagator and the initial condition is, in general, not enough is related to the generation of correlations between the system and the environment. This has recently been used

as an argument for the comparison of the two main witnesses of the degree of non-Markovianity available, namely the divisibility of the map and the so called information back-flow [142]. The same holds in classical stochastic processes [137, 138] where for non Markov maps the n-point relative probability density's evolution does depend on a hierarchy of relative density probabilities.

Since the effect of $\mathcal{P}$ is to factorize whatever it acts on then in $\mathcal{Q}[\hat{O}]$ we find the correlations between system and environment. A term such as

$$Tr_S\left[\hat{o}_1\, Tr_E\left[\mathcal{P}\, T(\tau,0)\, \hat{o}_2\, \mathcal{Q}\, T(t,t_0)\, \mathcal{P}\rho(t_0)\right]\right] \tag{5.23}$$

propagates the correlations generated by the joint system-environment evolution during the time interval $[t_0, t]$ from time $t$ up to time $t+\tau$. So we can define the Markov regime as the one in which these correlations are negligible recovering a nice and compact expression for the multivariate correlation functions. Moreover we maintain the physical implication of classical Markov approximation, *i.e.* we can calculate any quantity from the knowledge of the initial probability condition and the relative probability distribution density which in the quantum case is replaced by the functional $\Phi_{t_2,t_1}$. This fact was already pointed out by Grishanin [139, 140] in the study of an atom interacting with a strong electromagnetic field more than 30 years ago. Moreover we found the same definition of a Markov process proposed by Lindblad himself in an appendix of his book [123]. Now we can give to that proposal an explanation in terms of correlations generated in the joint system-environment dynamics.

In what follow we will apply this idea to two exemplary models: the decay of a two level atom in vacuum and the decoherence induced by a bosonic bath on a two level system. The choice of the two systems is motivated by the possibility to evaluate exactly the two point correlation functions $\langle\hat{o}_1(t+\tau)\hat{o}_2(t)\rangle$ and find the dynamical map $\Phi$ for the density operator. Our aim is to compare the exact value of the correlation functions $\langle\hat{o}_1(t+\tau)\hat{o}_2(t)\rangle_{exp} = Tr_S\left[Tr_E\left[\hat{o}_1(t+\tau)\hat{o}_2(t)\rho(t_0)\right]\right]$ with those calculated by means of expression (5.22) $\langle\hat{o}_1(t+\tau)\hat{o}_2(t)\rangle_M$. The suffixes "exp" and "M" stand for "experimental" and "Markov" since the first ones are correlation function that would be measured in a real experiment whereas the second ones are those calculated from the knowledge of the dynamical map $\Phi$ only and they would be exact in the Markov regime. Any difference between the two will be a signature of transition from the Markov to the non-Markov regime.

## 5.6 Decay of a two-level atom

In this section we consider the free decay of a two level atom coupled to a bosonic bath in its vacuum state. The Hamiltonian operator is given by

$$\begin{aligned}\hat{H} &= \hat{H}_0 + \hat{H}_I,\\ \hat{H}_0 &= \frac{\omega_0}{2}\hat{\sigma}_z + \sum_{\mathbf{k}} \omega_{\mathbf{k}}\, \hat{b}^\dagger_{\mathbf{k}}\hat{b}_{\mathbf{k}},\\ \hat{H}_I &= \hat{\sigma}_+ \sum_{\mathbf{k}} g_{\mathbf{k}}\, \hat{b}_{\mathbf{k}} + \hat{\sigma}_- \sum_{\mathbf{k}} g^*_{\mathbf{k}}\, \hat{b}^\dagger_{\mathbf{k}}.\end{aligned} \tag{5.24}$$

### 5.6.1 Exact solution

In order to calculate the multivariate correlation functions between $n$ operators $\hat{o}$ acting on the system's Hilbert space we need to obtain $\hat{o}(t) = e^{\imath\hat{H}t}\hat{o}e^{-\imath\hat{H}t}$. It is in general not possible to find a closed formula for it, but in the single excitation case as the evolution operator can be written as:

$$\begin{aligned}\hat{U}(t) = e^{-\imath\hat{H}t} = c_0(t)|0,0\rangle\langle 0,0| + c_1(t)|1,0\rangle\langle 1,0| + \sum_{\mathbf{q}} c_{\mathbf{q}}|0,1_{\mathbf{q}}\rangle\langle 0,1_{\mathbf{q}}|\\ + \sum_{\mathbf{q}}\sum_{\mathbf{p}\neq\mathbf{q}} c_{\mathbf{qp}}|0,1_{\mathbf{q}}\rangle\langle 0,1_{\mathbf{p}}|\\ + \sum_{\mathbf{q}} \lambda_{\mathbf{q}}|0,1_{\mathbf{q}}\rangle\langle 1,0| + \sum_{\mathbf{q}} \mu_{\mathbf{q}}|1,0\rangle\langle 0,1_{\mathbf{q}}|.\end{aligned} \tag{5.25}$$

Since $[\hat{U}(t), \hat{H}] = 0$ the following equalities hold to be true:

$$\begin{aligned}\mu_{\mathbf{q}}(t) &= \frac{g_{\mathbf{q}}}{g^*_{\mathbf{q}}}\,\lambda_{\mathbf{q}}(t)\\ c_{\mathbf{q}}(t) &= c_1(t) + \left(\frac{\omega_{\mathbf{q}}-\omega_0}{g^*_{\mathbf{q}}} - \sum_{\mathbf{p}\neq\mathbf{q}} \frac{g^*_{\mathbf{p}}}{g^*_{\mathbf{q}}}\frac{g_{\mathbf{p}}-g_{\mathbf{q}}}{\omega_{\mathbf{q}}-\omega_{\mathbf{p}}}\right)\lambda_{\mathbf{q}}(t),\\ c_{\mathbf{qp}}(t) &= \frac{g_{\mathbf{p}}-g_{\mathbf{q}}}{\omega_{\mathbf{q}}-\omega_{\mathbf{p}}}\lambda_{\mathbf{q}}(t),\end{aligned} \tag{5.26}$$

so that one has to solve only for the independent variables, namely $c_1(t)$ and $\lambda^*_{\mathbf{q}}(t)$. By using the equation $d\hat{U}(t)/dt = -\imath\hat{H}\hat{U}(t)$ and by mean of a change of variables $\tilde{c}_1(t) = c_1(t)e^{\imath\frac{\omega_0}{2}t}$ and $\tilde{\lambda}_{\mathbf{q}}(t) = \lambda_{\mathbf{q}}(t)e^{\imath\frac{\omega_0}{2}t}$ one is led to the following equations:

$$\begin{aligned}
\frac{d}{dt}c_0(t) &= \imath\,\omega_0\, c_0(t),\\
\frac{d}{dt}\tilde{c}_1(t) &= -\imath \sum_{\mathbf{q}} g_{\mathbf{q}}\,\tilde{\lambda}_{\mathbf{q}}(t),\\
\frac{d}{dt}\tilde{\lambda}_{\mathbf{q}}(t) &= -\imath\,(\omega_{\mathbf{q}}-\omega_0)\,\tilde{\lambda}_{\mathbf{q}}(t) - \imath\, g^*_{\mathbf{q}}\,\tilde{c}_1(t),
\end{aligned} \tag{5.27}$$

which are to be solved with the initial conditions $c_0(0)=1,\ \tilde{c}_1(0)=1,\ \tilde{\lambda}_{\mathbf{q}}(0)=0$. The solution to the first equation are given by $c_0(t)=e^{\imath\frac{\omega_0}{2}t}$. The solution for the last two is obtained by means of the Laplace transform as:

$$\begin{aligned}
s\,\mathcal{L}[\tilde{c}_1(t)](s)-\tilde{c}_1(0) &= -\imath\sum_{\mathbf{q}} g_{\mathbf{q}}(t)\mathcal{L}[\tilde{\lambda}_{\mathbf{q}}(t)](s),\\
s\,\mathcal{L}[\tilde{\lambda}_{\mathbf{q}}(t)](s)-\tilde{\lambda}_{\mathbf{q}}(0) &= -\imath(\omega_{\mathbf{q}}-\omega_0)\mathcal{L}[\tilde{\lambda}_{\mathbf{q}}(t)](s) - \imath g_{\mathbf{q}}(t)^*\mathcal{L}[\tilde{c}_1(t)](s),
\end{aligned} \tag{5.28}$$

hence we obtain:

$$\begin{aligned}
\mathcal{L}[\tilde{c}_1(t)](s) &= \left(s+\sum_{\mathbf{q}}\frac{|g_{\mathbf{q}}|^2}{s+\imath(\omega_{\mathbf{q}}-\omega_0)}\right)^{-1},\\
\mathcal{L}[\tilde{\lambda}_{\mathbf{q}}(t)](s) &= -\imath\frac{g_{\mathbf{q}}(t)^*}{s+\imath(\omega_{\mathbf{q}}-\omega_0)}\mathcal{L}[\tilde{c}_1(t)](s).
\end{aligned} \tag{5.29}$$

By taking the limit to the continuous we have

$$\sum_{\mathbf{q}}\frac{|g_{\mathbf{q}}|^2}{s+\imath(\omega_{\mathbf{q}}-\omega_0)} \to \int_0^\infty d\omega\,\frac{J(\omega)}{s+\imath(\omega-\omega_0)}, \tag{5.30}$$

where we introduced the "spectral density" of the bath $J(\omega)$. We next note that

$$\int_0^\infty d\omega \frac{J(\omega)}{s+\imath(\omega-\omega_0)} = \mathcal{L}\left[f(t)\right](s), \tag{5.31}$$

where $f(t)=\int_0^\infty d\omega J(\omega)e^{-\imath(\omega-\omega_0)t}$. The above equation then become:

$$\begin{aligned}
\mathcal{L}[\tilde{c}_1(t)](s) &= \frac{1}{(s+\mathcal{L}[f(t)](s))},\\
\mathcal{L}[\tilde{\lambda}_{\mathbf{q}}(t)](s) &= -\imath\frac{g_{\mathbf{q}}(t)^*}{s+\imath(\omega_{\mathbf{q}}-\omega_0)}\mathcal{L}[\tilde{c}_1(t)](s).
\end{aligned} \tag{5.32}$$

Thus we have the exact time evolution of any operator in the zero and one excitation sector of the Hilbert space.

### 5.6.2 Density matrix propagator

For the case of one excitation the total state of the system can be written as $a_0(t)|0,0\rangle + a_1(t)|1,0\rangle + \sum_{\mathbf{q}} a_{\mathbf{q}}(t)|0,1_{\mathbf{q}}\rangle$ It is possible to show [135] that in this limit and for the bath in the vacuum state the master equation governing the dynamics of the system is given by:

$$\begin{aligned} &\frac{d}{dt}\hat{\rho}_S(t) = \mathcal{W}(t)(\hat{\rho}_S(t)) \\ &\mathcal{W}(t)(\bullet) = -\frac{\imath}{2}\left(\omega_0 + \frac{S(t)}{2}\right)[\hat{\sigma}_z, \bullet] + \gamma(t)\left(\hat{\sigma}_- \bullet \hat{\sigma}_+ - \frac{1}{2}\left\{\hat{\sigma}_+\hat{\sigma}_-, \bullet\right\}\right), \end{aligned} \tag{5.33}$$

where $\gamma(t) + \imath S(t) = 2\int_0^t d\tau\ f(t-\tau)\, G(\tau,0)/G(t,0)$, $f(t) = \int_0^\infty d\omega J(\omega) e^{-\imath(\omega-\omega_0)t}$ and $G(t,0)$ such that $dG(t,0)/dt = -\int_0^t d\tau\ f(t-\tau)\, G(\tau,0)$.

The "propagator" is then given by $V(t,0) = Te^{\int_0^t d\tau\ \mathcal{W}(\tau)}$ where $T$ is the time-ordering operator. Since the coefficient $\gamma(t)$ can take on negative values the super-operator $\mathcal{W}(t)$ does not need to be of Lindblad form at all times. In what follow we will have to calculate the action of the super-operator on operators acting on the Hilbert space of the system. In order to simplify these calculations we will use the damping basis, i.e. the basis made up of operators $\hat{\Lambda}_i(t)$ such that $\mathcal{W}(t)[\hat{\Lambda}^i] = \lambda_i(t)\,\hat{\Lambda}_i(t)$. In fact the "eigen-operators" $\hat{\Lambda}_i$ are time independent:

$$\begin{aligned} &\hat{\Lambda}_0 = \tfrac{1}{2}(\hat{1} - \hat{\sigma}_z) && \lambda_0(t) = 0, \\ &\hat{\Lambda}_1 = \hat{\sigma}_+ && \lambda_1(t) = -\imath\left(\omega_0 + \tfrac{S(t)}{2}\right) - \tfrac{\gamma(t)}{2}, \\ &\hat{\Lambda}_2 = \hat{\sigma}_- && \lambda_2(t) = \imath\left(\omega_0 + \tfrac{S(t)}{2}\right) - \tfrac{\gamma(t)}{2}, \\ &\hat{\Lambda}_3 = \hat{\sigma}_z && \lambda_3(t) = -\gamma(t), \end{aligned}$$

We can thus write any operator as $\hat{o} = \sum_i c^i\,\hat{\Lambda}_i$ with $c^i = Tr(\check{\Lambda}^i\hat{o})$ where the dual of the damping basis's elements are such that $Tr(\check{\Lambda}^i\hat{\Lambda}_j) = \delta^i_j$.

Let now define the matrices $(A_\alpha)^j_i = Tr\left[\check{\Lambda}^j\hat{\sigma}_\alpha\hat{\Lambda}_i\right]$ in order to simplify the calculation of the multivariate correlation functions. The two-point ones are

$$\langle\ \hat{\sigma}_\alpha(t+\tau)\hat{\sigma}_\beta(t)\ \rangle_P = Tr\left[\hat{\sigma}_\alpha(0)\Phi_{\tau,0}\hat{\sigma}_\beta(0)\Phi_{t,t_0}\hat{\rho}_S(0)\right] = \sum_{i,j}(A_\alpha)^0_j(A_\beta)^j_i e^{L_j(\tau)}e^{L_i(t)}c^i, \tag{5.34}$$

where $L_i(t) = \int_0^t ds\ \lambda_i(s)$

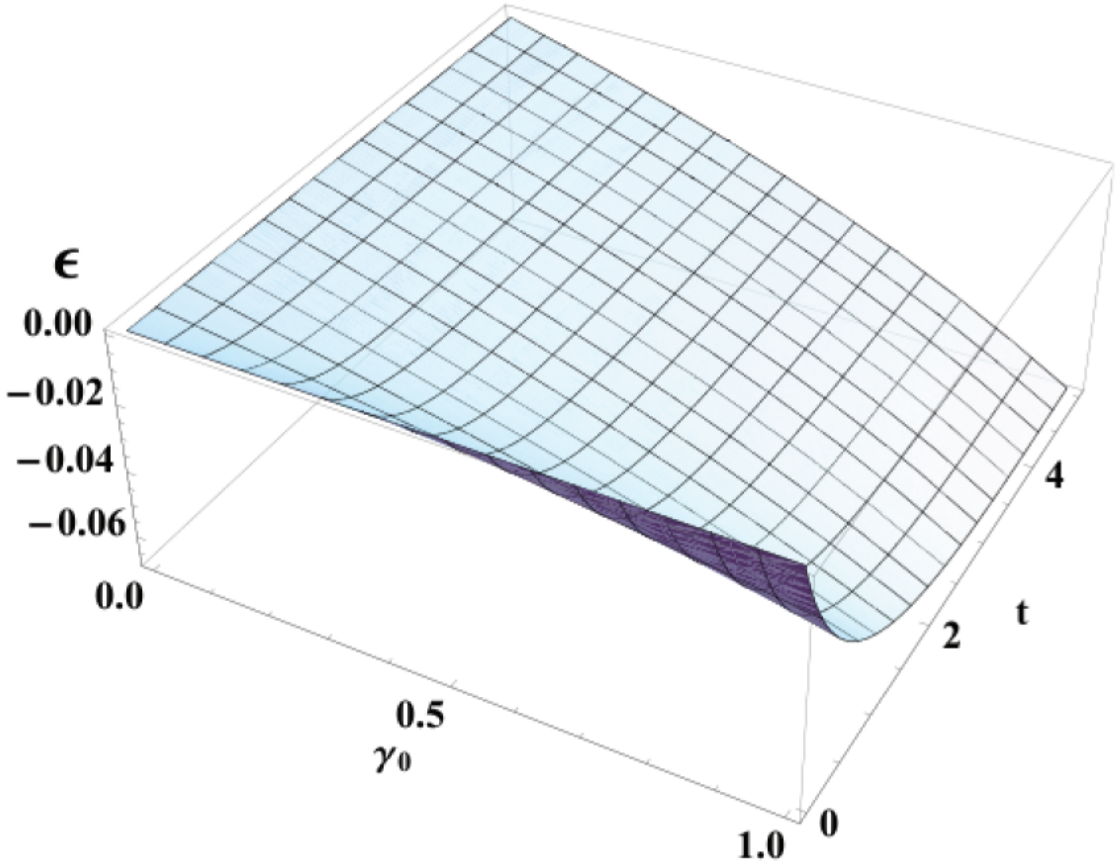



FIGURE 5.1: Plots of the relative errors for the correlation function $\langle\hat{\sigma}_+(0.1+\tau)\hat{\sigma}_-(0.1)\rangle$ for the case of the decay of a two level atom initially in its excited state interacting with a bosonic bath with spectral density in Eq. (5.35) initially in the vacuum state. The parameter used are $\omega_0 = 10,\ \lambda = 2.1,\ \Delta = 0.2$

Here we consider the case of a spectral density of the form

$$J(\omega) = \frac{1}{(2\pi)} \frac{\gamma_0 \lambda^2}{((\omega - \omega_0 + \Delta)^2 + \lambda^2)}. \tag{5.35}$$

This is the spectral density of an atom interacting with the vacuum of an electromagnetic cavity whose frequency is $\omega_0$.

We can see in Fig. 5.1 that for short times, regardless of the coupling constant $\gamma_0$ one gets $\langle\hat{o}_1(t+\tau)\hat{o}_2(t)\rangle_{exp} \approx \langle\hat{o}_1(t+\tau)\hat{o}_2(t)\rangle_M$ which is what is expected since in this limit one can determine the higher order correlation function from the one- and two-point ones. As time and coupling strength increase the deviation of the Markovian correlation functions from the real ones increase as well. It is interesting to note that both measures of non-Markovianity [127–129] so far defined give zero in the particular case considered in Fig. 5.1. We numerically checked Breuer's measure and we found that it is zero for

any value of the coupling strength $\gamma_0 \in [0,1]$. To check for the divisibility criterion we have to check that

$$\Phi_{t+\tau,t_0} = \Phi_{t+\tau,t}\Phi_{t,t_0} \tag{5.36}$$

with $\Phi_{t+\tau,t}$ being a complete positive map. We stress that the complete positivity is a requirement for the definition of Markovianity according to the work in [129] and this is one of the working assumption in Lindblad's original work [116, 117].

This is trivially true since in our case, which can be see by looking at

$$\Phi_{\tau_2,\tau_1}[\bullet] = \exp\left(-\frac{\imath}{2}\Omega(\tau_2,\tau_1)[\hat{\sigma}_z,\bullet] + \Gamma(\tau_2,\tau_1)\left(\hat{\sigma}_- \bullet \hat{\sigma}_+ - \frac{1}{2}\left\{\hat{\sigma}_+\hat{\sigma}_-,\bullet\right\}\right)\right), \tag{5.37}$$

where $\int_{\tau_1}^{\tau_2} d\tau \, \left(\omega_0 + \frac{S(\tau)}{2}\right)$ and $\Gamma(\tau_2,\tau_1) = \int_{\tau_1}^{\tau_2} d\tau \, \gamma(\tau)$

The super-operator appearing in the exponential in Eq. (5.37) admits a diagonal decomposition whose base elements are time independent. From this it is easy to see that relation (5.36) holds true and that the complete positivity of $\Phi_{t+\tau,t}$ in our case comes from the complete positivity of $\gamma(t)$ in the time interval considered.

## 5.7 Decoherence of a two-level atom

As a second example we consider in this section the decoherence of a qubit in vacuum. The Hamiltonian operator is given by

$$\begin{aligned} \hat{H} &= \hat{H}_0 + \hat{H}_I, \\ \hat{H}_0 &= \frac{\omega_0}{2}\hat{\sigma}_z + \sum_{\mathbf{k}} \omega_{\mathbf{k}}\, \hat{b}^\dagger_{\mathbf{k}}\hat{b}_{\mathbf{k}}, \\ \hat{H}_I &= \hat{\sigma}_z \sum_{\mathbf{k}} \left(g_{\mathbf{k}}\, \hat{b}_{\mathbf{k}} + g^*_{\mathbf{k}}\, \hat{b}^\dagger_{\mathbf{k}}\right). \end{aligned} \tag{5.38}$$

### 5.7.1 Exact solution

In the interaction picture the (total) time evolution operator is $\hat{U}(t) = \hat{1}_S \otimes \cosh(\hat{P}(t)) + \hat{\sigma}_z \otimes \sinh(\hat{P}(t))$ where $\hat{P}(t) = \sum_{\mathbf{k}} \left(\alpha^*_{\mathbf{k}}(t)\, \hat{b}^\dagger_{\mathbf{k}} - \alpha_{\mathbf{k}}(t)\, \hat{b}_{\mathbf{k}}\right)$ and $\alpha_{\mathbf{k}}(t) = g_{\mathbf{k}}(1 - e^{\imath\omega_{\mathbf{k}}t})/\omega_{\mathbf{k}}$. In order to evaluate the exact two-point correlation function of any two operators $\hat{o}_1$

and $\hat{o}_2$ acting only on the system's Hilbert space we have to calculate $\hat{o}_1(t_1)\hat{o}_2(t_2) = \hat{U}^\dagger(t_1-t_0)\hat{o}_1(t_0)\hat{U}(t_1-t_0)\hat{U}^\dagger(t_2-t_0)\hat{o}_2(t_0)\hat{U}(t_2-t_0)$. Assuming the electromagnetic field to be initially in a thermal state we find after lengthy calculations (we do not present them here because the expressions are cumbersome and the intermediate steps have been performed by using the software Mathematica):

$$\begin{aligned} Tr_E\big[\hat{o}_1(t_1)\hat{o}_2(t_2)\,\hat{\rho}_E\big] &= f_1(t_1,t_2)\,\hat{o}_1(t_0)\,\hat{o}_2(t_0) + f_2(t_1,t_2)\,\hat{\sigma}_z\,\hat{o}_1(t_0)\,\hat{o}_2(t_0)\,\hat{\sigma}_z \\ &\quad + f_3(t_1,t_2)\,\hat{o}_1(t_0)\,\hat{\sigma}_z\,\hat{o}_2(t_0)\,\hat{\sigma}_z + f_4(t_1,t_2)\,\hat{\sigma}_z\,\hat{o}_1(t_0)\,\hat{\sigma}_z\,\hat{o}_2(t_0), \end{aligned} \tag{5.39}$$

with

$$\begin{aligned} f_1(t_1,t_2) &= \frac{1}{4}\left(1+e^{-g(t_1)}+e^{-g(t_2)}+e^{-h(t_1,t_2)}\right), \\ f_2(t_1,t_2) &= \frac{1}{4}\left(1-e^{-g(t_1)}-e^{-g(t_2)}+e^{-h(t_1,t_2)}\right), \\ f_3(t_1,t_2) &= \frac{1}{4}\left(1+e^{-g(t_1)}-e^{-g(t_2)}-e^{-h(t_1,t_2)}\right), \\ f_4(t_1,t_2) &= \frac{1}{4}\left(1-e^{-g(t_1)}+e^{-g(t_2)}-e^{-h(t_1,t_2)}\right), \end{aligned} \tag{5.40}$$

where the continuous limit has been taken and we have defined the functions

$$g(t) = 4\int_0^\infty d\omega\,\frac{J(\omega)}{\omega^2}(1-\cos(\omega t))\coth\left(\frac{\beta\omega}{2}\right), \tag{5.41}$$

and

$$\begin{aligned} h(t_1,t_2) = 4\int_0^\infty d\omega\,\frac{J(\omega)}{\omega^2}\Bigg[&(1-\cos(\omega(t_1-t_2)))\coth\left(\frac{\beta\omega}{2}\right) \\ &+ \imath(\sin(\omega t_1)-\sin(\omega(t_1-t_2))-\sin(\omega t_2))\Bigg], \end{aligned} \tag{5.42}$$

where $\beta$ is the inverse temperature of the environment.

### 5.7.2 Density matrix propagator

In this case we find that calculating the density matrix map is an easier task since the interaction Hamiltonian commutes with the free Hamiltonian of the two level atom. By definition we have

$$\Phi_{t,t_0}[\hat{\rho}_S(t_0)] = Tr_E\Big[\hat{U}(t-t_0)\hat{\rho}(t_0)\hat{U}^\dagger(t-t_0)\Big], \tag{5.43}$$

where as usual $\hat{\rho}_S(t_0) = Tr_E\Big[\hat{\rho}(t_0)\Big]$.

For the dynamical map we have

$$\begin{aligned}\Phi_{t,t_0}[\hat{\rho}_S(t_0)] = \quad & \hat{\rho}_S(t_0) \quad Tr_E\Big[\cosh(\hat{P})\hat{\rho}_E(t_0)\cosh(\hat{P})\Big] \\ & - \hat{\sigma}_z\,\hat{\rho}_S(t_0)\,\hat{\sigma}_z\; Tr_E\Big[\sinh(\hat{P})\hat{\rho}_E(t_0)\sinh(\hat{P})\Big] \\ & - \quad \hat{\rho}_S(t_0)\,\hat{\sigma}_z\; Tr_E\Big[\cosh(\hat{P})\hat{\rho}_E(t_0)\sinh(\hat{P})\Big] \\ & + \hat{\sigma}_z\,\hat{\rho}_S(t_0) \quad Tr_E\Big[\sinh(\hat{P})\hat{\rho}_E(t_0)\cosh(\hat{P})\Big],\end{aligned} \tag{5.44}$$

where we have defined $\cosh(\hat{P}) = (e^{\hat{P}} + e^{-\hat{P}})/2$ and analogously for $\sinh(\hat{P})$. It is useful to note that $e^{\hat{P}} = \otimes_{\mathbf{k}} e^{(\alpha^*_{\mathbf{k}}\,\hat{b}^\dagger_{\mathbf{k}} - \alpha_{\mathbf{k}}\,\hat{b}_{\mathbf{k}})} = \otimes_{\mathbf{k}} D(\alpha^*_{\mathbf{k}})$ where $D(\bullet)$ is the displacement operator. The numerical values are easily calculated as shown below. The propagator is then given by:

$$\Phi_{t,t_0}[\hat{\rho}_S(t_0)] = \frac{1}{2}\left(\hat{\rho}_S(t_0)\left(1 + e^{-g(t-t_0)}\right) + \hat{\sigma}_z\,\hat{\rho}_S(t_0)\,\hat{\sigma}_z\left(1 - e^{-g(t-t_0)}\right)\right) \tag{5.45}$$

where again $g(t-t_0) = 4\int_0^\infty d\omega\, J(\omega)\omega^{-2}(1-\cos(\omega(t-t_0)))\coth(\beta\omega/2)$ .

### 5.7.3 Trace over the environment

In this section we show how to calculate the traces over the environment's degrees of freedom by means of phase space methods. We are interested in the case of an environment initially in equilibrium at a temperature $T$. The state can then be written as $\hat{\rho}_E(t_0) = \otimes_{\mathbf{k}}\hat{\rho}_{\mathbf{k}}$ with $\hat{\rho}_{\mathbf{k}} = (1 - e^{-\beta\omega_{\mathbf{k}}})\sum_{n_{\mathbf{k}}=0}^{\infty} |n_{\mathbf{k}}\rangle\langle n_{\mathbf{k}}| e^{-\beta n_{\mathbf{k}}\omega_{\mathbf{k}}}$.

The traces over the environmental degrees of freedom appearing in the density matrix propagator involve the evaluations of terms such as $Tr_{\mathbf{k}}(D(\alpha^*_{\mathbf{k}})\hat{\rho}_{\mathbf{k}}D(\alpha^*_{\mathbf{k}}))$ which traces can be easily calculated by noting the following:

- $D(\alpha)D(\beta) = e^{(\alpha\beta^* - \alpha^*\beta)/2}D(\alpha+\beta)$;
- $D(\alpha) = e^{-|\alpha|^2/2}e^{\alpha\hat{b}^\dagger}e^{-\alpha^*\hat{b}}$;
- By definition $\chi(\alpha,\alpha^*) = Tr(\hat{\rho}e^{\alpha\hat{b}^\dagger}e^{-\alpha^*\hat{b}})$ is the characteristic function which generates the Q-function corresponding to the state $\hat{\rho}$ in phase space;
- For the harmonic oscillator in a thermal state at temperature $\beta = (Tk_B)^{-1}$: $\chi(\alpha,\alpha^*) = e^{-|\alpha|^2/(e^{\beta\omega}-1)}$ .

Therefore we have:

$$\begin{aligned} Tr_{\mathbf{k}}(D(\alpha_{\mathbf{k}}^*)\hat{\rho}_{\mathbf{k}}D(\alpha_{\mathbf{k}}^*)) &= Tr_{\mathbf{k}}(\hat{\rho}_{\mathbf{k}}D(\alpha_{\mathbf{k}}^*)D(\alpha_{\mathbf{k}}^*)) \\ &= Tr_{\mathbf{k}}(\hat{\rho}_{\mathbf{k}}D(2\alpha_{\mathbf{k}}^*)) \\ &= e^{-2|\alpha_{\mathbf{k}}|^2}Tr_{\mathbf{k}}(\hat{\rho}_{\mathbf{k}}e^{2\alpha_{\mathbf{k}}^*\hat{b}^\dagger}e^{-2\alpha_{\mathbf{k}}\hat{b}}) \\ &= e^{-2|\alpha_{\mathbf{k}}|^2}\chi(2\alpha_{\mathbf{k}}^*, 2\alpha_{\mathbf{k}}) \\ &= e^{-2|\alpha_{\mathbf{k}}|^2}e^{-4|\alpha_{\mathbf{k}}|^2/(e^{\beta\omega_{\mathbf{k}}}-1)}, \end{aligned} \tag{5.46}$$

$$\begin{aligned} Tr_{\mathbf{k}}(D(-\alpha_{\mathbf{k}}^*)\hat{\rho}_{\mathbf{k}}D(-\alpha_{\mathbf{k}}^*)) &= Tr_{\mathbf{k}}(\hat{\rho}_{\mathbf{k}}D(-\alpha_{\mathbf{k}}^*)D(-\alpha_{\mathbf{k}}^*)) \\ &= Tr_{\mathbf{k}}(\hat{\rho}_{\mathbf{k}}D(-2\alpha_{\mathbf{k}}^*)) \\ &= e^{-2|\alpha_{\mathbf{k}}|^2}Tr_{\mathbf{k}}(\hat{\rho}_{\mathbf{k}}e^{-2\alpha_{\mathbf{k}}^*\hat{b}^\dagger}e^{2\alpha_{\mathbf{k}}\hat{b}}) \\ &= e^{-2|\alpha_{\mathbf{k}}|^2}\chi(-2\alpha_{\mathbf{k}}^*, -2\alpha_{\mathbf{k}}) \\ &= e^{-2|\alpha_{\mathbf{k}}|^2}e^{-4|\alpha_{\mathbf{k}}|^2/(e^{\beta\omega_{\mathbf{k}}}-1)}, \end{aligned} \tag{5.47}$$

$$\begin{aligned} Tr_{\mathbf{k}}(D(\alpha_{\mathbf{k}}^*)\hat{\rho}_{\mathbf{k}}D(-\alpha_{\mathbf{k}}^*)) &= Tr_{\mathbf{k}}(\hat{\rho}_{\mathbf{k}}D(-\alpha_{\mathbf{k}}^*)D(\alpha_{\mathbf{k}}^*)) \\ &= Tr_{\mathbf{k}}(\hat{\rho}_{\mathbf{k}}D(0)) = 1, \end{aligned} \tag{5.48}$$

$$\begin{aligned} Tr_{\mathbf{k}}(D(-\alpha_{\mathbf{k}}^*)\hat{\rho}_{\mathbf{k}}D(\alpha_{\mathbf{k}}^*)) &= Tr_{\mathbf{k}}(\hat{\rho}_{\mathbf{k}}D(\alpha_{\mathbf{k}}^*)D(-\alpha_{\mathbf{k}}^*)) \\ &= Tr_{\mathbf{k}}(\hat{\rho}_{\mathbf{k}}D(0)) = 1. \end{aligned} \tag{5.49}$$

By considering a spectral density of the form

$$J(\omega) = \frac{1}{2\pi}\omega\frac{\gamma_0\lambda^2}{\omega^2+\lambda^2}, \tag{5.50}$$

we can easily calculate the above expression for $g(t)$. The linear term $\omega$ that multiplies the otherwise Lorentzian spectral density guarantees that the function vanishes as $\omega \to 0$ avoiding unwanted singularities in the calculations. Surprisingly we find that in this case the system is always Markovian regardless of the coupling constant $\gamma_0$. We are not able to give an explanation for this behavior yet and we are currently working to better understand it.

## 5.8 Conclusions

We have shown that it is possible to define the Markov regime for quantum dynamics in analogy with the Markov assumption for classical stochastic processes. The idea behind

this definition is that the knowledge of both the density operator's propagator and the initial state of the system only is enough to *fully* characterize the system dynamics, *i.e.* be able to calculate any of the n-point (in time) correlation functions. We saw that in the quantum case the non Markov regime is due to the build up of correlations between system and environment that are propagated during the joint evolution. This implies, as in the classical case, that the n-point correlation functions need to be calculated by means of ad hoc n-point propagators $\Phi^{(n)}_{t_n,\cdots,t_1,t_0}$ which are in general not related to $\Phi$.

Moreover we stress that our definition of the Markov regime is not related to any of the two measures (or witnesses) previously proposed [130, 131]. The reason is that both these measures rely only on the "two points propagator" $\Phi_{t,t_0}$ and nothing is said about the correlation functions which nevertheless have a clear physical meaning. For instance the distinguishability criterion on which the measure of Markovianity by Breuer [127] is based deals with the mean value of the observables only. Given two state it describes how likely it is that one can distinguish them by performing a measurement of some observables. It is a static definition whereas (non-)Markovianity is based on the dynamical properties. One could think for instance of a process for which the mean values of the observables are the same ones but nevertheless their correlation functions are different. A similar argument holds for the comparison with the divisibility criterion [128, 129]. As already noticed by Lindblad our criterion is a natural generalization of the classical Markov assumption. Moreover we explicitly showed that the non-Markovian behavior arises as a consequence of the building up of coherences between system and environment. In real systems this is an important issue because it tells us that the environment plays an active role in the system's dynamics.

The work presented in this chapter has been done in collaboration with I. Sinaynskiy, Th. Busch and F. Petruccione.

# Conclusions and Outlook

In this thesis I have addressed different topics of quantum behavior at different scales. It can be divided into two parts that complement each other. In the first part I have analyzed quantum behavior in hybrid systems and Bose-Einstein condensates whereas in the second one I addressed the problem of the definition of Markov regimes for open quantum systems.

"Hybrid systems" refers to all those physical systems made up of different components such as photons, mechanical oscillators, (ultra-)cold gases, etc. They accomplish different tasks such as metrology in biological systems as well as in new generations of detectors, quantum computation, collectors of energy while at the same time offering a playground for fundamental questions. They have to be properly designed and built in order to be useful and I have suggested and investigated suitable setups. I particularly focused on their role as systems to test for quantum coherences on mesoscopic scales.

In the first work I studied the stability of vortex patterns in a two dimensional BEC held in a rotating anisotropic trapping potential. The study of vortex systems is useful to understand phenomena such as the properties of high $T_c$ superconductors or dissipation in super-fluids. BECs of alkali atoms offer a very clean and fully tunable setup to observe the behavior of vortex-like systems. In particular I studied how the spatial configuration of vortex patterns changes with the anisotropy of the trapping potential. For a small number of vortices I observed that the geometries of the possible vortex patterns are finite. Moreover there are critical values of the anisotropy at which changes between the spatial patterns suddenly occur. I then studied the stability of these patterns and found that they are all unstable. Nevertheless I found that there is a clear signature of the change of patterns' geometries in the eigenvalues of the pattern modes. This work has been published in Phys. Rev. A **81**, 053625 (2010).

It is interesting to look at a three dimensional BECs where the vortex patterns become vortex filaments and their motion is described Kelvin waves. This is the ultra-cold gases version of the II-type superconductors in an external magnetic field. In this case in fact the current flowing through the superconductor would dissipate energy due to vortex

filaments motion. Moreover the inclusion of dissipation balancing the external forcing could result in stable oscillations of the vortex patterns and thereby stabilize the system.

I then addressed the problem of scaling entanglement up from microscopic to mesoscopic scales. I proposed an experimental scheme in order to transfer entanglement from photons to BECs. An entangled photon pair was obtained from parametric down conversion and interacted with a BEC. The two photons are entangled in the orbital angular momentum degree of freedom and the scheme is designed such that during the interaction with a BEC each photon transfers a quantum of angular momentum to the BEC it is interacting with. The two BECs are spatially separated and they do not interact with each other. I showed that in a finite transition time it is possible to transfer the angular momentum initially distributed between the two photons to the two BECs. The net effect is that the two BECs become entangled at the end of the protocol. The entanglement is due to the indistinguishability of particles belonging to the BEC phase. This work has been published in Phys. Rev. A **83**, 053612 (2011).

It would be interesting to extend this work by looking at the BECs as part of a quantum repeater and study the advantages of it with respect to non-rotating ultra-cold quantum gases.

In the last work of the first part I addressed the problem of revealing quantum behavior in the state of a mechanical oscillator. In recent years significant efforts have been put in reaching the quantum regime for such objects. Nevertheless we know that such a regime would be fragile due to decoherence processes that would rapidly drive the system back to a classical regime. The detection of quantum coherences in the state of the mechanical oscillator has therefore to be performed in a non invasive way. In particular I considered the case of a single clamped cantilever equipped with a magnetic molecule. I then proposed to use a BEC as an ancillary system that couples to the cantilever to monitor the cantilever state. The interaction between the cantilever and the BEC is mediated by the magnetic molecule whose magnetic moment does interact with the spin of the atoms in the BEC. The spin of the BEC then undergoes a precession motion which can be related to coherent superposition of different states of the cantilever. In order to detect the presence of these coherences I proposed the use of Faraday rotation of the polarization of a laser beam traveling through the atomic cloud. This work has been published in Phys. Rev. A **84**, 063815 (2011).

In order to make this study more applicable to a real system dissipation effects have to be taken into account. Moreover the scheme presented does not allow for the reconstruction of the state of the cantilever, which is an important requirement. A next step would be to modify the experimental scheme in order to reconstruct the cantilever state.

In the second part of the thesis I addressed a more fundamental problem. The evolution of a closed system in quantum mechanics is given by a unitary evolution, however most systems we encounter are "open" systems. It means that they interact with an external environment and this interaction has to be take into account for a proper description of the system's dynamics. The resulting equation of motion for the system can be quite complicated except in one case where the master equation is of a special form: the Gorini-Sudarshan-Kossakowski-Lindblad form. This equation has always been associated with Markov behavior for the system dynamics. The concept of a Markov process is borrowed from the theory of classical stochastic processes where, in order to simplify the mathematical description of the system dynamics, the so-called Markov assumption is made. The main implication of Markov assumption for classical systems is that the system is fully characterized by the initial condition and the Green's function for the two point probability distribution. Hence I used this physical implication to extend the definition of Markov regime for quantum open system dynamics. Nowadays it is important to know whether a system undergoes a Markov or non-Markov dynamics for at least two reasons. The first is that the mathematical description of the dynamics in a Markov regime is greatly simplified. Most importantly the deviation from Markovian behavior tells us the importance of the system-environment correlations in the system's dynamics. This is important in facing problems such as charge transport in macromolecules where the environment is a complex one (ions in solution, molecular vibrations, etc.) and it is not simple to identify the single contribution. By means of state tomography I proposed a feasible way of determining whether the Markov assumption is valid or not.

As a future work it would be useful to extend this formalism to the space of the operators (rather than focusing only on the density matrix operator) and look for effective description of the operator's dynamics.

# Bibliography


[1] O. Carnal, J. Mlynek, Phys. Rev. Lett. **66**, 2689 (1991);

[2] A. Auerbach, *Interacting Electrons and Quantum Magnetism*, Springer (1994)

[3] V. Gogonea, D. Surez, A. van der Vaart, K. M. Merz Jr, Current Opinion in Structural Biology **11**, 217;

[4] M. Wallquist, K Hammerer, P Rabl, M. Lukin, P. Zoller, Phys. Scr. **T137**, 014001 (2009);

[5] J. Huang, A.-P. Jauho, *Quantum kinetics in transport and optics of semiconductors*, (Springer, 1996);

[6] I. Bloch, J. Dalibard, W. Zwerger, Rev. Mod. Phys. **80**, 885 (2008);

[7] U.R. Fischer, R. Schtzhold, Phys. Rev. A **70**, 063615 (2004);

[8] M. Köhl, Th. Busch, K. Molmer, T. W. Hänsch, T. Esslinger, Phys. Rev. A **72**, 063618 (2005)

[9] A. Einstein, Sitzber. Kgl. Preuss. Akad. Wiss., 3 (1924);

[10] S.N. Bose , Z. Phys., 26 (1924);

[11] L.D. Landau, J. Phys USSR **5**, 71 (1941);

[12] N.N. Bogoliubov, J. Phys USSR **11**, 23 (1947);

[13] M.H. Anderson, J.R. Ensher, M.R. Matthews, C.E. Wieman, and E.A. Cornell, Science **269**, 198 (1995);

[14] J. Vewinger F. Klaers, J. Schmitt and M. Weitz., Nature **468**, 545 (2010);

[15] L. E. Sadler, J. M. Higbie, S. R. Leslie, M. Vengalattore and D. M. Stamper-Kurn, Nature **443**, 312 (2006); A. Görlitz, T. L. Gustavson, A. E. Leanhardt, R. Löw, A. P. Chikkatur, S. Gupta, S. Inouye, D. E. Pritchard, and W. Ketterle, Phys. Rev. Lett. **90**, 090401 (2003);

[16] W. Bao, H. Wang, P.A. Markowich, Comm. Math. Sci. **3**, 57 (2005).

[17] L. Pitaevskii and S. Stringari, *Bose-Einstein condensation*, (Claredon Press, 2003);

[18] M. Tinkham, *Introduction to Superconductivity*, (McGraw-Hill, 1996);

[19] V.I. Yukalov, Laser Phys. Lett. **3**, 406 (2006);

[20] J. R. Abo-Shaeer, C. Raman, J. M. Vogels, and W. Ketterle, Science **292**, 476 (2001);

[21] Y. Castin, R. Dum, Eur. Phys. J. D **7**, 399 (1999);

[22] C.J. Foot, *Atomic Physics*, (Oxford University Press, 2005);

[23] S. Chu, L. Hollberg, J.E. Bjorkholm, A. Cable, A. Ashkin, Phys. Rev. Lett. **55**, 48 (1985);

[24] W.D. Phillips, J.V. Prodan, H.J. Metcalf, J. Opt. Soc. Am. B **2**, 1751 (1985);

[25] J. Dalibard, C. Chen-Tannoudji, J. Opt. Soc. Am. B **6**, 2023 (1989);

[26] I. Buluta, F. Nori, Science **326**, 108 (2009); J. Simon, W. S. Bakr, R. Ma, M.E. Tai, P.M. Preiss, and M. Greiner, Nature **472**, 307 (2011);

[27] G. D. Bruce, S. L. Bromley, G. Smirne, L. Torralbo-Campo, D. Cassettari, Phys. Rev. A **84**, 053410 (2011);

[28] C. Chin, R. Grimm, P. Julienne, and E. Tiessinga, Rev. Mod. Phys. **82**, 1225 (2010);

[29] A.J. Leggett, Rev. Mod. Phys. **73**, 307 (2001);

[30] E. Majorana, Nuovo Cimento, 6 (1932);

[31] Y. Castin and R. Dum, Eur. Phys. J. D **7**, 399 (1999); A. Aftalion and Q. Du, Phys. Rev. A **64**, 063603 (2001);

[32] S. McEndoo and Th. Busch, Phys. Rev. A **79**, 053616 (2009); *ibid.* **82**, 013628 (2010);

[33] M.R. Matthews, *et al.* Phys. Rev. Lett. **83**, 2498 (1999); A.E. Leanhardt, *et al.*, *ibid.* **89**, 190403 (2002);

[34] K.W. Madison, *et al.*, Phys. Rev. Lett. **84**, 806 (2000); J.R. Abo-Shaeer, *et al.*, Science **292**, 476 (2001);

[35] V. Schweikhard, I. Coddington, P. Engels, V. P. Mogendorff, and E.A. Cornell, Phys. Rev. Lett. **92**, 040404 (2004);

[36] J. Kasprzak *et all*, Nature **443**, 409 (2006);

[37] G. Birkl, S. Kassner, and H. Walther, Nature **357**, 310 (1992); I. Waki, *et al.*, Phys. Rev. Lett. **68**, 2007 (1992); J.P. Schiffer, *ibid.* **70**, 818 (1993); G. Morigi and S. Fishman, *ibid.* **93**, 170602 (2004).

[38] G. Baym, Phys. Rev. Lett. **91**, 110402 (2003); T. Mizushima, *et al.*, *ibid.* **92**, 060407 (2004);

[39] I. Coddington, *et al.*, Phys. Rev. Lett. **91**, 100402 (2003);

[40] S.I. Matveenko, *et al.*, Phys. Rev. A **80**, 063621 (2009).

[41] J.W. Reijnders and R.A. Duine, Phys. Rev. A **71**, 063607 (2005).

[42] L.J. Campbell, Phys. Rev. A **24**, 514 (1981).

[43] L.D. Landau and E.M. Lifshitz, *Statistical Physics* (Pergamon, Oxford, 1958).

[44] R. Ignat and V. Millot, J. Funct. Anal. **233**, 260 (2006); Rev. Math. Phys. **18**, 119 (2006).

[45] N.G. Parker and C.S. Adams, Phys. Rev. Lett. **95**, 145301 (2006);

[46] E. Kozik and B. Svistunov, Phys. Rev. B **72**, 172505 (2005).

[47] C. Lobo, A. Sinatra and Y. Castin, Phys. Rev. Lett. **92**, 020403 (2004).

[48] V. K. Tkachencko, Sov. Phys. JETP **22**, 1049 (1282); *ibid.* **23**, 1049 (1966).

[49] B.I. Halperin and D.R. Nelson, J. Low. Temp. Phys. **36**, 599 (1979); K. Mullen, Phys. Rev. B **60**, 4334 (1999).

[50] J. Pearl, in *Low temperature physics* **LT9**, J.G. Daunt, D.O. Edwards, F.J. Milford and M. Yagub eds. (Plenum, New York, 1965).

[51] D.A. Luzhbin, Phys. Solid State **43**, 1823 (2006).

[52] C. Bruder, *et al.*, Ann. der Phys. **14**, 566 (2005).

[53] C.W. Gardiner, P. Zoller, *Quantum noise*, (Springer, 1991);

[54] P. Caruthers. M.M. Nieto, Rev. Mod. Phys. **40**, 411 (1968);

[55] A. Fedrizzi, *et al.*, Nature Phys. **5**, 389 (2009); R. Ursin *et al.*, *ibid.* **3**, 481 (2007); D. Rosenberg, *et al.*, Phys. Rev. Lett. **98**, 010503 (2007); T. Schmitt-Manderbach, *et al.*, *ibid.* **98**, 010504 (2007); C.-Z. Peng *et al. ibid.* **98**, 010505 (2007);

[56] Y.-A. Chen, *et al.*, Nature Phys. **4**, 103 (2008); Z.-S. Yuan, *et al.*, Nature (London) **454**, 1098 (2008); C.-W. Chou *et al.*, Science **316**, 1316 (2007); K. S. Choi, H. Deng, J. Laurat, and H. J. Kimble, Nature (London) **452**, 67 (2008);

[57] P. Kok, *et al*, Rev. Mod. Phys. **79**, 135 (2007) and references within; S. Braunstein and P. van Loock, *ibid.* **77**, 513 (2005) and references within; J.-W. Pan, *et al.*, Rev. Mod. Phys. **84** 777 (2012) and references within;

[58] S. Franke-Arnold, L. Allen, and M. Padgett, Laser & Photon. Rev. **2**, 299 (2008);

[59] G. Gibson, J. Courtial, M. J. Padgett, M. Vasnetsov, V. Pas'ko, S. M. Barnett, and S. Franke-Arnold, Opt. Express **12**, 5448 (2004);

[60] H. He, M. E. J. Friese, N. R. Heckenberg, and H. Rubinsztein Dunlop, Phys. Rev. Lett. **75**, 826 (1995);

[61] A. Mair, A. Vaziri, G. Weihs, and A. Zeilinger, Nature **412**, 313 (2001);

[62] A. Vaziri, G. Weihs, and A. Zeilinger, Phys. Rev. Lett. **89**, 240401 (2002); A. Vaziri, J.-W. Pan, T. Jennewein, G. Weihs, and A. Zeilinger, Phys. Rev. Lett. **91**, 227902 (2003);

[63] S. Barz, G. Cronenberg, A. Zeilinger, and P. Walther, Nature **4**, 553 (2010);

[64] G. Molina-Terriza, J. P. Torres, and Ll. Torner, Nature Phys. **3**, 605 (2007);

[65] M. Barbieri, F. De Martini, P. Mataloni, G. Vallone, and A. Cabello, Phys. Rev. Lett. **97**, 140407 (2006);

[66] S. Gröblacher, T. Jennewein, A. Vaziri, G. Weihs, and A. Zeilinger, New J. Phys. **8**, 75 (2006);

[67] M. F. Andersen, *et al.*, Phys. Rev. Lett. **97**, 170406 (2006); R. Inoue, *et al.* Phys. Rev. A **74**, 053809 (2006); Z. Dutton, and J. Ruostekoski, Phys. Rev. Lett. **93**, 193602 (2004);

[68] K.-P. Marzlin, W. Zhang, and E. M. Wright, Phys. rev. Lett. **79**, 4728 (1997);

[69] S. Thanvanthri, K. T. Kapale, and J. P. Dowling, Phys. Rev. A **77**, 053825 (2008);

[70] K. T. Kapale and J. P. Dowling, Phys. Rev. Lett. **95**, 173601 (2005);

[71] R. Kanamoto, E. M. Wright, and P. Meystre, Phys. Rev. A **75**, 063623 (2007); W. Chen, D. Meiser, and P. Meystre, *ibid.* **75**, 023812 (2007);

[72] M. Paternostro, G. Adesso, and S. Campbell, Phys. Rev. A **80**, 062318 (2009); M. Paternostro, G. Falci, M. Kim, and G. M. Palma, Phys. Rev. B **69**, 214502 (2004); M. Paternostro, W. Son, M. Kim, G. Falci, and G. M. Palma, Phys. Rev. A **70**, 022320 (2004); F. Casagrande, A. Lulli, and M. G. A. Paris, Phys. Rev. A **75**, 032336 (2007); D. McHugh, M. Ziman, and V. Bužek, Phys. Rev. A **74**, 042303 (2006); D. Cavalcanti, J. G. Oliveira, J. G. de Faria, M. O. Cunha, and M. França Santos, Phys. Rev. A **74**, 042328 (2006);

[73] W.P. Schleich, *Quantum Optics in Phase Space*, (Wiley-VCH, 2001);

[74] C.T. Lee, Phys. Rev. A **44** R2775 (1991); M.A. Marchiolli, V.S. Bagnato, Y. Guimares, B. Basilea, Phys. Rev. Lett. **279**, 294 (2001);

[75] A. Kenfack, K. Życzkowski, J. Opt. B **6**, 396 (2004);

[76] J.P. Bizarro, Phys. Rev. A **49**, 3255 (1994);

[77] S. Bose and V. Vedral, Phys. Rev. A **61**, 040101(R) (2000).

[78] A. Peres, Phys. Rev. Lett. **77**, 1413, (1996); M. Horodecki, P. Horodecki, and R. Horodecki, Phys. Lett. A **223**, 1 (1996).

[79] K. Zyczkowski, *et. al.*, Phys. Rev. A, **58**, 883 (1998); G. Vidal and R. F. Werner, Phys. Rev. A **65**, 032314 (2002).

[80] I. Rigas, L. L. Sanchez-Soto, A. B. Klimov, J. Rehacek, Z. Hradil, Phys. Rev. A, **78**, 060101 (2008).

[81] D. Kazlikowski, L. C. Kwek, J. L. Chen, M. Zukowski, and C. H. Oh, Phys. Rev. A **65**, 032118 (2002); D. Collins, N. Gisin, N. Linden, S. Massar, and S. Popescu, Phys. Rev. Lett. **88**, 040404 (2002); A. Acín, T. Durt, N. Gisin, and J. I. Latorre, Phys. Rev. A **65**, 052325 (2001).

[82] Z. Hradil, J. Rehacek, Z. Bouchal, R. Celechovsky, and L. L. Sancher-Soto, Phys. Rev. Lett. **97**, 243601 (2006).

[83] A. I. Lvovsky, M. G. Raymer, Rev. Mod. Phys. **81**, 299 (2009).

[84] M. Lassen, G. Leuchs, and U. L. Andersen, Phys. Rev. Lett. **102**, 163602 (2009);

[85] F.G. Bosco, E.-T. Hwu, C.-H. Chen, S. Keller, M. Bache, M. H. Jakobsen, I.-S. Hwang, A. Boisen, Lab Chip **11**, 2411 (2011);

[86] D. Hungera, S. Camerera, M. Korppia, A. Jöckela,T.W. Hänscha, P. Treutlein, Comptes Rendus Physique **12**, 871 (2011);

[87] G. Binnig, C. F. Quate, Ch. Gerber, Phys. Rev. Lett. **56**, 930 (1986);

[88] A.V. Tsukanov, Russian Microelectronics **40**, 254 (2011);

[89] D. Hunger, S. Camerer, T. W. Hänsch, D. König, J. P. Kotthaus, J. Reichel, and P. Treutlein, Phys. Rev. Lett. **104**, 143002 (2010).

[90] A. D. OConnell, M. Hofheinz, M. Ansmann, R. C. Bialczak, M. Lenander, E. Lucero, M. Neeley, D. Sank, H. Wang, M. Weides, J. Wenner, J. M. Martinis, A. N. Cleland, Nature **464**, 697 (2010);

[91] J. D. Thompson, B. M. Zwickl, A. M. Jayich, F. Marquardt, S. M. Girvin, J. G. E. Harris, Nature **452**, 72 (2008);

[92] M. Sato, B. E. Hubbard, A. J. Sievers, Rev. Mod. Phys. **78**, 137 (2006);

[93] T. J. Kippenberg and K. J. Vahala, Science **321**, 1172 (2008); F. Marquardt and S. M. Girvin, Physics **2**, 40 (1993); M. Aspelmeyer, S. Gröblacher, K. Hammerer, and N. Kiesel, J. Opt. Soc. Am. B **27**, A189 (2010);

[94] G. Binnig,C.F. Quate, Ch. Gerber,Phys. Rev. Lett. **56**, 930 (1986);

[95] M. Paternostro, S. Gigan, M. S. Kim, F. Blaser, H. Böhm, and M. Aspelmeyer, New J. Phys. **8**, 107 (2006); M. Paternostro, D. Vitali, S. Gigan, M. S. Kim, C. Brukner, J. Eisert, and M. Aspelmeyer, Phys. Rev. Lett. **99**, 250401 (2007); Donner Nature (London) (2011); Painter Nature (London) (2011);

[96] P. Treutlein, D. Hunger, S. Camerer, T.W. Hänsch, and J. Reichel, Phys. Rev. Lett. **99**, 140403 (2007).

[97] A.D. Armour and M. Blencowe, New J. Phys. **10**, 095004 (2008); J.D. Teufel, T. Donner, Dale Li, J.W. Harlow, M.S. Allman, K. Cicak, A.J. Sirois, J.D. Whittaker, K.W. Lehnert and R.W. Simmonds, Nature (London) **478**, 89 (2011); M. Paternostro, G. De Chiara, and G. M. Palma, Phys. Rev. Lett. **104**, 243602 (2010); G. De Chiara, M. Paternostro, and G. M. Palma, Phys. Rev. A **83**, 052324 (2011);

[98] H. Jing, D. Goldbaum, L. Buchmann, and P. Meystre, Phys. Rev. Lett. **106**, 223601 (2011);

[99] H. Pu, C.K. Law, S. Raghavan, J. H. Eberly and N. P. Bigelow, Phys. Rev. A **60**, 1463 (1999);

[100] R. Barnett, J. D. Sau, S. Das Sarma Phys. Rev. A **82**, 031602 (2010); R. Barnett, H.-Y. Hui, C.-H. Lin, J. D. Sau, S. Das Sarma, Phys. Rev. A **83**, 023613 (2011);

[101] T. L. Ho, Phys. Rev. Lett. **81**, 742 (1998); C. K. Law, H. Pu and N. P. Bigelow, *ibid.* **81**, 5257 (1998); T. Ohmi and K. Machida, J. Phys. Soc. Jpn. **67**, 1822 (1998);

[102] E.G.M. van Kempen, S.J.J.M.F. Kokkelmans, D.J. Heinzen, B.J. Verhaar, Phys. Rev. Lett. **88**, 093201 (2001);

[103] M.-S Chang, Q Qin, W. Zhang, L.You and M.S. Chapman, Nature Phys. **1**, 111 (2005);

[104] S. Inouye, M. R. Andrews, J. Stenger, H.J. Miesner, D. M. Stamper-Kurn, W. Ketterle, Nature (London) **392**, 151 (1998);

[105] E. Arimondo, M. Inguscio, P. Violino, Rev. Mod. Phys. **49**, 31 (1977);

[106] Y. J. Wang, M. Eardley, S. Knappe, J. Moreland, L. Holberg and J. Kitching, Phys. Rev. Lett. **97**, 227602 (2006).

[107] I. H. Deutsch, P. S. Jessen, Phys. Rev. A **57**, 1972 (1998);

[108] Y. Takahashi, K. Honda, N. Tanaka, K. Toyoda, K. Ishikawa, T. Yabuzaki Phys. Rev. A **60**, 4974 (1999);

[109] G. A. Smith, S. Chaudhury, P. S. Jessen J. Opt. B: Quantum Semiclass. Opt. **5**, 323 (2003);

[110] Y. Liu, E. Gomez, S.E. Maxwell, L.D. Turner, E. Tiesinga, and P.D. Lett, Phys. Rev. Lett. **102**, 125301 (2009); *ibid.* **102**, 225301 (2009);

[111] L. Chang, Q. Zhai, R. Lu, Y. You, Phys. Rev. Lett. **99**, 080402 (2007);

[112] M. Kitagawa, M. Ueda, Phys. Rev. A **47**, 5138 (1993);

[113] S. K. Steinke, S. Singh, M. E. Tasgin, P. Meystre, K. C. Schwab, and M. Vengalattore, Phys. Rev. A **84**, 023841 (2011);

[114] S. Gigan *et al.*, Nature (London) **444**, 67 (2006); O. Arcizet *et al.*, *ibid.*) **444**, 71 (2006); A. Schliesser *et al.*, Phys. Rev. Lett. **97**, 243905 (2006);

[115] S. Gröblacher *et al.*, Nature (London) **460**, 724 (2009); A. D. O' Connell *et al.*, *ibid.* **464**, 697 (2010);

[116] V. Gorini, A. Kossakowski, E.C.G. Sudarshan, J. Math. Phys. **17**, 821 (1976);

[117] G. Lindlbad, Commun. Math. Phys. **48**, 119 (1976);

[118] H.P. Breuer, B. Vacchini, Phys. Rev. Lett. **101**, 140402 (2008);

[119] A. Shaji, E.C.G. Sudarshan, Phys. Lett. A **341**, 48 (2005);

[120] M. Žnidarič, T. Prosen, G. Benenti, G. Casati, D. Rossini, Phys. Rev. E **81**, 051135 (2010);

[121] M. Esposito, K. Lindenberg, C. Van den Broeck, New J. Phys. 12, 013013 (2010); S. Deffner, E. Lutz, Phys. Rev. Lett. **107**, 140404 (2011);

[122] R. Biele, R. D'Agosta, J. Phys **24**, 273201 (2012);

[123] G. Lindblad, *Non-Equilibrium Entropy and Irreversibility*, (D. Reidel Publishing Company,1940);

[124] R. Brown Phil. Mag. **4**, 161 (1828); A. Einstein, Ann. der Phys. **17**, 549 (1905);

[125] J.M. Steele, *Stochastic calculus and financial applications*, (Springer, 2000);

[126] D. Helbing, *Quantitative sociodynamics*, (Springer, 2010);

[127] H.-P. Breuer, E.-M. Laine, J. Piilo, Phys. Rev. Lett. **103**, 210401 (2009);

[128] M. M. Wolf, J. Eisert, T. S. Cubitt and J. I. Cirac, Phys. Rev. Lett. **101**, 150402 (2008);

[129] Á . Rivas, S.F. Huelga, and M.B. Plenio, Phys. Rev. Lett. **105**, 050403 (2010);

[130] D. Chruściński, A. Kossakowsi, Á. Rivas, Phys. Rev. A **83**, 052128 (2011);

[131] P. Hakika, J. D. Cresser, S. Maniscalco, Phys. Rev. A **83**, 012112 (2011);

[132] B. Vacchini, A. Smirne, E.-M. Laine, J. Piilo, H.-P. Breuer, New J. Phys. **13**, 093004 (2011);

[133] M. Lax, Phys. Rev. **129**, 2342 (1963);

[134] M. Lax, Phys. Rev. **172**, 350 (1968);

[135] H.-P. Breuer, F. Petruccione, *The theory of open quantum systems*, (Oxford University Press, 2002);

[136] E. Hille, R. S. Phillips, *Functional analysis and semi-groups*, (American Mathematical Society, 2000);

[137] P. Hänggi, H. Thomas, Z. Physik B **26**, 85 (1977);

[138] P. Hänggi, H. Thomas, Physics Reports **88**, 207 (1982);

[139] B. A. Grishanin, Kvantovanya Elektron **6**, 1409 (1979);

[140] B. A. Grishanin, Teoreticheskaya i Matematicheckaya Fizika **48**, 396 (1981);

[141] D. Chruściński, A. Kossakowsi, Eur. Phys. Lett. **97**, 20005 (2012);

[142] L. Mazzola, C. A. Rodriguez-Rosario, K. Modi, M. Paternostro, Phys. Rev. A **86**, 010102 (2012);

[143] M. Mohseni, A.T. Rezakhani, and D. A. Lidar, Phys. Rev. A **77**, 032322 (2008);